

AD-A246 085



L (2)

# NAVAL POSTGRADUATE SCHOOL Monterey, California



**DTIC**  
**S** **ELECTE** **D**  
**D** FEB 20 1992

## THESIS

THE CONVERSION OF A SINGER GAT-1B™  
ANALOG FLIGHT SIMULATOR INTO A DIGITAL  
FLIGHT SIMULATOR

by

George Demetrius Duchak

March 1990

Thesis Advisor:  
Co-Advisor:

James P. Hauser  
Louis V. Schmidt

Distribution is ~~limited~~ to U.S. Government Agencies only: Thesis contains proprietary information; 15 March 1990. Other requests for this document must be referred to Link Flight Simulation Systems, Binghamton, N.Y. 13902 ~~via the Defense Technical Information Center, Cameron Station, Alexandria, VA 22304-6145~~

92-03697



92 2 12 160

Unclassified

Security Classification of this page

REPORT DOCUMENTATION PAGE				
1a Report Security Classification <b>Unclassified</b>		1b Restrictive Markings		
2a Security Classification Authority		3 Distribution Availability of Report		
2b Declassification/Downgrading Schedule		<del>Distribution Statement B</del>		
4 Performing Organization Report Number(s)		5 Monitoring Organization Report Number(s)		
6a Name of Performing Organization <b>Naval Postgraduate School</b>	6b Office Symbol (If Applicable) <b>39</b>	7a Name of Monitoring Organization <b>Naval Postgraduate School</b>		
6c Address (city, state, and ZIP code) <b>Monterey, CA 93943-5000</b>		7b Address (city, state, and ZIP code) <b>Monterey, CA 93943-5000</b>		
8a Name of Funding/Sponsoring Organization	8b Office Symbol (If Applicable)	9 Procurement Instrument Identification Number		
8c Address (city, state, and ZIP code)		10 Source of Funding Numbers		
		Program Element Number	Project No	Task No
		Work Unit Accession No		
11 Title (Include Security Classification) <b>The Conversion of a Singer/Link GAT-1B™ Analog Flight Simulator into a Digital Flight Simulator</b>				
12 Personal Author(s) <b>George D. Duchak</b>				
13a Type of Report <b>Engineer's Thesis</b>	13b Time Covered From To	14 Date of Report (year, month, day) <b>1990 March</b>	15 Page Count <b>144</b>	
16 Supplementary Notation <b>The views expressed in this thesis are those of the author and do not reflect the official policy or position of the Department of Defense or the U.S. Government.</b>				
17 Cosati Codes		18 Subject Terms (continue on reverse if necessary and identify by block number)		
Field	Group	Subgroup		
		Flight Simulator, Singer GAT-1B™		
19 Abstract (continue on reverse if necessary and identify by block number) <p>This thesis was a proof of concept engineering project. A portion of a Singer GAT-1B™ motion based analog flight simulator was converted into its digital equivalent. The attitude analog card was partially replicated in digital hardware and software. An IBM PS/2™ Model-50 with a National Instruments® Analog to Digital board and Lab Windows™ software was used for the conversion and manipulation of the signals. Movement of a control surface changed a potentiometer position on the simulator. This change in voltage was analogous to a force causing an acceleration on the flight vehicle. The angular accelerations were integrated to determine the angular rotation rates. These rotation rates were combined with the components of the other forces effecting simulator position and attitude. The results were integrated to determine the appropriate Euler angles of the flight simulator. The digital response to a one Hertz square wave input as a control surface deflection was compared to the analog response. The analog and digital responses were identical for the roll and yaw rate computations. The pitch rate digital response was approximately a factor of two greater than the analog response.</p>				
20 Distribution/Availability of Abstract		21 Abstract Security Classification		
<input checked="" type="checkbox"/> unclassified/unlimited <input type="checkbox"/> same as report <input type="checkbox"/> DTIC users		<b>Unclassified</b>		
22a Name of Responsible Individual <b>James P. Hauser</b>		22b Telephone (Include Area code) <b>(408) 646-2892</b>	22c Office Symbol <b>Code 67HS</b>	

DD FORM 1473, 84 MAR

83 APR edition may be used until exhausted

All other editions are obsolete

security classification of this page

Unclassified

~~Distribution is limited to U.S. Government Agencies only: Thesis contains proprietary information; 15 March 1990. Other requests for this document must be referred to Link Flight Simulation Systems, Binghamton, N.Y. 13902 via the Defense Technical Information Center, Cameron Station, Alexandria, VA 22304-6145~~

**The Conversion of a Singer GAT-1B Analog Flight Simulator into a  
Digital Flight Simulator**

by

**George Demetrius Duchak**  
**Lieutenant Commander, United States Navy**  
**B.S.M.E., United States Naval Academy, 1977**  
**M.B.A., The Ohio State University, 1985**  
**M.S.A.E., Naval Postgraduate School, 1989**

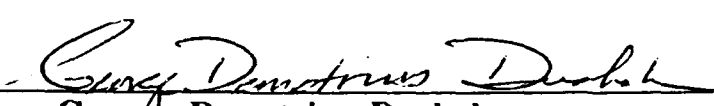
Submitted in partial fulfillment of the requirements  
for the degree of

**AERONAUTICAL ENGINEER**

from the

**NAVAL POSTGRADUATE SCHOOL**  
**March 1990**

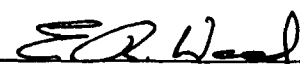
Author:

  
George Demetrius Duchak

Approved by:

  
James P. Hauser, Thesis Advisor

  
Louis V. Schmidt, Co-Advisor

  
E. Roberts Wood, Chairman, Department of Aeronautics and  
Astronautics

  
Dean of Faculty and Graduate Studies

## ABSTRACT

This thesis was a proof of concept engineering project. A portion of a Singer GAT-1B™ motion based analog flight simulator was converted into its digital equivalent. The attitude analog card was partially replicated in digital hardware and software. An IBM PS/2™ Model-50 with a National Instruments® Analog to Digital board and Lab Windows™ software was used for the conversion and manipulation of the signals. Movement of a control surface changed a potentiometer position on the simulator. This change in voltage was analogous to a force causing an acceleration on the flight vehicle. The angular accelerations were integrated to determine the angular rotation rates. These rotation rates were combined with the components of the other forces effecting simulator position and attitude. The results were integrated to determine the appropriate Euler angles of the flight simulator. The digital response to a one Hertz square wave input as a control surface deflection was compared to the analog response. The analog and digital responses were identical for the roll and yaw rate computations. The pitch rate digital response was approximately a factor of two greater than the analog response.

iii

Accession For	
NTIS	CRA&I
DTIC	TAB
Unannounced	<input checked="checked" type="checkbox"/>
Justification	
By _____	
Distribution /	
Availability Codes	
Dist	Avail and/or Special
B-3	
(A)	

## TABLE OF CONTENTS

I. INTRODUCTION .....	1
A. SCOPE .....	3
1. The Task .....	3
2. Reasons/Need for Flight Simulation .....	4
B. A BRIEF HISTORY .....	5
C. ORGANIZATION OF THIS THESIS .....	16
II. NATURE OF THE PROBLEM.....	17
A. ANALOG TO DIGITAL AND DIGITAL TO ANALOG CONVERSION .....	18
B. THE MATH MODEL .....	21
C. EULER ANGLE EQUATIONS OF MOTION DEVELOPED .....	22
III. THE HARDWARE AND THE SOFTWARE .....	45
A. GAT-1B™ SYSTEM DESCRIPTION .....	45
1. Attitude Card.....	45
a. Some Preliminaries.....	49
b. Roll Circuitry Described .....	52
c. Pitch Circuitry Described .....	57
d. Yaw Circuitry Described .....	62
2. Time Division Multiplier Circuitry Card Described.....	68
B. IBM PS/2™ MODEL-50 HARDWARE .....	70
1. National Instruments® MC-MIO-16 Interface Board .....	70

2. Lab Windows™ .....	74
IV. ENGINEERING APPROACH .....	75
A. INSTALLING THE DIGITAL COMPUTER .....	75
B. ANALOG/DIGITAL UMBILICAL INSTALLATION.....	77
C. SIGNAL FLOW .....	78
1. Input Signal Flow.....	78
a. WOG Circuit .....	81
b. A/D Trigger Signal.....	82
2. Output Signal.....	83
D. SUPPORTING SOFTWARE .....	92
1. Explanation of Variables .....	92
a. buffer%() .....	92
b. chan.vector%() .....	92
c. gain.vector%() .....	93
d. volt.array%() .....	93
e. bin.val%() .....	94
2. Explanation of Constants.....	95
3. Explanation of Rate Equation Calculations.....	96
a. Roll Rate Calculations .....	97
b. Pitch Rate Calculations .....	98
c. Yaw Rate Calculations .....	99
E. EXPERIMENTAL VERIFICATION OF NUMERICAL INTEGRATION TECHNIQUE USED .....	101
F. MATCHING WAVEFORMS .....	103

G. CORRECTIONS TO THE SCHEMATICS .....	107
H. A PICTURE IS WORTH A THOUSAND WORDS .....	109
V. RESULTS AND CONCLUSIONS .....	114
A. RESULTS .....	114
1. Digital Tracked Analog Signal .....	114
2. Unexplained Gain .....	114
3. Difficulty Relating Constants from the Circuit to the Equations of Motion .....	115
B. AREAS FOR FUTURE MODIFICATIONS .....	115
1. Construct a Special Purpose A/D Circuit .....	115
2. Digitize All Analog Boards .....	116
3. Add X-Y Plot .....	116
4. Add Visual Display .....	117
5. Multi-engine .....	117
6. Helicopter Equations of Motion .....	119
C. CONCLUSIONS .....	119
APPENDIX A - COMPUTER CODE .....	121
LIST OF REFERENCES .....	126
BIBLIOGRAPHY .....	128
INITIAL DISTRIBUTION LIST .....	131

## LIST OF FIGURES

1-1	THE WRIGHT FLYER (1903) .....	2
1-2	EARLY LINK TRAINER (1935) .....	8
1-3	GENERALIZED DIGITAL DATA FLOW .....	14
2-1	GROSS SIGNAL FLOW .....	17
2-2	EXAMPLE OF A 3-BIT ADC .....	20
2-3	A GENERAL MATH MODEL .....	21
2-4	REFERENCE SYSTEM .....	24
2-5	POSITION VECTORS .....	25
2-6	EULER ANGLE ROTATIONS.....	36
3-1	N-TYPE CHANNEL FET .....	49
3-2	PIN CONNECTIONS FOR ANALOG MOTHER BOARD .....	51
3-3	ROLL RATE BLOCK DIAGRAM.....	52
3-4	ROLL RATE AND BANK MOTION SYSTEM SCHEMATIC .....	56
3-5	PITCH RATE BLOCK DIAGRAM.....	57
3-6	PITCH RATE AND PITCH MOTION SYSTEM SCHEMATIC.....	61
3-7	YAW RATE BLOCK DIAGRAM .....	62
3-8	TURN RATE AND HEADING MOTION SYSTEM SCHEMATIC..	67
3-9	TIME DIVISION MULTIPLIER SCHEMATIC.....	69
3-10	ANALOG OUTPUT CIRCUITRY BLOCK DIAGRAM.....	71
3-11	ANALOG INPUT AND DATA ACQUISITION CIRCUITRY .....	72
3-12	RTSI BUS INTERFACE BLOCK DIAGRAM .....	73



4-1	POWER CONVERSION .....	76
4-2	CB-50 I/O BLOCK DIAGRAM .....	78
4-3	INPUT ARRAY .....	79
4-4	VOLTAGE DIVIDER.....	80
4-5	INPUT SIGNAL FLOW .....	81
4-6	WOG CIRCUIT .....	82
4-7	TIMING CIRCUIT .....	85
4-8	TIMING DIAGRAM .....	88
4-9	NAND LOGIC .....	88
4-10	1 OF 8 SWITCH CONCEPT .....	89
4-11	TIMING LOGIC.....	91
4-12	VOLTAGE ARRAY .....	94
4-13	EXPERIMENTAL INTEGRATION CIRCUIT .....	101
4-14	ANALOG AND DIGITAL INTEGRATION OSCILLOSCOPE DISPLAY.....	102
4-15	DIGITAL AND ANALOG ROLL RATE RESPONSE TO A SQUARE WAVE INPUT SIGNAL.....	104
4-16	DIGITAL AND ANALOG PITCH RATE RESPONSE TO A SQUARE WAVE INPUT SIGNAL AFTER ADJUSTING RESISTOR VALUE .....	105
4-17	DIGITAL AND ANALOG YAW RATE RESPONSE TO A SQUARE WAVE INPUT SIGNAL.....	107
4-18	RESISTOR VALUES FOR TIME CONSTANTS .....	108
4-19	OVERALL SYSTEM PHOTOGRAPH .....	110

4-20	DIGITAL COMPUTER INSTALLATION.....	111
4-21	ANALOG MOTHER BOARD CLOSE-UP .....	112
4-22	AMALOG MOTHER BOARD AND PROTOTYPE CIRCUIT BOARD CLOSE-UP .....	112
4-23	CLOSE-UP OF THE PROTOTYPE CIRCUIT BOARD .....	113
5-1	SYNCHRO TO ANALOG CONVERTER CIRCUIT .....	118

## DEFINITIONS

<b><u>Symbol</u></b>	<b><u>Name</u></b>
$\beta$	Side Slip Angle
$C_L$	Coefficient of Lift
$\delta_a$	Aileron Deflection
$\delta_e$	Elevator Deflection
$\delta_{e t}$	Elevator Trim Deflection
$\delta_{FW}$	Wing Flap Deflection
$\delta_r$	Rudder Deflection
$\phi$	Roll Angle
$T_N$	Net Thrust
$\theta$	Pitch Angle
$P_A$	Rate of Roll
$Q_A$	Rate of Pitch
$R_A$	Rate of turn
$q$	Dynamic pressure
$V_{ind}$	Indicated Airspeed
$1/V_{ind}$	Reciprocal of Indicated Airspeed

## ACKNOWLEDGEMENTS

To my family, without whose love, encouragement, patience, understanding, and support, the successful completion of this program would not have been possible. I owe them incalculable gratitude.

The patience, guidance, brilliant insight, and invaluable assistance of Professor James P. Hauser are most sincerely appreciated. During his brief tenure his contributions to the avionics program at the Naval Postgraduate School have been most significant. The void left by his absence will be clearly felt by the students, faculty and staff.

The sage advice, thoughtful comments, and generous assistance of Professor Louis V. Schmidt are most gratefully applauded. His uncommon dedication to the Navy and the Naval Postgraduate School over the past 25 years has been extraordinary. The school and the Navy have greatly benefited from his presence.

## I. INTRODUCTION

The mid morning air was crisp and a cool stiff breeze blew over the sands of Kill Devil Hills approximately four miles south of Kitty Hawk, North Carolina. Orville Wright was at the controls of the Wright Flyer as his brother Wilbur ran along the starboard side supporting the wing to ensure it didn't drag in the sand. As the throttle of the 12 hp engine advanced, the Wright Flyer, Figure 1-1, lifted off under its own power at 1035 on Thursday 17 December 1903. Frozen in time, man's first flight lasted 12 seconds, traversed 120 feet with a maximum altitude of 10 feet and attained a top speed of 30 miles per hour. In Orville Wright's own words:

"the first in the history of the world in which a machine carrying a man had raised itself by its own power into the air in full flight, had sailed forward without reduction of speed, and had finally landed at a point as high as that from which it started." (Wolko, Anderson, 1985, p.2)

Before the Wright's first flight, it was widely perceived that powered fixed wing flight would be relatively as stable as airship flight and as such require no a priori skills. The Wright's discovered that their aircraft (as well as others of the era) required a skilled operator to maintain equilibrium.

The driving philosophy of aviation became to fly faster, further, and higher. Logically, it would be prudent to have a training device which helped develop flight skills while the operator was safely on the ground.

Flight simulators have become so pervasive that today type rating for airline pilots occurs fully in the simulator. A newly rated pilot's first flight in the actual aircraft occurs with paying passengers.

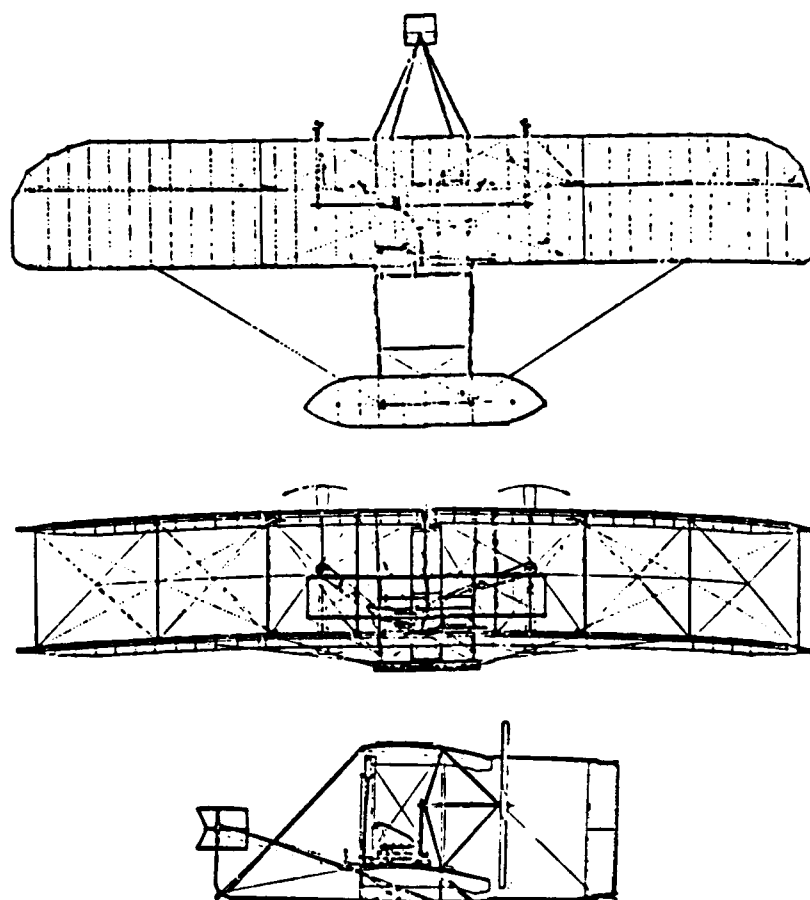


Figure 1-1. The Wright Flyer I 1903. (Anderson, 1985, p.2)

## **A. SCOPE**

The Department of Aeronautics and Astronautics at the Naval Postgraduate School in Monterey, California is currently in possession of a Singer Link GAT-1B™ (General Aviation Trainer), serial number 357.

This thesis is a proof of concept engineering project which digitally replicates a portion of the analog flight attitude control card on the GAT-1B. Once the concept has been validated, the logical extension would be to digitize all of the analog cards making the GAT-1B fully digitally controlled. That however is beyond the scope of this project. This project does however lay the groundwork for that eventuality, namely to validate the practicality of using digital verse analog control logic in the GAT-1B simulator.

### **1. The Task**

Flight simulation engineering crosses many disciplines; aeronautics, mechanical, electrical, mathematics, computer science, and even psychological and biological sciences. Within the area of aeronautics, flight simulation engineering can be further subdivided into requiring knowledge of flight dynamics, performance, and stability. Within the area of electrical engineering, required knowledge includes electromechanical devices, electronic devices, control systems, and digital machines. Software engineering becomes paramount in sophisticated real-time, full motion, visual flight simulators. In short, all the engineering areas involved in the design and construction of a real aircraft are involved in flight simulation engineering. Even wind-tunnel testing provides the parameters which are to be used in the model.

The objective of this project was to digitize the analog information necessary to compute roll, pitch, and yaw. That is, the Euler Angles were computed digitally. These signals were then reintroduced into the analog circuitry to allow the GAT-1B to retain its full motion capability.

It should be apparent that representing an analog computation digitally in software enables tremendous flexibility over the dynamic stability and performance characteristics which are simulated by the trainer. Equations can be easily modified to vary the simulated aircraft performance and handling characteristics.

## **2. The Reasons**

Most will surely recognize that advances in technology have made it possible for the latest state of the art flight simulators to be perceived by the pilot as virtually identical to actual flight. As early as 1973 the Government Accounting Office, GAO, recommended that increased simulator training lowers costs and increases the safety of pilot training (GAO, 1973, pp. 21-22). There have been both advocates and opponents of full motion simulators. P.W. Caro suggests that there are more economic alternatives to motion based simulator (Third Annual Symposium on Flight Simulation, 1976, p. E-1). Generally however, the pilots, the ones actually using the flight simulators, agree that motion queues are most useful. J. B. Keegan has called flight simulation a "confidence trick" where the kinesthetic queues force a perception of actual flight (Third Annual Flight Simulation Symposium, 1976, p. 6-1).

The Department of Aeronautics and Astronautics at the Naval Postgraduate School has the opportunity to improve its instructional capabilities



by modifying the GAT-1B. Different handling characteristics can be programmed and students can actually fly (simulated) aircraft with differing handling characteristics. The cost and benefits arising from this project are not in teaching the students how to fly (most already know how), but rather in the academic arena of taking classroom concepts and actually getting a "real world" feel of the reprogrammed changes on the handling characteristics of the modified aircraft.

## **B. A BRIEF HISTORY OF FLIGHT SIMULATION**

In order to gain an appreciation for the evolution, complexities, and number of engineering disciplines involved in flight simulation, a brief history is presented. Highlights from various texts on flight simulation by Parrish, Rolfe and Staples are condensed and presented in the ensuing discussion.

One of the first "flight simulators" was the Sanders Teacher (circa 1910) which was a crude device mounted on a universal ball joint which the pilot attempted to maintain balanced. Other simulators of this basic design were produced by the British, French, and Italians between 1910 and 1920.

World War I saw the need to teach flight skills in large numbers to military aviators. Simulators however were not used much due to their questionable benefit. Many would-be aviators died in training. The Army however, believed that the ones who perished in flight training didn't have the right innate skills so simulators were developed which could test reaction time and coordination.

By the 1920's equations of aircraft flight dynamics were being developed. Between 1920 and 1930 the most common simulator design used a pivoted cockpit and compressed air to actuate motion in response to stick and rudder

deflections. It was widely believed at the time that the inner ear was responsible for determining aircraft orientation in flight.

In the early days of aviation, aircraft were flown only when the weather permitted. As aviation evolved and became less of a romantic curiosity and more of commercial venture, the need for safe and reliable transportation became paramount. This meant that aircraft needed to be capable of flight in most weather conditions. A method of flying during adverse weather conditions utilizing instruments which gave the pilot attitude, airspeed, altitude, various engine data, and radio navigation information was eventually developed.

In 1929 Lieutenant James Doolittle, U.S. Army Air Forces, convincingly proved that an aircraft could take off, fly, and land using only cockpit instruments as a guide. Also that same year, Edwin A. Link, the son of a piano and organ, manufacturer<sup>1</sup> was teaching himself to fly in a homebuilt "aircraft" which was never intended to leave the ground. Link described the first fixed-base flight simulator as, "part piano, part organ, and even a little bit of airplane." (Parrish, 1969, p. 13) Link developed his trainer in the basement of the piano and organ factory between 1927 and 1929. His patent for the device was first filed in 1930. Link however fine-tuned the motion of his trainer by trial and error until it "felt right" rather than using any sort of math model. This first trainer was intended only to simulate the feel of flight. No instruments were installed. In the early 1930's Link fitted his trainer with instruments and began to teach "blind flight training" to the U.S. Army Air Corps who were recently given the responsibility of carrying the U.S. mail. His trainer soon

---

<sup>1</sup> Link Piano and Organ Company of Binghamton, N.Y.

became the standard for teaching instrument procedures to airmen and thus enabling the safer, longer range flight.

Figure 1-2 shows Link's first successful simulator known as the "blue and yellow box" which bore little resemblance to any aircraft. Consisting of a fuselage of plywood with only the rudiments of wings and a tail for esthetic reasons and cacophony of bellows, pumps and gauges, the box had motion in the three major flight axes. It rolled, pitched, and yawed. The simulator was totally without external visual references as the cockpit canopy consisted of an opaque cover. Instruments in the simulator all responded to changes in the flight controls and the "box" itself would move to reflect the instrument positions giving a crude kinesthetic feel of flight. While the trainer lacked the instrumentation of any particular aircraft and replicated the motions (stability dynamics) of no aircraft, it did serve the purpose of indoctrinating the airmen in instrument procedures while safely on the ground where mistakes or misinterpretation of the instruments was far less costly physically and fiscally. During the 1930's Link sold his trainer to Japan, the USSR, France, Britain, and Germany.

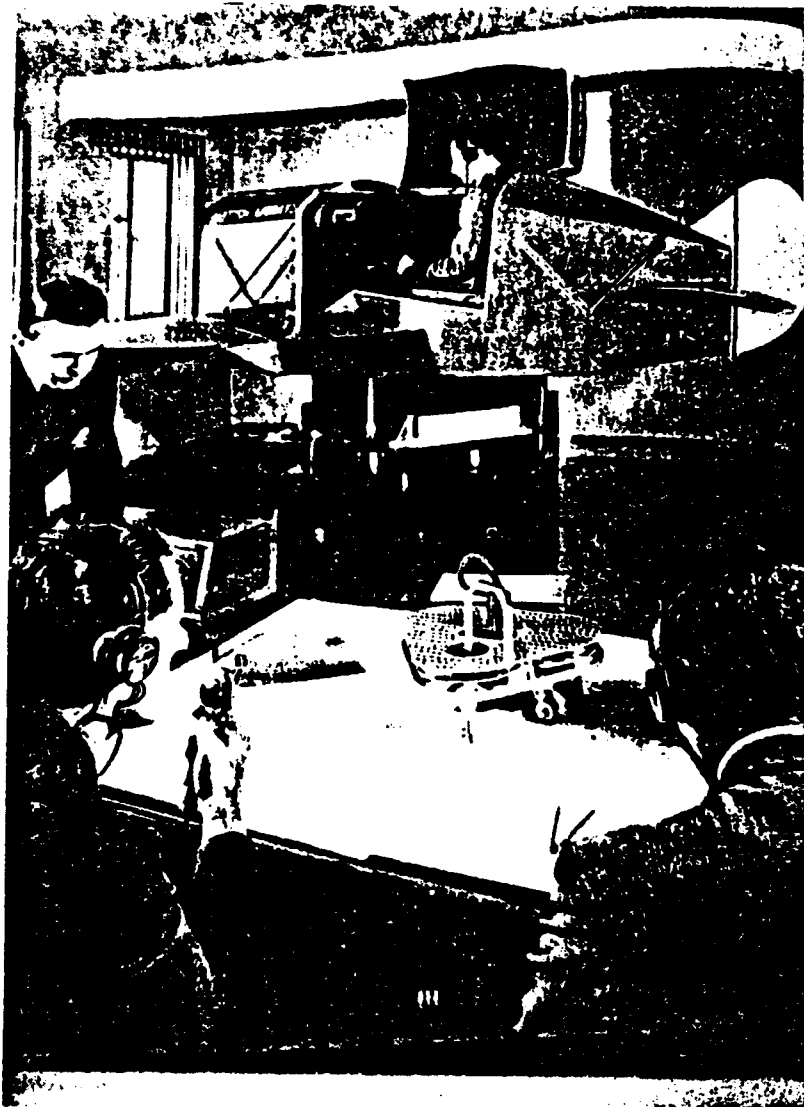


Figure 1-2. Early Link Trainer, 1935. (Rolfe and Staples, 1986, p. 23)

The rudiments of electric analog flight simulation began in 1936 when Professor Mueller of MIT described an analog computer which would be capable of solving in real time the aircraft equations of motion.

In 1937 American Airlines became the first commercial airline to purchase the Link trainer. By World War II, Link's trainers were used by virtually every major air force.

In 1939 the British contracted Link to construct a celestial navigation trainer to improve night bombing accuracy. The trainer, completed in 1941 was housed in a gargantuan, for the day, 45 foot silo. The cockpit was large enough for a pilot, navigator, and bombardier. An elaborate celestial representation changed position with respect to latitude and longitude as the aircraft simulated transiting the earth's surface. Aircrewmembers practiced fixing the aircraft position with respect to the twelve major stars. Radio navigation aids were also incorporated. The RAF was impressed enough with the simulator to order 60. However, most were never delivered to the RAF but rather diverted to use by U.S. forces.

Between 1939 and 1940, Travis developed the fixed base "Aerostructor" which was electrically operated but used visual rather than instrument cues to simulate aircraft dynamics. It used a film loop which responded to roll, pitch, and yaw. This design was later modified by the U.S. Navy and became the "Gunairstructor" to teach aerial gunnery.

Telecommunications Research Establishment (TRE), most noted for their early work in radar, developed a radar intercept trainer to complement their radar in 1941.

During World War II Link developed the ANT-18 which was first used more specifically for SNJ and AT-6 aircraft indoctrination. Thousands of Link's follow-on simulators, the ANT-19, were eventually used. The trainer still used bellows that were driven by a vacuum pump which responded differentially to

flight control inputs. The differential pressures in the bellows caused the motion. Early simulators used an assortment of gears, pinions and cranks to move the cockpit instruments. Audio engine noise was incorporated much in the way a child would attach a baseball card to the frame of his bicycle allowing the card to strike the wheel spokes. Trainers of the day were limited to the level of technology available, mainly electromechanical devices.

A glimpse of digital computing was on the horizon. Aiken constructed the first general purpose digital computer, Mark I, between 1937 and 1944. It was an electromechanical device. In 1942 Crawford of MIT authored a thesis prescribing "Automatic Flight Control by Arithmetic Operators." The U.S. Navy funded the development of ASCA (Airplane Stability and Control Analyzer) in 1943 which became a digital project.

By 1943 Bell Telephone Labs produced the first trainer designed specifically to simulate the characteristics of an operational aircraft, specifically the PBM-3. It electronically solved the equations of motion using potentiometers and servo integrators. No motion or visual simulation was incorporated, however.

Simulators prior to the end of the War were basically procedural trainers with few noted exceptions. After the War, the explosive growth of flight trainers subsided somewhat. The value of motion base simulation was questioned since they didn't really simulate the actual forces experienced in flight. The argument was made that modern pilots should know how to fly by instruments rather than by the seat of their pants. The trend was now towards fixed base simulators. Advanced by technology developed during the War more

sophisticated trainers using analog computation were being introduced and the first real simulators were born.

The War brought greatly enhanced methods and mathematical models for aircraft and propulsion design. Onboard avionics, navigation equipment, radar, armament, ordnance, and tactics all increased in their level of sophistication. Simulation designers now approached the simulation problem on a different tact. Using the math models developed by the airframe and propulsion engineers, the designers worked backwards to make the simulator respond according to these math models and equations of motion.

These equations had to be updated in response to flight control inputs. Analog computers, comprised of special purpose electronic circuits, were developed which modeled the aircraft equations of motion responding in real time. Analog computers offered several advantages. Modifying the list contained in the text by Ostendorf (Ostendorf, p. 11-11):

- information was computed in parallel, that is, all computational elements worked simultaneously
- dependent variables within the computer were treated in a continuous fashion due to the nature of the circuitry
- non-linear functions could be generated as well as the mathematical operations of integration, addition, and multiplication
- computational speeds were limited by the characteristics of the electronic circuit computing elements, not by the complexity of the problem

However, as the level of sophistication of the simulator increased so did the amount of hardware required to implement the model. More complicated simulations required more circuits for their model. For complex simulators, it was not unusual to find literally rooms filled with analog computer cabinets. Analog computers however, had several inherent disadvantages:

- errors were cumulative
- essentially non-robust; results could not be identically replicated for each run of the simulator
- maintenance problems due to increased size and complexity
- accuracy limited by the quality of the individual electronic components
- amplitude scale of the computer was limited by amplifier saturation
- a limited ability to make logical decisions and store data
- low frequencies tended to have drift and high frequencies showed phase shift and attenuation

In 1948 Pan American Airways became the first airline to use a full aircraft simulator. Developed by Curtiss-Wright, the simulator replicated the performance and handling characteristics of the Boeing 377 Stratocruiser. No motion or visual cues were simulated. The flight instruments did replicate the behavior of the Boeing 377, however. This simulator design was licensed by Rediffusion of the U.K. and a similar simulator was built for BOAC.

In 1949 Link developed an analog computer for the fixed base C-11 jet-trainer simulator used by the U.S. Air Force. Over 1000 were produced.

As analog designs became increasingly more complex, any errors in the signal accumulated and diminished effectiveness. By 1950 the development of



the digital computer had progressed to the point where almost over night, simulator designers switched from analog to digital designs. Concurrently, sophistication in test and evaluation of aircraft provided much more data to the simulation engineer. Better math models could be constructed and run on a digital computer without the degradation of cumulative analog error signal effects. During 1950 the U.S. Navy funded UDOFT (Universal Digital Operational Flight Trainer) which was the first truly digital flight simulator. Also during the 1950's, digital computers found their way into military applications such as the AN/FSQ-7 computer used in the USAF SAGE Air defense System. By the late 1950's the airlines were requesting flight simulators which had six degrees of freedom digitally controlled.

In 1960 Link built the Mark I special purpose digital computer for use in their simulators. The special purpose digital computer offered a computational speed advantage over general purpose digital computers. Digital computers found their way into the flight simulation problem offering the advantages of reduced hardware requirements and robustness. Digital approaches offered greater stability, repeatability, greater precision, and no precise temperature control was necessary for the cooling of analog electronic components. A new problem of converting the analog flight control input information to digital information for computation by the math model and then converting the computed digital information back to analog information emerged. Figure 1-3 illustrates the digital data flow. (Parrish, 1969, p. 41) Note the use of analog to digital and digital to analog converters.

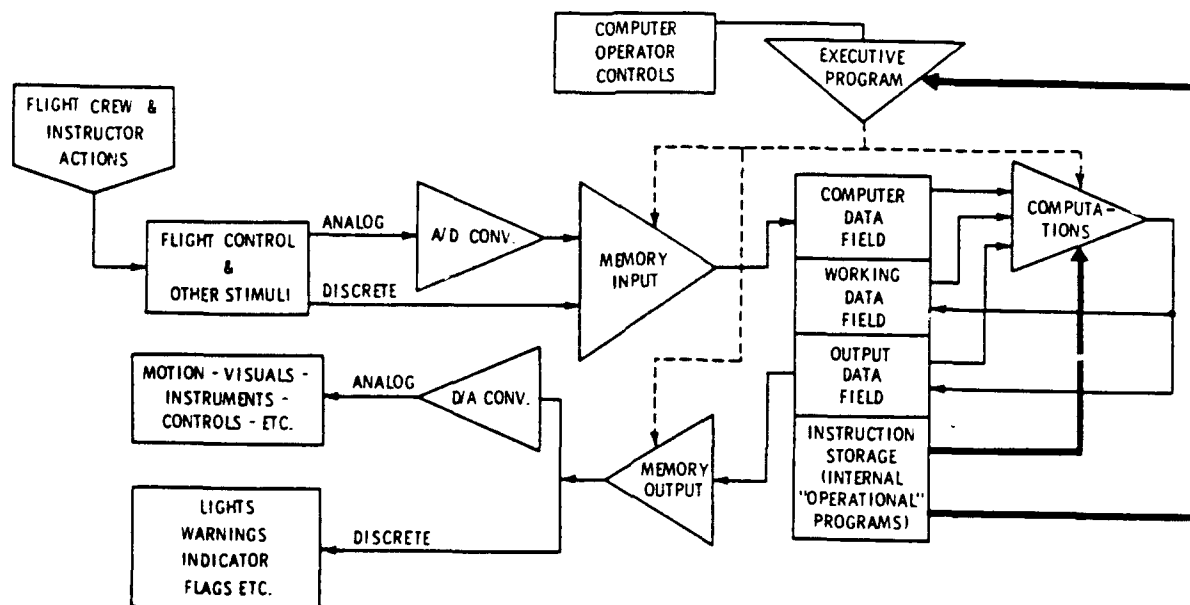


Figure 1-3. Generalized Digital Data Flow. (Parrish, 1969, p.41)

The digital computer uses discrete data and manipulates individual numbers. They have a logic capability as well as the ability to store data in memory. A closed loop system design was utilized as opposed to earlier open loop systems. The growth of digital computers ushered in the last remaining hurdle to realistic flight in a ground based simulator, that is the display of out of the cockpit visual information.

Eighty percent of learning is accomplished through the visual senses. Out of cockpit displays which provide realistic visual perceptory cues greatly improved the quality of the simulation. Visual cues give a much more realistic perception of motion than vestibular cues.

The first visual displays were static physical models of the local terrain on a large board on the order of 20 feet by 20 feet. A camera was mounted on a device which allowed the camera to translate (in three dimensions), roll, pitch and yaw above the model. The visual image seen by the camera above the terrain model was projected in front of the simulator as a visual cue of aircraft position and attitude. The pilot essentially flew the camera over the terrain model. There was an economic as well as a practical level of detail for a physical model.

Other less successful devices employing the same sort of techniques utilized fixed film projection (a terrain snapshot) and film transparencies to project visual images in response to control inputs.

Computer image generation was first developed by General Electric in 1967 for the U.S. Space program and in 1971 McDonnell-Douglas developed the Vital II. Electronic image generation simulated night and low visibility conditions. An electronic terrain map was computed and recomputed based on flight control inputs to give accurate sensory displays. This method was limited to night and low visibility projections due to the computational intensity of the manipulation of graphics images. Only lights of varying brightness were in the model.

As the development of the microprocessor continued, flight simulation techniques progressed in a parallel manner. More detailed math models required faster computational speeds and more computer memory. Currently, through the use of high speed computers, the ability to accurately represent full color digital terrains exists. These computationally intensive models project a near lifelike real-time image which corresponds to flight control input.

### **C. ORGANIZATION OF THIS THESIS**

Chapter two will discuss the nature of the problem. A generalized math model for aircraft simulations and the Euler angle equations of motion are described and related to the GAT-1B flight simulator. Analog to digital and digital to analog conversion in general is also presented. Chapter three will present a detailed explanation of the signal flow of the analog flight attitude card. A description of the hardware and software that was available for use for this project is also presented. Chapter four will explain the engineering approach taken to meet the objectives of this project. Detailed digital signal flow is presented and the software written for this project is described. Chapter five reports the results of the conversion and suggests avenues for further enhancement.

## II. NATURE OF THE PROBLEM

With the introduction of digital computers to solve the flight simulation math model came the need to convert the analog voltages which represent actions taken by the pilot to a digital form for manipulation by the computer. As mentioned in the brief history contained in Chapter I, it became necessary not only to convert the analog signals to digital but equally important to convert the digital results onto analog form to drive the motion, instruments and other peripheral equipment. Additionally, the simulation is only as good as the math model which drives it. Figure 2-1 gives a gross illustration of the signal flow for this problem.

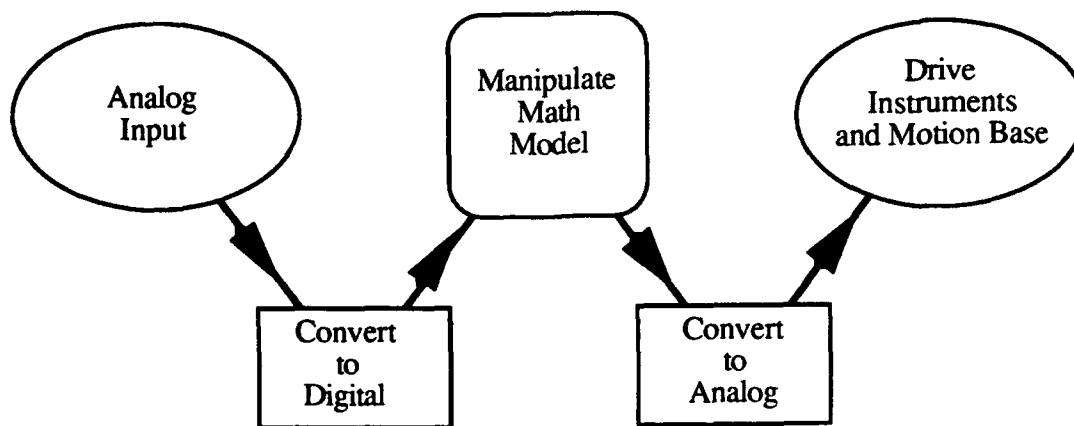


Figure 2-1. Gross Signal Flow.

Rolfe and Staples (Rolfe and Staples, 1986, p. 17) state that good simulation requires,

- model
- real time solution
- presentation

The elements of the above requirements will be discussed.

#### **A. ANALOG TO DIGITAL / DIGITAL TO ANALOG COMPUTATION**

An analog to digital converter is an electronic device which takes a continuous voltage input and determines its value for input to a digital computer. The voltage is binary coded and the resolution of the device depends on the size (number of bits) of the microprocessor device being used. A comparator is a device which compares a reference voltage to an incoming voltage and determines which is the greater. The comparator in conjunction with the microprocessor will commonly<sup>1</sup> use a successive approximation scheme to determine the incoming voltage. The resolution becomes:

$$\text{digitized voltage} = \text{full scale voltage} \div 2^n$$

where n is the number of bits of the micro processor. In actuality, the error is a function of the least significant bit (LSB) of the microprocessor, 1/2 LSB. The

---

<sup>1</sup> Other techniques of converting analog signal to digital words include integration, counting, and parallel conversion.

A/D converter used in this project had 12 bits and the input signal was scaled to  $\pm 10$  volts so the resolution was 0.004883 volts or  $\pm 0.002441$  volts using a successive approximation scheme. Figure 2-2 is an illustration of a three bit A/D conversion using a successive approximation scheme. Notice how the analog input voltage (7.0 volts) is compared to the reference voltage. The first guess is at half the full scale. Since the input is greater than half the full scale, 5 volts, a  $1_{\text{binary}}$  is written in the most significant bit. The output register would read  $100_{\text{binary}}$ . The next approximation is half the difference between the last approximation and full scale, 7.5 volts. This is greater than the actual so a  $0_{\text{binary}}$  is written, so the output register remains  $100_{\text{binary}}$ . The last approximation splits the difference to 6.25 volts and compares this voltage to the input. Since it is less than the analog signal, a  $1_{\text{binary}}$  is written and the output register reads  $101_{\text{binary}}$  or 6.25 volts.

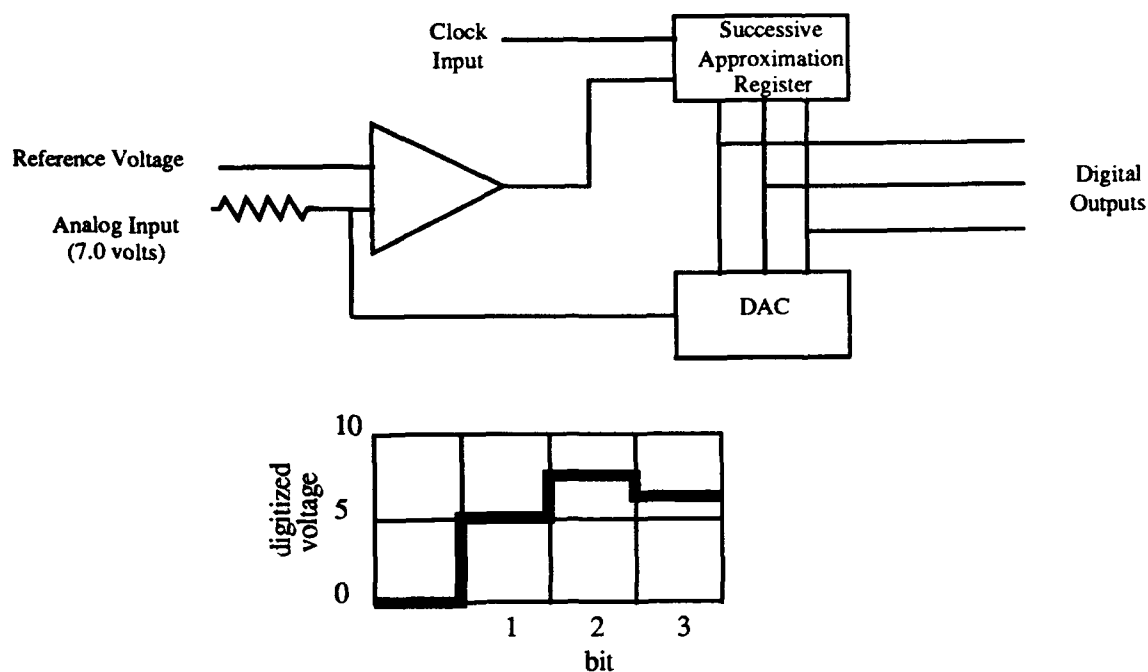


Figure 2-2. Example of a 3-bit ADC.

Notice how the digitized voltage of 6.25 volts differs from the actual analog voltage of 7.0 volts. This is due to the number of bits of resolution. The resolution of a three bit DAC is 1.25 volts so the range of the analog voltage which is digitized to 6.25 volts is from 5.0 to 7.5 volts.

A digital to analog converter performs essentially the reverse operation however the digital word produces a single analog output whereas the analog input can have a range (depending upon the resolution) of values but only a single digital word results.



## B. THE MATH MODEL

At the core of the simulation project is the math model which is simply the collection of equations which describe in a physical sense the aircraft and its interaction or movement within a three dimensional environment. These equations are coupled with circular logic (feedback) where the outputs of one are the inputs for another, the output of which effects the original. Figure 2-3 is a conceptual representation of the math model incorporated in the GAT-1B flight simulator.

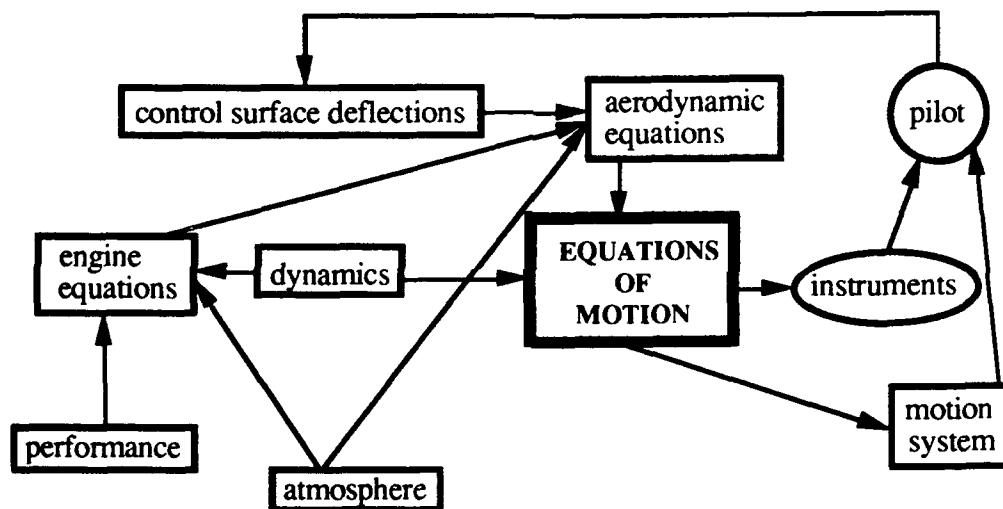


Figure 2-3. A General Math Model

The function of the math model is identical whether it is constructed in an analog manner using resistors, capacitors, FETs<sup>2</sup> and operational amplifiers or software based upon using a digital representation.

---

<sup>2</sup> Field Effect Transistors

The Link GAT-1B™ has specific aircraft parameters (i.e the math model) hard wired into its circuit boards. In order to change the aircraft parameters to modify the simulators handling characteristics, the appropriate analog circuit boards must be identified, the precise component located and then replaced by another which modifies the circuit to respond appropriately. This difficult and time consuming task can be greatly eased by using a general purpose digital computer to perform the necessary calculations. The analog signals are fed into the digital computer where these values are used as the inputs to the preprogrammed aircraft equations. Rates are computed and the digital output is then converted to an analog signal and returned to the analog simulator circuit boards on the GAT-1B™.

The focus of this project was to take a 16 element analog input vector to the flight attitude control card and perform the integration in a digital computer then put the signal back into the circuit. Therefore, in the grand scheme of the full math model for the simulator, this project only manipulated the Euler angle equations of motion shown in bold capital letters in the center of the math model, Figure 2-3.

These equations of motion however, determine the trajectory of the aircraft. In order to gain an appreciation for the approach the GAT-1B flight simulator uses to replicate aircraft motion, attitude and position with its analog circuitry, a derivation of the Euler angle equations is presented.

### **C. EULER ANGLE EQUATIONS OF POSITION DEVELOPED**

Knowing the orientation of the aircraft with respect to the reference frame of the observer, the inertial reference frame, is most useful. An elegant method

of determining the aircraft orientation with respect to a fixed reference frame is to translate the inertial reference frame in a specific order (yaw, pitch, then roll) to align with the aircraft reference frame. The three rotations yield a resultant vector which describes the orientation of the aircraft with respect to the inertial frame of reference. The rotation angles are commonly referred to as Euler angles. A detailed derivation can be found in flight dynamics texts by Etkin, Nelson, or Roskam. The following discussion develops this result using a combination of the approaches taken in the aforementioned texts.

The quintessential governing equation describing aircraft dynamics is simply Newton's Second Law conserving both linear and angular momentum. The following relations must hold:

$$\text{applied forces} = \Delta \text{ linear momentum} \quad (2-1)$$

$$\sum \vec{F} = \frac{d}{dt} m \vec{v}$$

$$\text{applied moments} = \Delta \text{ angular momentum} \quad (2-2)$$

$$\sum \vec{M} = \frac{d}{dt} \vec{H}$$

Before proceeding further, Figure 2-4 defines the coordinate reference system to be used. The x, y, and z axes define the inertial earth fixed nonrotating reference frame and  $x_A$ ,  $y_A$ , and  $z_A$  define the aircraft fixed rotating reference frame. L, M, and N represent the rolling, pitching, and yawing

moments.  $P$ ,  $Q$ , and  $R$  represent the rolling, pitching, and yawing velocities.  $U$ ,  $V$ , and  $W$  represent the components of the aircraft velocity relative to the aircraft center of mass. Lastly,  $X$ ,  $Y$ , and  $Z$  represent the components of the resultant aerodynamic forces.

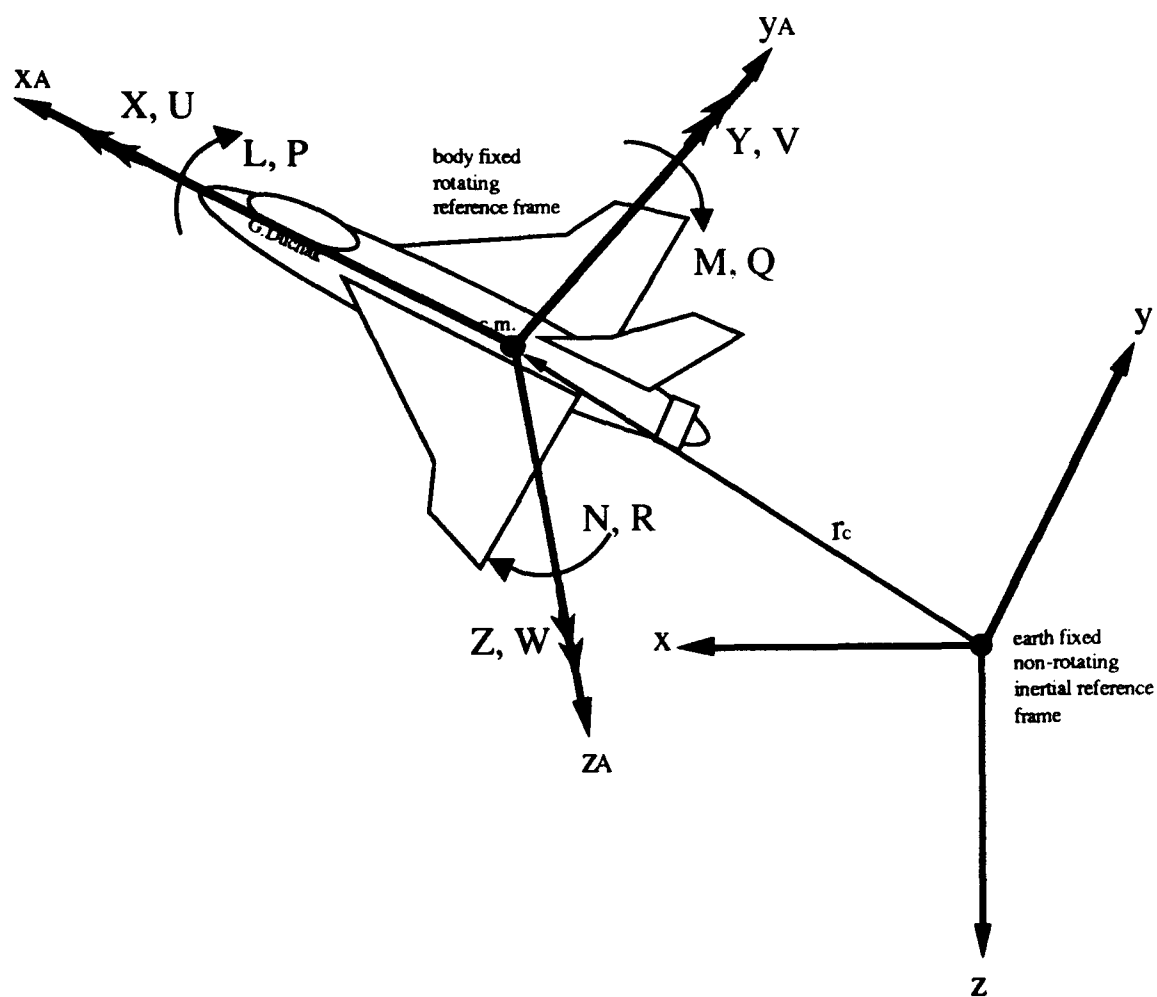


Figure 2-4. Reference System.

For a differential element of mass of an aircraft,  $\delta m$  where  $\mathbf{v}$  is the velocity of the elemental mass relative to the inertial reference frame then,

(2-3)

$$\delta \vec{F} = \delta m \frac{d\vec{v}}{dt}$$

The total external force on the aircraft would be the summation of the elemental forces,

(2-4)

$$\Sigma \delta \vec{F} = \vec{F}$$

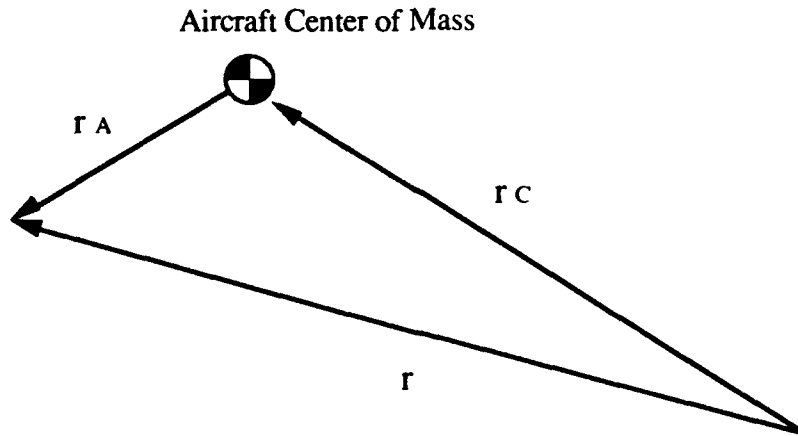


Figure 2-5. Position vectors.

In the above figure,  $\mathbf{r}_A$  is the vector from the aircraft center of mass to the differential element of mass,  $\mathbf{r}_C$  is the vector from an inertial reference frame to the aircraft center of mass, and  $\mathbf{r}$  is the vector from the inertial reference frame to the differential element of mass. The vector  $\mathbf{r}$  can be represented as,

(2-4)

$$\vec{r} = \vec{r}_C + \vec{r}_A$$

The time rate derivative of the position vector is then,

(2-5)

$$\frac{d\vec{r}}{dt} = \frac{d\vec{r}_C}{dt} + \frac{d\vec{r}_A}{dt}$$

so the velocity of the differential element of mass,  $\delta m$ , can be represented as,

(2-6)

$$\vec{v} = \vec{v}_C + \frac{d\vec{r}_A}{dt}$$

If  $\vec{v}$  is substituted into equation (2-1), Newton's Second Law becomes,

(2-7)

$$\sum \delta \vec{F} = \vec{F} = \frac{d}{dt} m \vec{v} = \sum \frac{d}{dt} \left( \vec{v}_C + \frac{d\vec{r}_A}{dt} \right) \delta m$$

It can be safely assumed that the aircraft's mass and distribution of mass are constant over small time intervals. The derivative of the momentum becomes,

(2-8)

$$\frac{d}{dt} (m \vec{v}_C) = m \frac{d\vec{v}_C}{dt} + \vec{v}_C \frac{dm}{dt}$$

but it is assumed that,

(2-9)

$$\frac{dm}{dt} = 0$$

so,

(2-10)

$$\frac{d}{dt}(m\vec{v}_C) = m\frac{d\vec{v}_C}{dt}$$

Since the mass is assumed constant, equation (7) can be rewritten as

(2-11)

$$\vec{F} = m\frac{d\vec{v}_C}{dt} + \frac{d}{dt}\sum \frac{d\vec{r}_A}{dt} \delta m$$

(2-12)

$$\vec{F} = m\frac{d\vec{v}_C}{dt} + \frac{d^2}{dt^2}\sum \vec{r}_A \delta m$$

If  $\vec{r}$  is measured from the center of mass then by definition,

(2-13)

$$\sum \vec{r} \delta m = 0$$

So the force equation becomes

(2-14)

$$\vec{F} = m\frac{d\vec{v}_C}{dt}$$

The force vector can be represented as the sum of the gravity, aerodynamic, and thrust vectors so,

(2-15)

$$\sum \vec{F} = m\vec{g} + \vec{F}_A + \vec{F}_T$$

Which is equivalent to,

(2-16)

$$m \frac{d\vec{v}_C}{dt} = m\vec{g} + \vec{F}_A + \vec{F}_T$$

Equation (2-16) simply says that time rate of change of the linear momentum is equal to the sum of the externally applied forces on the aircraft.

Equation (2-2) can be developed to arrive at a similar result but in terms of angular momentum. In an inertial reference frame, the angular momentum about a point is defined as the sum of the moments of the linear momenta about that point. That is, angular momentum is the moment of the momenta.

(2-17)

$$\vec{H} = \sum_{i=1}^N (\vec{r}_i \times m_i \vec{v}_i)$$

Equation (2-2) can be rewritten for a differential mass as,

(2-18)

$$\delta \vec{M} = \frac{d}{dt} \delta \vec{H} = \frac{d}{dt} (\vec{r}_A \times \vec{v}) \delta m$$



If the velocity of the differential element of mass is expressed in terms of the velocity of the center of mass and the relative velocity of the center of differential element mass to the aircraft center of mass then,

(2-19)

$$\vec{v} = \vec{v}_C + \frac{d\vec{r}_A}{dt} = \vec{v}_C + \vec{\omega} \times \vec{r}_A$$

The total angular momentum can then be expressed as,

(2-20)

$$\vec{H} = \sum \delta \vec{H} = \sum (\vec{r}_A \times \vec{v}_C) \delta m + \sum [\vec{r}_A \times (\vec{\omega} \times \vec{r}_A)] \delta m$$

Since the vector  $\vec{r}_A$  is measured from the center of mass, the velocity of the center of mass,  $\vec{v}_C$ , is constant with respect to the summation so,

(2-21)

$$\vec{H} = \sum \vec{r}_A \delta m \times \vec{v}_C + \sum [\vec{r}_A \times (\vec{\omega} \times \vec{r}_A)] \delta m$$

By equation (2-13) the first summation term is zero by definition so the angular momentum becomes,

(2-22)

$$\vec{H} = \sum [\vec{r}_A \times (\vec{\omega} \times \vec{r}_A)] \delta m$$

The total angular velocity of the aircraft can be represented by its component velocities.

(2-23)

$$\vec{\omega} = P\vec{i} + Q\vec{j} + R\vec{k}$$

The position vector  $\vec{r}$  (refer to Figure 3-4) can likewise be represented by its components as,

(2-24)

$$\vec{r} = x\vec{i} + y\vec{j} + z\vec{k}$$

Expanding equation (2-22) by applying the vector triple product rule (Etkin, 1982, p. 297),

(2-25)

$$\vec{A} \times (\vec{B} \times \vec{C}) = \vec{B} (\vec{A} \cdot \vec{C}) - \vec{C} (\vec{A} \cdot \vec{B})$$

(2-26)

$$\vec{r}_A \times (\vec{\omega} \times \vec{r}_A) = \vec{\omega} (\vec{r}_A \cdot \vec{r}_A) - \vec{r}_A (\vec{\omega} \cdot \vec{r}_A)$$

The angular momentum becomes,

(2-27)

$$\vec{H} = \sum \left[ \vec{\omega} r_A^2 - \vec{r}_A (\vec{\omega} \cdot \vec{r}_A) \right] \delta m$$

Expanding equation (2-27) gives,

(2-28)

$$\begin{aligned}\vec{H} = & \sum \left[ (\vec{P}\hat{i} + \vec{Q}\hat{j} + \vec{R}\hat{k}) \left| x\hat{i} + y\hat{j} + z\hat{k} \right|^2 \right] \delta m \\ & - \sum \left\{ (x\hat{i} + y\hat{j} + z\hat{k}) \left[ (\vec{P}\hat{i} + \vec{Q}\hat{j} + \vec{R}\hat{k}) \cdot (x\hat{i} + y\hat{j} + z\hat{k}) \right] \right\} \delta m\end{aligned}$$

Rearranging and regrouping terms of equation (2-28) gives,

$$\vec{H} = (\vec{P}\hat{i} + \vec{Q}\hat{j} + \vec{R}\hat{k}) \sum (x^2 + y^2 + z^2) \delta m + \sum (x\hat{i} + y\hat{j} + z\hat{k}) (Px + Qy + Rz) \delta m \quad (2-29)$$

$$\vec{H} = \vec{\omega} \sum (x^2 + y^2 + z^2) \delta m + \sum \vec{r}_A (Px + Qy + Rz) \delta m$$

Rewriting equation (2-29) in terms of its components gives,

(2-30)

$$H_x = P \sum (y^2 + z^2) \delta m - Q \sum xy \delta m - R \sum xz \delta m$$

(2-31)

$$H_y = -P \sum xy \delta m + Q \sum (x^2 + z^2) \delta m - R \sum yz \delta m$$

(2-32)

$$H_z = -P \sum xz \delta m - Q \sum yz \delta m + R \sum (x^2 + y^2) \delta m$$

By definition, the mass moments and products of inertia for the aircraft are;

(2-33)

$$I_{xy} = \sum xy \delta m$$

(2-34)

$$I_{xz} = \sum xz \delta m$$

(2-35)

$$I_{yz} = \sum yz \delta m$$

(2-36)

$$I_x = \sum (y^2 + z^2) \delta m$$

(2-37)

$$I_y = \sum (x^2 + z^2) \delta m$$

(2-38)

$$I_z = \sum (x^2 + y^2) \delta m$$

Substituting the definitions, equations (2-33) through (2-38) into the equations for the components of the angular momentum, equations (2-30) to (2-32) gives,

(2-39)

$$H_x = PI_x - QI_{xy} - RI_{xy}$$

(2-40)

$$H_y = -PI_{xy} + QI_y - RI_{yz}$$

(2-41)

$$H_z = -PI_{xz} - QI_{yz} + RI_z$$

Since the moments and products of inertia were determined for a fixed reference frame, they will vary as the aircraft rotates. To avoid this problem and allow the moments and products of inertia to remain constant, the reference system is fixed to the aircraft and moves as the aircraft moves. This constraint however requires that the derivatives of the velocity and angular momentum be determined in the rotating frame of reference.

Applying the rules for the derivative of a vector (Etkin, p. 298) it can be shown that,

(2-42)

$$\frac{d\vec{A}}{dt}_{\text{inertial}} = \frac{d\vec{A}}{dt}_{\text{aircraft}} + \vec{\omega} \times \vec{A}$$

where

(2-43)

$$\frac{d\vec{A}}{dt}_{\text{aircraft}} = \frac{dA_x}{dt} \vec{i} + \frac{dA_y}{dt} \vec{j} + \frac{dA_z}{dt} \vec{k}$$

If the property illustrated by equation (2-42) is applied to equations (2-1) and (2-2) then Newton's laws for the conservation of linear and angular momenta become,

(2-44)

$$\vec{F} = m \frac{d\vec{v}_C}{dt}_{\text{aircraft}} + m(\vec{\omega} \times \vec{v}_C)$$

(2-45)

$$\vec{M} = \frac{d\vec{H}}{dt}_{\text{aircraft}} + \vec{\omega} \times \vec{H}$$

In component form, equations (2-44) and (2-45) become,

$$F_x = m(\dot{U} + QW - RV) \quad (2-46)$$

$$F_y = m(\dot{V} + RU - PW) \quad (2-47)$$

$$F_z = m(\dot{W} + PV - QU) \quad (2-48)$$

$$L = \dot{H}_x + QH_z - RH_y \quad (2-49)$$

$$M = \dot{H}_y + RH_x - PH_z \quad (2-50)$$

$$N = \dot{H}_z + PH_y - QH_x \quad (2-51)$$

Note that the force components  $F_x$ ,  $F_y$ , and  $F_z$  of equations (2-46), (2-47) and (2-48) are total forces which include aerodynamic, thrust, and gravity forces as shown in equation (2-16). The gravity component however, depends upon the orientation of the aircraft with respect to the inertial reference frame.

Assuming symmetry about the x-z plane of the aircraft so the cross products of inertia  $I_{xy}$  and  $I_{yz} = 0$ , then the moment equations become,

(2-52)

$$L = I_x \dot{P} - I_{xz} \dot{R} + QR(I_z - I_y) - I_{xz} PQ$$

(2-53)

$$M = I_y \dot{Q} + RP(I_x - I_z) + I_{xz}(P^2 - R^2)$$

(2-54)

$$N = -I_{xz} \dot{P} + I_z \dot{R} + PQ(I_y - I_x) - I_{xz} QR$$

The forces and moments in equations (2-46) to (2-48) and (2-52) to (2-54) have been defined as functions of the variables  $P, Q, R, U, V,$  and  $W$ .

It is desired to know the orientation of the aircraft relative to a non-rotating, inertial, earth fixed reference system so orientation of the aircraft fixed reference system is describe relative to earth fixed coordinate system. At time  $t = 0$  the two reference systems will be co-located. As time passes, the two systems and their relative orientations with respect to each other will change.

In order to determine the relationship of the aircraft fixed system to the earth fixed reference frame, the two systems are superimposed upon one another. The relative orientation is then described by means of three consecutive rotations. The order in which these rotations is carried out is important. These angular rotations are commonly referred to as Euler angles. Quoting Euler, (Halfman, p183, 1962)

“Any number of rotations about different axes through a point must in the end remain equivalent to a single rotation”.

Figure 2-6 shows the Euler angles for the prescribed order of rotation. The Euler angles are  $\psi$  for azimuth angle,  $\theta$  for pitch angle, and  $\phi$  for bank angle.

Rotate the fixed reference frame through an angle  $\psi$ , then rotate through an angle  $\theta$  and lastly rotate through an angle  $\phi$ .

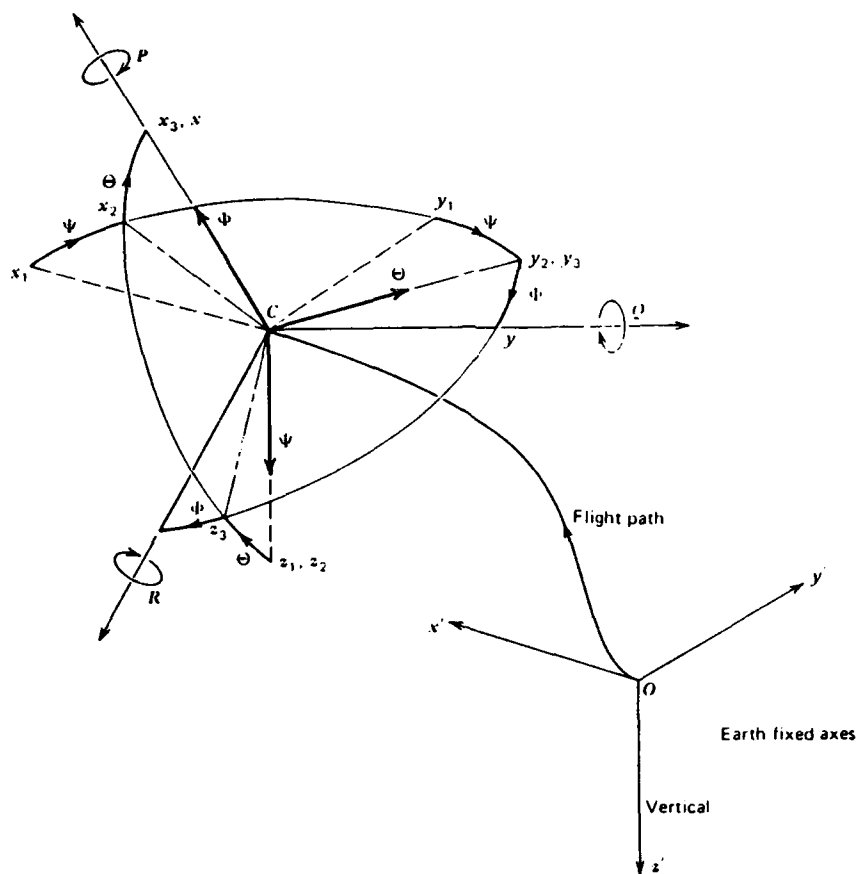


Figure 2-6. Euler Angle Rotations (Etkin, 1982, p. 89)



Knowing the flight velocity components relative to the fixed reference frame, the flight path of the aircraft can be determined. Referring to figure 2-4, the velocities U, V, and W in the aircraft (rotating)  $x_A$ ,  $y_A$ , and  $z_A$  reference frame must be related to the inertial x, y, and z reference frame. Letting

(2-55)

$$\frac{dx}{dt} = u_1$$

(2-56)

$$\frac{dy}{dt} = v_1$$

(2-57)

$$\frac{dz}{dt} = w_1$$

and applying the orthogonal transformation which relates the rotation,  $\psi$  from the fixed reference frame to the first intermediate coordinate system,  $x_1$ ,  $y_1$ , and  $z_1$ ,

(2-58)

$$\begin{pmatrix} u_1 \\ v_1 \\ w_1 \end{pmatrix} = \begin{bmatrix} \cos \psi & -\sin \psi & 0 \\ \sin \psi & \cos \psi & 0 \\ 0 & 0 & 1 \end{bmatrix} \begin{pmatrix} u_2 \\ v_2 \\ w_2 \end{pmatrix}$$

then applying the  $\theta$  rotation,

(2-59)

$$\begin{pmatrix} u_2 \\ v_2 \\ w_2 \end{pmatrix} = \begin{bmatrix} \cos \theta & 0 & \sin \theta \\ 0 & 1 & 0 \\ -\sin \theta & 0 & \cos \theta \end{bmatrix} \begin{pmatrix} u_3 \\ v_3 \\ w_3 \end{pmatrix}$$

and lastly applying the  $\phi$  rotation gives,

(2-60)

$$\begin{pmatrix} u_3 \\ v_3 \\ w_3 \end{pmatrix} = \begin{bmatrix} 1 & 0 & 0 \\ 0 & \cos \phi & -\sin \phi \\ 0 & \sin \phi & \cos \phi \end{bmatrix} \begin{pmatrix} U \\ V \\ W \end{pmatrix}$$

Successive substitution of equations (2-60) and (2-59) into (2-58) yields,

(2-61)

$$\begin{pmatrix} u_1 \\ v_1 \\ w_1 \end{pmatrix} = \begin{pmatrix} \dot{x} \\ \dot{y} \\ \dot{z} \end{pmatrix} = \begin{bmatrix} \cos \psi & -\sin \psi & 0 \\ \sin \psi & \cos \psi & 0 \\ 0 & 0 & 1 \end{bmatrix} \begin{bmatrix} \cos \theta & 0 & \sin \theta \\ 0 & 1 & 0 \\ -\sin \theta & 0 & \cos \theta \end{bmatrix} \begin{bmatrix} 1 & 0 & 0 \\ 0 & \cos \phi & -\sin \phi \\ 0 & \sin \phi & \cos \phi \end{bmatrix} \begin{pmatrix} U \\ V \\ W \end{pmatrix}$$

Performing the multiplication gives,

(2-62)

$$\begin{pmatrix} \dot{x} \\ \dot{y} \\ \dot{z} \end{pmatrix} = \begin{bmatrix} \cos \theta \cos \psi & \sin \phi \sin \theta \cos \psi - \cos \phi \sin \psi & \cos \phi \sin \theta \cos \psi - \sin \phi \sin \psi \\ \cos \theta \sin \psi & \sin \phi \sin \theta \sin \psi - \cos \phi \cos \psi & \cos \phi \sin \theta \sin \psi - \sin \phi \cos \psi \\ -\sin \theta & \sin \phi \cos \theta & \cos \phi \cos \theta \end{bmatrix} \begin{pmatrix} U \\ V \\ W \end{pmatrix}$$

Equation (2-62) relates the velocity components in an inertial fixed reference frame system,  $x$ ,  $y$ , and  $z$  to the velocity components in the rotating aircraft fixed reference system,  $x_A$ ,  $y_A$ , and  $z_A$ .

A relationship between the time rate derivatives of the Euler angle and the rotational velocity components, P, Q, and R is necessary.

Recalling equation (2-23) that total rotational velocity is the sum of the component velocities, then,

(2-63)

$$\vec{\omega} = P\vec{i} + Q\vec{j} + R\vec{k}$$

Equation (2-63) must, according to Euler, also be equal to

(2-64)

$$\vec{\omega} = \vec{\psi} + \vec{\theta} + \vec{\phi}$$

Since the order of the rotations is  $\psi$ ,  $\theta$ , then  $\phi$ , from Figure 2-6 it can be seen that,

(2-65)

$$\vec{\psi} = k_3\dot{\psi} = k_2\dot{\psi} \text{ for rotation about the } z_1 \text{ axis}$$

(2-66)

$$\vec{\theta} = j_2\dot{\theta} = j_3\dot{\theta} \text{ for rotation about the } y_2 \text{ axis}$$

(2-67)

$$\vec{\phi} = i_3\dot{\phi} = i_1\dot{\phi} \text{ for rotation about the } x_3 \text{ axis}$$

Substituting equations (2-65), (2-66), and 2-(67) into the expression for  $\omega$ , equation (2-64) becomes,

(2-68)

$$\vec{\omega} = k_2 \dot{\psi} + j_3 \dot{\theta} + i \dot{\phi}$$

Projecting the components of  $\omega$  onto the body fixed coordinate system,  $x_A$ ,  $y_A$ , and  $z_A$  fixed at the body's center of mass then, the angular velocities in the aircraft reference frame are,

(2-69)

$$P = \dot{\phi} - \dot{\psi} \sin \theta$$

(2-70)

$$Q = \dot{\theta} \cos \phi + \dot{\psi} \cos \theta \sin \phi$$

(2-71)

$$R = \dot{\psi} \cos \theta \cos \phi - \dot{\theta} \sin \phi$$

Solving equations (2-69), (2-70), and (2-71) for the Euler angle rates  $d\phi/dt$ ,  $d\theta/dt$ , and  $d\psi/dt$ ,

(2-72)

$$\dot{\phi} = P + Q \sin \phi \tan \theta + R \cos \phi \tan \theta$$

(2-73)

$$\dot{\theta} = Q \cos\phi - R \sin\phi$$

(2-74)

$$\dot{\psi} = (Q \sin\phi + R \cos\phi) \sec\theta$$

and integrating equations (2-72), (2-73), and (2-74) gives,

(2-75)

$$\phi = \int_0^t (P + Q \sin\phi \tan\theta + R \cos\phi \tan\theta) dt$$

(2-76)

$$\theta = \int_0^t (Q \cos\phi - R \sin\phi) dt$$

(2-77)

$$\psi = \int_0^t [(Q \sin\phi + R \cos\phi) \sec\theta] dt$$

For small angles of pitch, like those observed in the GAT-1B flight simulator,  $\sec\theta \approx 1$ .

Equation (2-75) can be factored as  $P + (Q \sin\phi + R \cos\phi) \sec\theta \sin\theta$ . This is identically equal to  $(d\psi/dt) \sin\theta$ . The approximation effects  $d\psi/dt$  directly and therefore  $d\phi/dt$  indirectly. Note that digitally these approximations do not have to be made. Equations (2-75), (2-76) and (2-77) can be rewritten as,

(2-78)

$$\dot{\phi} = P + \dot{\psi} \sin \theta$$

(2-79)

$$\dot{\theta} = Q \cos \phi - R \sin \phi$$

(2-80)

$$\dot{\psi} = Q \sin \phi + R \cos \phi$$

Equations (2-78), (2-79), and (2-80) are the Euler rates if small pitch angle is presumed. A 10 degree pitch angle introduces an error of only 1.5% in  $\sec \theta$ .

The preceding discussion illustrated how the Euler angles were formed in order to determine the orientation and position of the aircraft with respect to a fixed reference frame.

The GAT-1B replicates and solves the Euler angle equations (2-78), (2-79), and (2-80) using electrical and electromechanical devices. The motion of the simulator is driven by the  $\phi$ ,  $\theta$ , and  $\psi$  angle equations. It is important to understand the method of computation when examining the analog circuitry to determine how motion is computed and achieved by the GAT-1B flight simulator.

The Link referenced documentation for the GAT-1B purports the rate equations created in analog hardware to be as shown in equations (2-81), (2-82), and (2-83). The rate equations determined from inspection of the analog attitude board, J22, on the simulator were somewhat different. Equations (4-2), (4-3),

and (4-4) were the ones actually implemented in software. These will be discussed in Chapter IV.

(2-81)

$$P_A = 338 \int \left[ \begin{aligned} & q \left( -0.00177 \beta - 0.0260 \delta_a + 0.0148 \right) \\ & + v_{ind} \left( 0.057 \times 10^{-3} R_A - 0.084 \times 10^{-3} P_A \right) \\ & - 0.223 \times 10^{-3} T_N - \left( 5.53 \sin \phi + 0.0205 P_A \right) WOG \end{aligned} \right] dt$$

(2-82)

$$Q_A = 37.7 \int \left[ \begin{aligned} & q \left( \begin{aligned} & -0.3 \delta_e - 0.00288 - 0.314 C_L - 0.55 \delta_{stall} \\ & - 0.0183 \delta_{FW} + 0.0933 \times 10^{-3} T_N + 0.31 \delta_{trim} \end{aligned} \right) \\ & - 1.62 \times 10^{-3} Q_A v_{ind} + 0.141 \times 10^{-3} T_N - K_{CG} \\ & + \left( -0.402 Q_A - 78 \sin \theta + 3.66 - 1.33 WOG \right) WOG \end{aligned} \right] dt$$

(2-83)

$$R_A = 173 \int \left[ \begin{aligned} & q \left( -0.0292 \delta_r + 0.00131 \beta + 0.00240 C_L \delta_a \right) \\ & - 0.0346 \times 10^{-3} R_A v_{ind} - \left( 0.00575 R_A + 1.2 \delta_r \right) WOG \end{aligned} \right] dt$$

Equations (2-69), (2-70), and (2-71), roll, pitch, and yaw rate equations are modeled by equations (2-81), (2-82), and (2-83). The appropriate summation of moments due to control surface deflections, aerodynamic damping, and aerodynamic attitude changes produce the Euler angle rate equations (2-78), (2-79), and (2-80). These equations are then mechanically integrated by the motion drive motors to obtain the Euler angle positions of the simulator.

Chapter III of this thesis describes in detail the analog signal flow and Chapter IV describes the modifications made to digitally replicate the analog function of the attitude card which contains the circuitry for computing the motion of the aircraft.



### **III. THE HARDWARE AND SOFTWARE**

The primary criteria used to select the hardware and software used for this project was availability and cost. The hardware used to capture the analog signal vector, digitize and process the vector, and reconvert it to an analog signal came from inventory or surplus supply. Ancillary circuits were built from miscellaneous hardware.

Bill Lawton (607-648-6125)<sup>1</sup>, a leading and possibly only expert on the Link GAT-1B™ simulator, said that Singer had designed and built a digital conversion kit for the GAT-1B which removed all analog cards, except the motion amplifier cards. The conversion kit had an estimated cost of \$70,000.

#### **A. GAT-1B™ SYSTEM DESCRIPTION**

The Link references can be consulted for a more comprehensive description of the total system. Although more comprehensive, the accuracy is questionable. Examination of the applicable portions of the Link manuals revealed several errors. The description contained herein accurately reflects the configuration of the portions of the flight simulator modeled.

The Link General Aviation Trainer, GAT-1B™, is a motion based analog single engine aircraft simulator. This electromechanical device was developed by the Link Division of Singer during the early 1960's to provide general aviation flight instrument training. It was the first in a series of trainers designed to train both prospective and experienced pilots to fly-single reciprocating engine type aircraft. The actual cockpit instrument arrangement is

---

<sup>1</sup> The author spoke with Bill Lawton in August 1989.

generic and replicates no particular aircraft but is representative of basic single engine aircraft. Instruments and controls include:

- ignition switch
- master switch
- throttle control
- mixture control
- carburetor heat control
- yoke
- rudder peddles
- flap switch
- elevator trim wheel with position indicator
- parking brake
- engine RPM indicator
- airspeed indicator
- altitude indicator
- attitude indicator
- rate of climb indicator
- turn and slip indicator
- directional gyro
- fuel quantity gages (left and right)
- cylinder head temperature gages
- engine oil pressure gage
- engine oil temperature gage

The actual physical dimensions are:

height	80.0 in
fuselage width	35.5 in
wingspan	139.0 in
length	137.0 in
turning radius	91.0 in
weight	1300.0 lbs

The simulator can physically roll 12.5 degrees left and right, pitch 16 degrees up, 8 degrees down, and yaw 360 degrees. The instruments in the cockpit indicate  $\pm 75$  degrees for roll, +48 degrees to -24 degrees for pitch, and 360 degrees for yaw. Motion is achieved through a system of gears and cables driven by electrical motors. The fundamental operation is the development of actual attitude information by solving the Euler rate equations to determine  $\phi$ ,  $\theta$ , or  $\psi$ .

Recall from the math model description (Figure 2-3) that many factors influence the aircraft motion. These factors are modeled on 10 analog circuit boards within the GAT-1B™. They are:

<u>Board Designation No.<sup>2</sup></u>	<u>Function of Board</u>
J15	Rough Air Generator
J16	Sound Generator
J18	Engine
J19	Altitude
J20	Wind
J21	Time Division Multiplier
J22	Attitude
J23	Pitch Power Amplifier
J24	Roll Power Amplifier
J25	Yaw Power Amplifier

A portion of the attitude board, J22, was replicated in software.

### **1. Attitude Card**

The function of the attitude card is to provide the appropriate voltages to the motion drive motors. The drive motors roll, pitch, and yaw the simulator in response to pilot actions.

In the most basic sense, the inputs which create a moment on the aircraft and produce a change in the acceleration about an aircraft axis are summed and then added to components of other forces effecting these moments, forming the rate equations. This was done digitally by replicating in software the hardware found on analog card J21.

The three systems contained on the analog attitude control card are roll rate and bank motion, pitch rate and pitch motion, and yaw rate and heading motion. While they are similar in the design, they each have certain nuances which had to be deciphered before any software replication of the circuit could

---

<sup>2</sup> The board designation number refers to the method of identifying the board on a circuit schematic.

take place. A somewhat time consuming endeavor was the deciphering of the schematics for the roll rate, pitch rate, yaw rate, and timing circuitry.

Each circuit will be explained in detail in order to better understand some of the finer points of this project.

***a. Some Preliminaries***

The rate circuitry has two modes of operation depending on whether the simulated aircraft is airborne or on the ground. All three circuits behave similarly but certain differences exist. For the following discussions of these circuits refer to the schematics, Figures 3-4, 3-6, and 3-8. Figures 3-3, 3-5, and 3-7 are simplified block diagrams of the roll, pitch, and yaw rate systems. A Weight on Wheels (WOG) switch modifies the analog circuit to respond differently for airborne or on the ground motion.

In each circuit a number of field effect transistors, FETs, are used simply as electronic switches. The schematics label these FETs as Q1, Q2, Q3...Q# and they appear as shown in Figure 3-1.

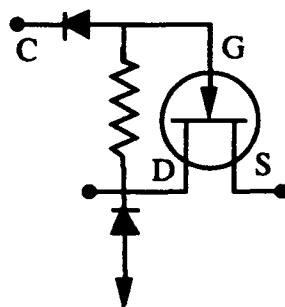


**Figure 3-1. N-type Channel FET.**

All the FETs used are N-channel type. When a positive 15 volts is applied to terminal C, the FET is on and acts to complete the connection allowing current to flow from the drain, D to the source, S. As the voltage goes more negative, the current flow through the FET is reduced effectively to zero. For example, the WOG FET(Q15 in Figure 3-6) voltage is either +15 volts if on the ground or -15 volts if airborne. This has the effect of making the switch either on (current flowing through from D to S) or off (opening the circuit). The other FETs used for the time division multiply function similarly but they are switched on and off at a rate equal to the time divided input signal to the gate.

It may be helpful to think of the FET as a voltage controlled variable resistor. The current through a FET obeys the relation shown in equation 3-1

(3-1)

$$I_D = \frac{V_{DS}}{R}$$

Figure 3-2 is a representation of the pin connections located on the back (port) side of the analog mother board in the aft section of the flight simulator. Ten analog circuit cards slide into this mother board. The numbers reflect the pin configuration printed on the analog circuit boards. The signals necessary for computation were extracted from the mother board rather than soldering any connections directly to the analog board.

Y bar	43
X bar	42
W bar	41
V bar	40
U bar	39
T bar	38
S bar	37
R bar	36
P bar	35
N bar	34
M bar	33
L bar	32
K bar	31
J bar	30
H bar	29
F bar	28
E bar	27
D bar	26
C bar	25
B bar	24
A bar	23
Z	22
Y	21
X	20
W	19
V	18
U	17
T	16
S	15
R	14
P	13
N	12
M	11
L	10
K	9
J	8
H	7
F	6
E	5
D	4
C	3
B	2
A	1

Figure 3-2. Pin Connections for Analog Mother Board.

### b. Roll Circuitry Described

Figure 3-3 is a simplified block diagram of the roll rate circuitry as it would operate airborne.

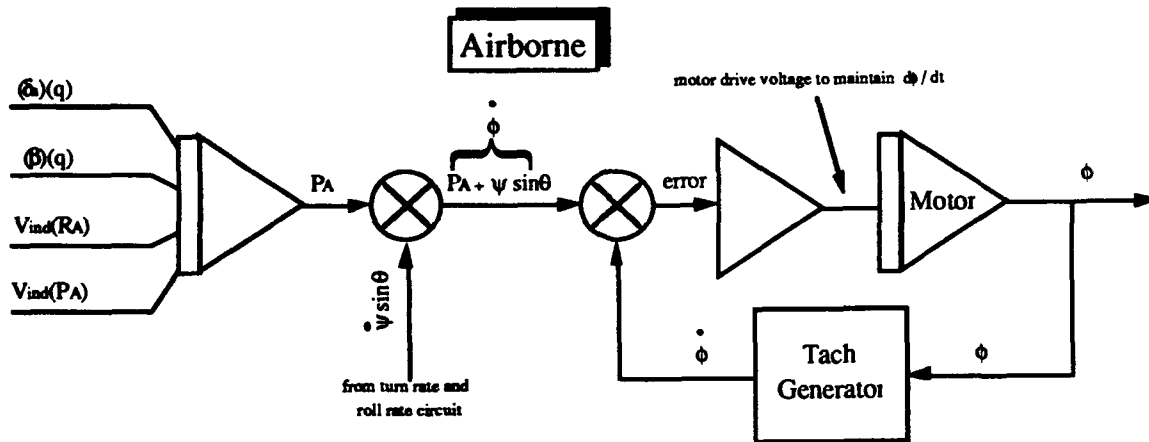


Figure 3-3. Roll Rate Block Diagram.

Rolling moments created by aileron deflection,  $\delta_a$  and sideslip,  $\beta$  are multiplied by the dynamic pressure,  $q$ . Turn rate,  $R_A$  and roll rate,  $P_A$  are multiplied by indicated velocity,  $V_{ind}$ . These moment creating inputs are then summed to produce roll acceleration which is then integrated to produce roll rate,  $P_A$ . The product of heading rate (from the turn rate circuit) times the sine of the pitch angle (from the pitch rate circuit) is then summed with  $P_A$ . The result is the bank motion rate,  $d\phi/dt$ .

For example, in straight and level flight the pitch angle is zero. The roll angle rate becomes simply a function of roll rate alone. If the pitch angle is



90 degrees then the roll angle rate is the sum of the pitch rate and the turning angle rate.

The voltage representing the bank motion rate is sent through a differential amplifier then to drive the motor. The motor mechanically integrates the bank motion rate to get position. The position is fed back through a tach<sup>3</sup> generator where position rate from the tach generator is then compared to the requested rate. If they are different, an error signal is produced. This error signal modifies the voltage through the differential amplifier which in turn modifies the motor turning rate. The purpose of the tach generator feedback is to ensure the rate commanded equals the rate realized by the motor.

Referring to Figure 3-4, beginning on the left side, the base of the simulator contains a sine-cosine potentiometer which is mechanically connected, through gears and chain pulleys, to the bank motion motor, B2. The voltage out is  $\pm 15$  volts times  $\sin\phi$  and  $\pm 15$  volts times  $\cos\phi$ . The signal,  $\sin\phi$ , enters the attitude card, J22, at pin number 30. This signal is used in two places; a roll motion limiting circuit and a wings leveling circuit.

To electrically limit the roll motion,  $\sin\phi$  goes through the  $100\text{ k}\Omega$ , R18 resistor to operational amplifier, AR3. When the motion is at the limits of  $\pm 75$  degrees cockpit indicated, the output voltage of AR3 is approximately zero. For example, in a maximum bank  $\phi = 75$  degrees. The voltage out of the sine-cosine potentiometer R2 is  $(15)(\sin\phi) = 14.48$  volts dc. This signal enters the bank limiting operational amplifier, AR3 via the  $100$

---

<sup>3</sup> A tach generator is simply a device which measures the speed at which the input changes. In short it differentiates the input. In this application the tach generator is a dc generator.

k $\Omega$  R18 resistor and is balanced by the -15 volt dc reference voltage going through the 100 k $\Omega$  R16 resistor. This has the effect of turning off both FET Q5 and Q6 (depending on if the roll is right or left) since the output from AR3 is -15 volts dc. With FETs Q5 or Q6 off, no signal can pass through to the bank angle motor servo amplifier, AR4. At the same time, the signal goes through zener diodes CR8 and CR9 and resistors R21 and R22. The voltage drops to 5 volts and enters AR4 and causes the simulator to bank in a direction away from the electrical limit. This action prevents damage to the simulator.

The signal,  $\sin\phi$ , also goes through a 24.9 k $\Omega$  resistor, R2 via the WOG, FET Q1. The WOG signal is either +15 volts dc indicating the simulator is on the ground or -15 volts dc indicating airborne. With a +15 volts (on ground) to FET Q1, Q1 is turned on which allows the  $\sin\phi$  signal to enter the summing amplifier AR1. While on the ground, with no velocity,  $q$  and  $V_{ind}$  are both zero, so the only input to AR1 is  $\sin\phi$ . This strong voltage while the simulator is on the ground will overcome any other voltage to AR1. With the feedback loop through the 75 k $\Omega$  resistor R1, wings will be kept level.

When the engine is on and the brakes are released, dynamic pressure increases as airspeed increases. FET Q2 turns on proportional to the increase in dynamic pressure. Moment inputs, aileron deflection,  $\delta_a$  and sideslip  $\beta$ , to Q2 are multiplied by dynamic pressure and summed. Additionally, roll rate feedback through the 68 k $\Omega$  resistor R8 and turn rate through the 200 k $\Omega$

resistor R9 are multiplied proportional to the indicated velocity,  $V_{ind}$  by FET Q3. These products are also summed at AR1.

Airborne, operational amplifier AR1, is an integrating amplifier whose output is determined by integrating the control surface and attitude effects. The output is proportional to the rotation rate of the aircraft about the body axes,  $x_A$ . This is the roll rate  $P_A$ . The output of AR1,  $P_A$ , is then summed with the product  $(d\psi/dt)(\sin\theta)$  giving  $d\phi/dt$ .

This signal  $d\phi/dt$  is sent to the bank angle servo amplifier, AR4. The output of this amplifier produces a voltage to the bank drive motor which is necessary to maintain the commanded bank rate  $(d\phi/dt)_c^4$ . The motor physically integrates this rate to obtain a position. However, position rate feedback  $(d\phi/dt)_a$  is sent back to AR4 via a tach generator G2 and a 113 k $\Omega$  resistor R20. Resistor R20 controls the rate at which the motor responds to the commanded input. The actual rate and the commanded rate are both inputs to AR4 and the difference between the two results in a error signal which modifies the voltage signal to the drive motor to maintain the commanded rate.

In short, the Euler angle rate equation  $d\phi/dt$ , is computed and then this rate is sent to bank drive motor in the motion base via the power amplifier board, from pin 10 on the attitude board J22 to position the simulator. The resulting position is the Euler angle  $\phi$ . Feedback from the motor is used to ensure that the commanded rate and the actual rate are equal.

---

<sup>4</sup> The subscript c denotes a commanded rate and the subscript a denotes the actual rate achieved by the motor.



### c. Pitch Circuitry Described

The pitch rate circuitry is very similar to the roll rate circuitry. Figure 3-5 is a simplified block diagram of the pitch rate and motion circuitry. Notice that unlike the roll rate circuit, the pitch rate is multiplied by the cosine component of the roll rate vector which effects the pitch rate.

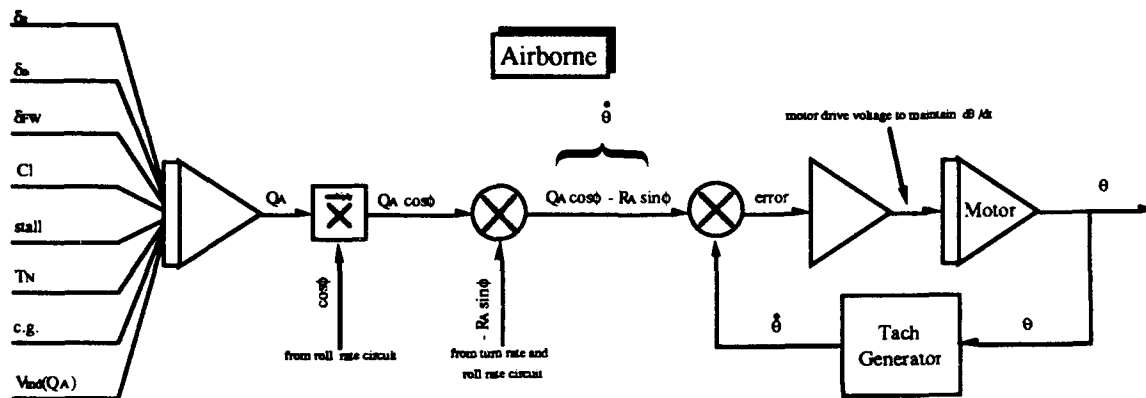


Figure 3-5. Pitch Rate Block Diagram.

The basic function is to take moments which contribute to the overall pitching moment of the aircraft. Summing and integrating these moments gives pitch rate. The pitch rate,  $Q_A$ , is multiplied by the cosine of the roll (bank) angle. Pitch angle is the angle between the aircraft x-axis and the horizon (level) in a ground-fixed reference system. Only the vector component of the roll angle which is perpendicular to the ground is used to determine pitching motion. The result is  $Q_A \cos \phi$ . This result is summed with the effects of the rotation of the nose of the aircraft in a vertical plane due to the turning of

the aircraft about the z-axis,  $R_A \sin \phi$  term, to determine the pitch angle rate,  $d\phi/dt$ .

For example, if the roll angle is zero, as would be the case for straight and level flight, the term  $R_A \sin \phi$  drops out and the pitch angle rate becomes  $Q_A \cos \phi$  or simply  $Q_A$ . That is, in level flight, the pitch angle rate is simply due to the pitch rate. Conversely, for a roll angle of 90 degrees, the cosine term is zero and the pitch rate becomes  $R_A$ . That is, in a 90 degree bank the pitch angle rate is due solely to the turn rate.

The remaining signal flow is identical in all the roll, pitch, and yaw rate circuitry. The signal is sent to a differential operational amplifier then to a power amplifier to drive the pitch motor. The motion is integrated and the Euler pitch angle,  $\theta$  is produced. Feedback is provided to ensure the commanded pitch rate equals the actual pitch rate driven by the motor.

Referring to top left corner of Figure 3-6, the pitching rate schematic,  $\theta$  enters from a sine-cosine potentiometer which is physically connected to the pitch drive motor shaft. The  $\sin \theta$  output signal is sent to the time division multiplier card and then via pin 21 on board J22 through operational amp AR10 where it is reduced by 2/3rds. This signal,  $-\sin \theta$  is sent to three other analog cards, lift, altitude, and attitude indicator, as an input.

$\sin \theta$  is also sent through motion limiting circuitry which prevents the pitch angle from over driving the limits of the trainer. This circuitry was

described in the roll rate circuitry description and is essentially the same for the pitch.

$\sin\theta$  from the sine-cosine potentiometer is also sent through the 4.7 k $\Omega$  resistor, R63 and FET Q15 as part of a  $\sin\theta$  follow up signal for pitch attitude into the summing amplifier AR9. On the ground, +15 volts is applied to the gate of Q15 which turns the FET fully on so the  $\sin\theta$  signal enters AR9. Additionally, while on the ground with no airspeed, the voltage represented by the dynamic pressure  $q$ , into the gate of FET Q16 is zero so Q16 is fully off. None of the moment signals,  $\delta_{\alpha}$ ,  $\delta_e$ ,  $\delta_{FW}$ ,  $C_L$ , or stall can enter AR9. The only inputs are then  $\sin\theta$ , net thrust,  $T_N$ , and center of gravity, c.g. location.

Once brakes are released,  $V_{ind}$  and  $q$  become greater than zero. Inputs from the moment signals,  $\delta_{\alpha}$ ,  $\delta_e$ ,  $\delta_{FW}$ ,  $C_L$ , and stall, and pitch rate feedback are now summed by AR9 since FET Q16 now turns on and off proportional to the dynamic pressure. Additionally, since the weight may not necessarily be on the ground, input from weight on the nose wheel (WOW) is summed as well. WOW simply accounts for ground effects of the aircraft. Once airborne, the WOG signal goes negative and the FET Q15 is turned off so no  $\sin\theta$  follow up or WOW signals are summed with the other moment producing signals.

The output of the summing amplifier AR9 is the pitch rate,  $Q_A$ . This signal is multiplied with the  $\cos\phi$  from the roll rate circuitry. This product

$Q_A \cos \phi$  is then summed with the product  $R_A \sin \phi$  from the turn and roll rate circuits to yield the pitch rate,  $d\theta/dt$ . The multiplication of  $Q_A \cos \phi$  is done by FETs Q17 and Q18. As in the roll rate circuit,  $d\theta/dt$  is sent to a pitch angle servo amplifier AR12 where the commanded rate is compared to the feedback motor pitch rate by feeding back the pitch angle through the tach generator, G3. The  $d\theta/dt$  feedback loop is identical to the loop employed by the roll rate circuit where the 162 kW R86 resistor determines the rotation rate of the motor. The Euler angle,  $\theta$ , results from the integration of  $d\theta/dt$  by the motor and associated gears and pulleys.



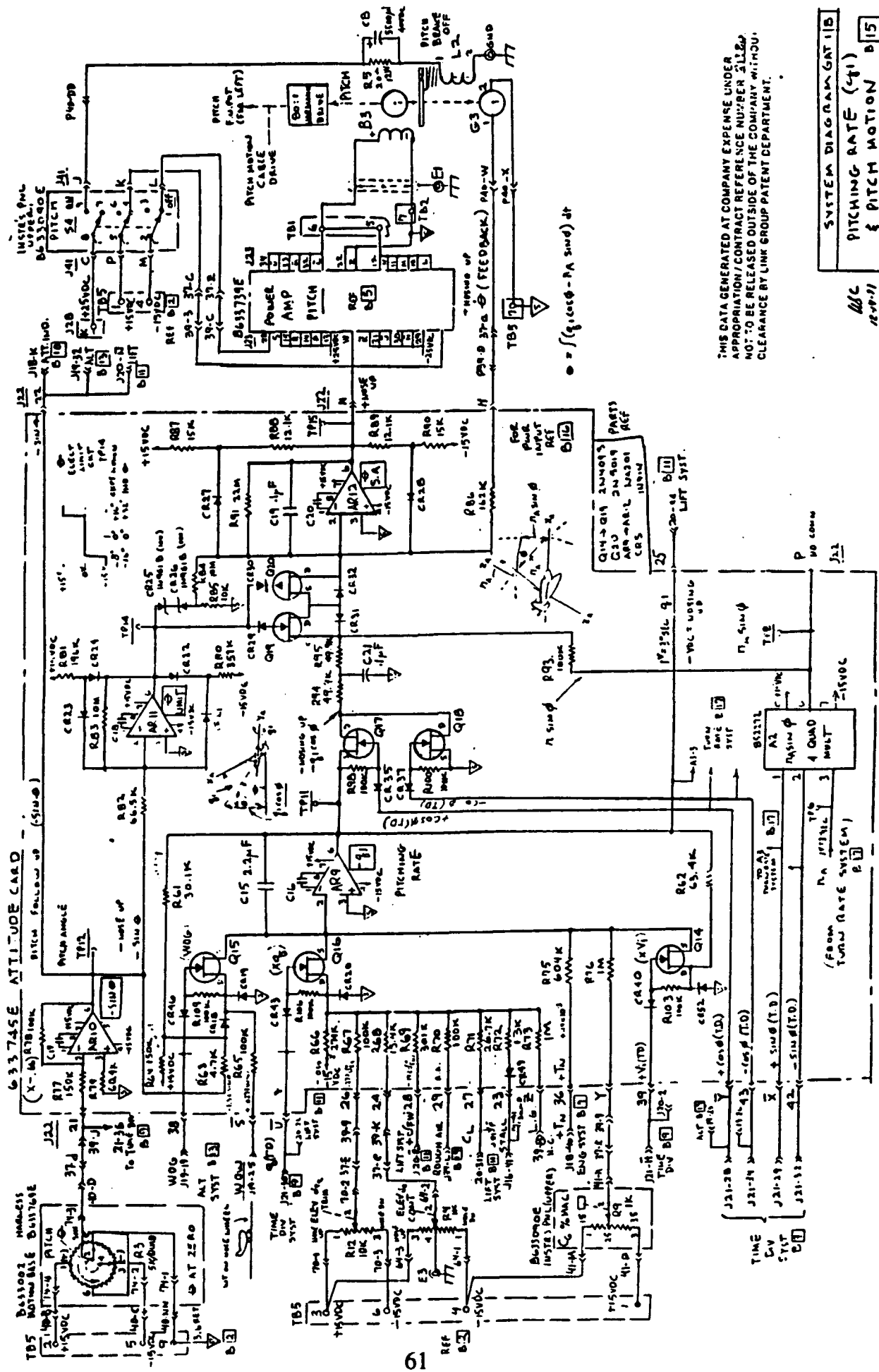


Figure 3-6. Pitch Rate and Pitch Motion System Schematic.

#### d. Yaw Circuitry Described

The yaw rate circuitry is very similar to the roll and pitch rate circuitry previously described. Figure 3-7 is a simplified block diagram. Like the pitch rate circuit, the yaw rate is multiplied by the cosine component of the roll angle which effects the yaw rate. Notice that all three of the simplified block diagrams which produce the Euler angles are similar for the airborne mode. What the block diagrams don't show are the minor differences that enter into the computations while the aircraft is on the ground, rolling down the runway in ground effect.

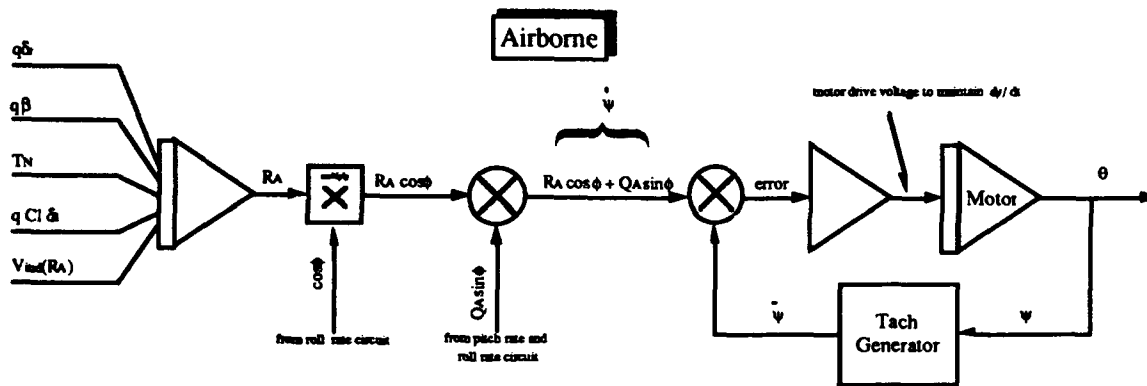


Figure 3-7. Yaw Rate Block Diagram.

Like the previous systems, moments created by control surface deflections and by aircraft attitude now with respect to the z-axis, are summed and integrated to obtain the yaw rate,  $R_A$ . The yaw rate is then multiplied by the vector component of the portion of the turn rate about the z-axis, due to the bank angle  $\phi$  which is horizontal with respect to an inertial reference frame. This

gives  $R_A \cos\phi$ . This term is added to the vector component of the aircraft pitch rate about the y-axis due to bank angle, which is horizontal to the inertial reference frame. This gives  $Q_A \sin\phi$ . The sum of these two terms,  $R_A \cos\phi + Q_A \sin\phi$ , yields the yaw rate,  $d\psi/dt$ .

Note that if the bank angle is zero, the yaw angle rate,  $d\psi/dt$ , will be simply a function of the turn rate,  $R_A$ . If the bank angle is 90 degrees, the yaw angle rate,  $d\psi/dt$ , will be equal to the pitch rate,  $Q_A$ .

The combined input along with heading rate feedback goes to the heading servo amplifier then to the turn rate motor where it is integrated to obtain the Euler yaw angle,  $\psi$ .

Referring to the turn rate schematic, Figure 3-8, notice the absence of a sine-cosine potentiometer in the upper left corner of the drawing. This is because it does not matter which direction the trainer is pointed when power is applied. There is no physical limit on the amount of rotation about the z axis. The simulator simply follows a rate command and the instruments track accordingly.

In order to maintain the aircraft on a steady heading at very slow (essentially zero) speeds,  $V_p$  is brought in at pin 11 on board J22 and goes through the 10 k $\Omega$  resistor R42 to operational amplifier AR7. If  $V_p$  is less than eight miles per hour then the output of AR7 is +15 volts. This +15 volts turns on FETs Q7 and Q13. FET Q7 when on, acts to short the output of the summing amplifier AR5 and FET Q13 when on, acts to short the servo amplifier AR8.

The effect of shorting these two amplifiers when the speed is less than eight miles per hour is to ensure that zero volts goes to the turn pointer and drive motor, keeping the aircraft heading and indicator from drifting about.

Operational amplifier AR7 has -15 volts through a 301 k $\Omega$  resistor R47 as an input along with  $V_p$ . When  $V_p$  is great enough to balance the effect of the -15 volt input, the output of AR7 will be approximately -15 volts and FETs Q7 and Q13 will be turned off opening the circuit. This allows normal inputs to AR5 and AR8.

While on the ground, the WOG input is latched at +15 volts which turns on Q10 FET. With Q10 on, the signal from the rudder pedal deflection,  $\delta_r$  goes through to the summing amplifier AR5. Other signals which are multiplied by  $q$  or  $V_{ind}$  are essentially zero so the rudder pedal deflection is the dominate input. This has the effect of giving the simulator a nose wheel steering capability. At takeoff however, the WOG signal is latched to -15 volts and FET Q10 is turned off opening the circuit and not allowing the nose wheel steering signal to dominate.

As the brakes are released velocity increases. The dynamic pressure,  $q$  increases proportionally. The time divided signals  $V_{ind}$  and  $q$ , stay on for increasingly longer intervals. Indicated velocity is multiplied with  $R_A$  feedback through the 45.3 k $\Omega$  resistor R42. Dynamic pressure is multiplied with  $\delta_r$  and  $\beta$  through the 35.7 k $\Omega$  and 27.4 k $\Omega$  resistors R38 and R39 respectively. The net thrust,  $T_N$  signal enters AR5 directly through the 1 m $\Omega$  resistor R31. This

relatively small input has the effect of inducing a slight left turn rate due to propeller wash of the vertical stabilizer and rudder. The slight turn rate is proportional to the net thrust.

The effects of aileron drag are considered by taking aileron deflection,  $\delta_a$ , through the 665 k $\Omega$  resistor R13. The sign of this input is such that a slight momentary turn in the opposite direction of the yoke motion will occur due to asymmetric drag created by the aileron deflection. This simulates the effect of adverse yaw. Aileron deflection,  $\delta_a$ , is also multiplied, by a  $C_L$  input through FET Q4, to simulate the effects of increased drag at higher angle of attack which affects the turn rate. Both the  $\delta_a$  and  $C_L \delta_a$  signals go through AR2 enroute to AR5 via FET Q9 which multiplies these signals by dynamic pressure.

Airborne, the signals  $\delta_r$ ,  $\beta$ ,  $\delta_a$ , and  $C_L \delta_a$  are all multiplied by  $q$  and  $T_N$  is added. This combined signal is integrated by AR5 to produce the turning rate,  $R_A$ . Operational amplifier AR6 simply inverts the signal,  $R_A$ .  $R_A$  is then multiplied by vector component of the bank angle,  $\phi$  which contributes to the turn motion, that is  $R_A \cos \phi$ . The cosine of the bank angle comes from the roll rate circuit and is multiplied by the turn rate via FET Q11 or Q12 depending upon the whether the roll is to the right or to the left. The signal  $R_A \cos \phi$  is added to the product of the pitch rate and the vector component of the bank angle which also produces a turning moment about the z-axis. The

$Q_A \sin \phi$  signal enters the circuit via A3, a four quad multiplier.<sup>5</sup> The sum  $R_A \cos \phi + Q_A \sin \phi$ , which is the commanded yaw angle rate,  $d\psi/dt$ , enters the servo motor amplifier, AR8 along with turn rate feedback,  $d\psi/dt$ . This signal, as modified by the feedback through the tach generator G1, drives the turn motor.

The physical turning rate that the motor produces is effected by the 10 k $\Omega$  resistor R112 in the feedback loop. The motor, as was the case in the previous descriptions for roll and pitch, mechanically integrates the yaw angle rate to arrive at the Euler angle,  $\psi$ .

---

<sup>5</sup> A four quad multiplier simply performs the multiplication of the two signals while retaining the signs of the angles in each quadrant.



## **2. Time Division Multiplier Circuit Description**

The time division multiplier circuit shown in Figure 3-9, converts a dc voltage, which is proportional to either a rate such as  $q$  or  $v_{ind}$ , or an angle such as  $\phi$ ,  $\theta$ , or  $\psi$ , into a 1000 Hertz square wave whose time period is proportional to those rate or angles. The duration of the square pulse changes proportionally to a change in amplitude of the controlling dc input. These time divided signals provide the multiplication factors which represent the magnitude of their respective signals.



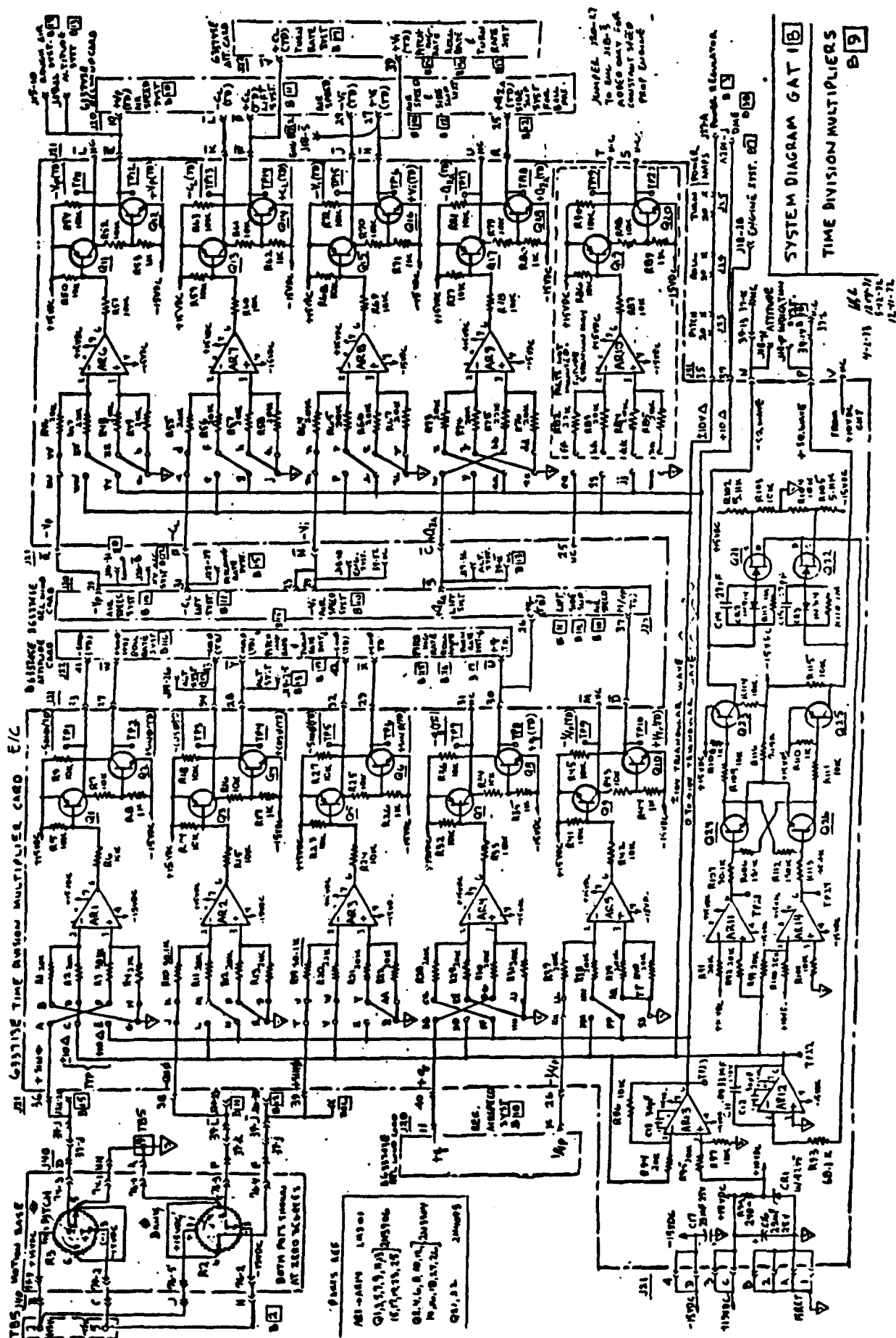


Figure 3-9. Time Division Multiplier Schematic.

## **B. IBM PS/2™ MODEL-50 HARDWARE**

The hardware selected for this project was the IBM Personal System/2™ Model 50 which utilizes the Intel® 80286 microprocessor. The criteria used for selections was one of expediency and availability. The IBM PS/2™ was configured with an Intel® 80287 math coprocessor to enhance floating-point arithmetic operations.

### **1. National Instruments® MC-MIO-16 Interface Board**

The National Instruments® MC-MIO-16 Interface Board is a multifunction analog, digital and timing input/out board designed for compatibility with the IBM Personal System/2™ computer. The MC-MIO-16 Interface Board uses a 12 bit, 25  $\mu$ sec analog-to-digital (A/D) converter. The board was configured for ground referenced, bipolar input from -10 volts to + 10 volts. The output was configured as binary, bipolar with externally referenced voltage. Figure 3-10 shows the analog output circuitry block diagram.

The conversion pulse was triggered externally by an algorithm generated square wave function. The A/D conversion begins upon detection of the low-to-high edge of the square wave pulse. The trigger pulse was set for 16 msec. Figure 3-11 illustrates the analog input and data acquisition circuitry.

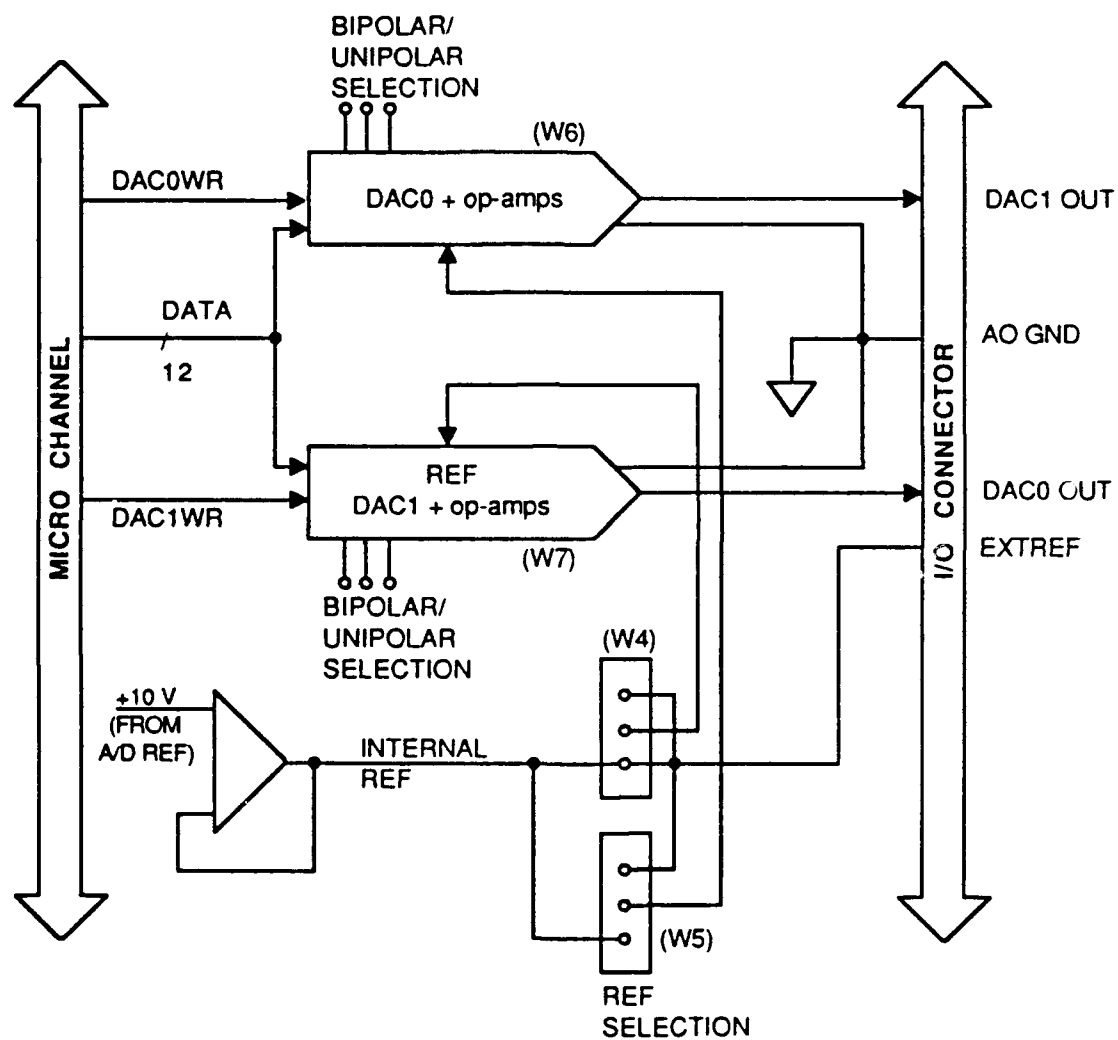


Figure 3-10. Analog Output Circuitry Block Diagram.  
(MC-MIO-16 User Manual p. 4-11)

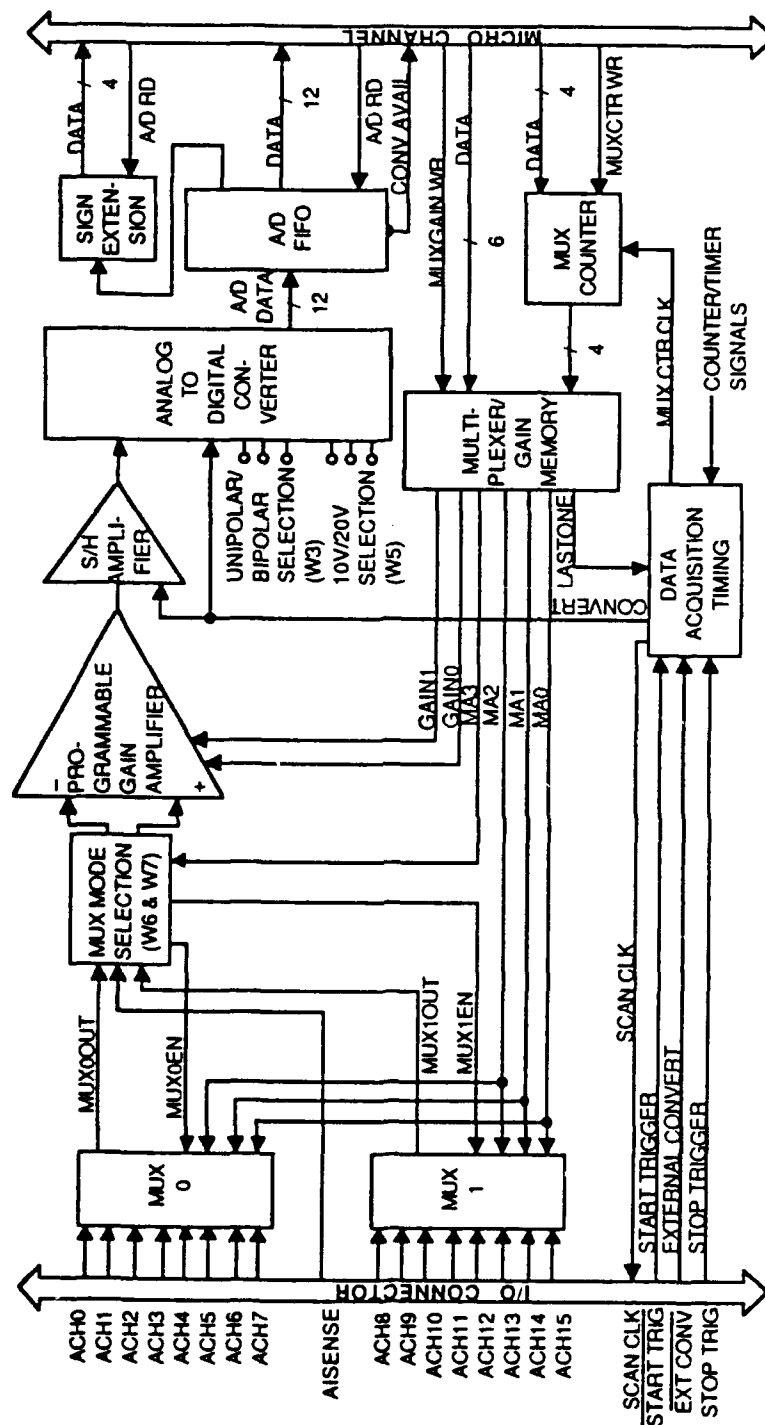


Figure 3-11. Analog Input and Data Acquisition Circuitry  
(MC-MIO-16 User Manual, p. 4-5)

There are 16 analog input channels available (ACH0 through ACH15) and two analog output channels (DAC0 out and DAC1 out). Additionally, there are eight digital I/O lines which are divided into two ports of four lines each (ADIO0,1,2,3 and BDIO0,1,2,3).

The board is configured with a Real Time System Integration (RTSI) bus to allow for easy connection, cross connection, or disconnection of signals. Any signal can be connected to any trigger line. Figure 3-12 shows the RTSI Bus Interface Circuitry Block Diagram. The RTSI bus was configured to connect the square wave generated trigger signal (OUT 5) to the start trigger line. This initiated the A/D conversion.

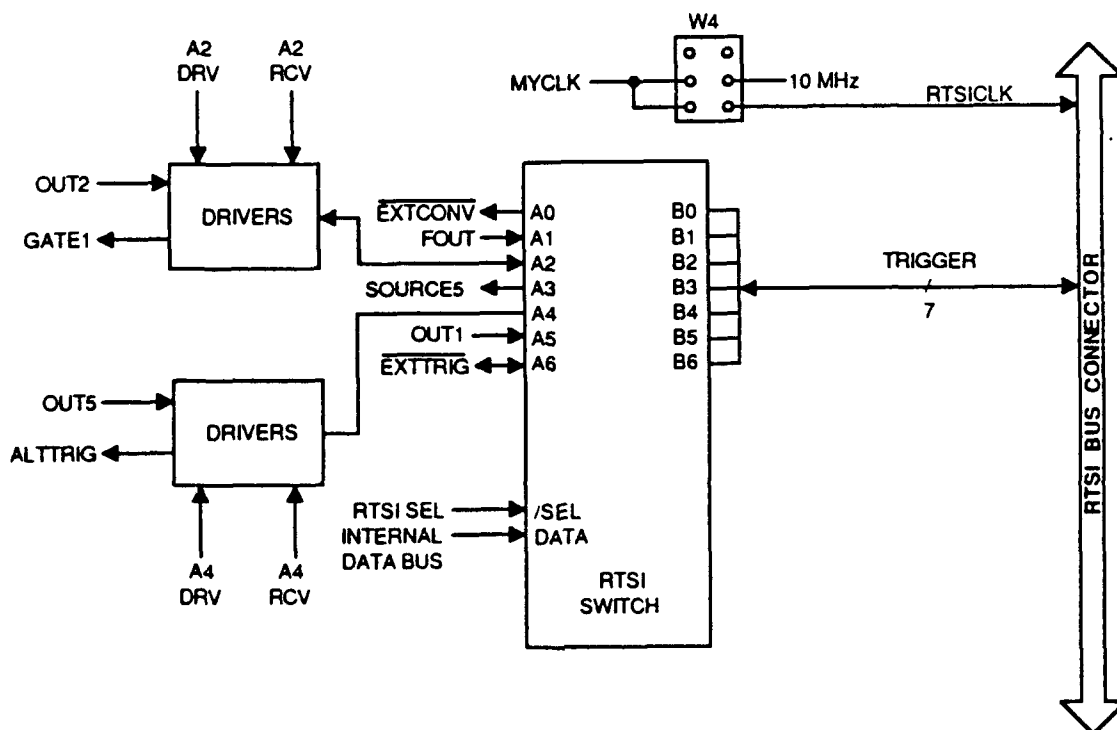


Figure 3-12. RTSI Bus Interface Circuitry Block Diagram.  
(MC-MIO-16 User Manual. p. 4-7)

## **2. Lab Windows™**

Lab Windows™ is an interactive development software package for use with National Instruments data acquisition boards. It facilitates engineering or scientific program development in Microsoft QuickBASIC and Microsoft C. A supplement to Lab Windows™, The Data Acquisition Library, was used fairly extensively as an expedient method of assembling code which made use of the National Instruments data acquisition board.

Using Lab Windows™ greatly expedited the development of software to acquire and transfer data to and from the analog flight simulator circuitry. However, the price paid for this convenience feature was a large compiled program. The sample rate of approximately 62 samples per second could have been quicker but it is by no means unacceptable.

## **IV. ENGINEERING APPROACH**

A detailed description of the actual engineering and modifications made to the Link GAT-1™ trainer will be presented. It will include a description of the installation of the digital computer, wiring modifications made, interface circuits designed, and discovered deviations from the 1972-1973 working schematic provided by the Link Flight Simulation Division of Singer Aerospace and Marine Systems which was used as the primary source of documentation for the GAT-1™ installed at the Naval Postgraduate School, Monterey, California. The wiring schematics presented in Figures 3-4, 3-6, and 3-8 as well as the software program contained in Appendix A will be referred to repeatedly. Software line code will be presented in *Helvetica italics* print to differentiate it from the text. National Instruments Lab Windows™ documentation should be consulted for a complete description of the subroutine calls used.

### **A. INSTALLING THE DIGITAL COMPUTER**

In order to replicate in software a portion of the analog circuitry while still retaining the full motion capability of the flight simulator, the digital computer used to run the software had to move as the simulator moved. Additionally, the wiring to the digital computer's A/D board had to be such as to allow the unrestricted motion of the simulator.

The instructors seat, which is attached to the rotating base, was removed and a platform built to accommodate an IBM PS/2™ Model-50 computer. Line power is brought into the simulator and passes through a slip ring assembly.

Figure 4-1 is a sketch showing the wiring for the power to the computer. The line power terminates at TB4. TB4 is located on the port side of the simulator immediately aft of the wire screen which separates the cockpit from the analog computer bay. Three line wire was run from TB4 to the computer. On TB4, the neutral (white) line was connected to pin 2, the high (black) line was connected to pin 1 and the ground (green) was connected to ground. Since power came from the slip ring assembly, the computer mounted on the instructor's stand was free to rotate 360 degrees without encumbrances due to a power cord.

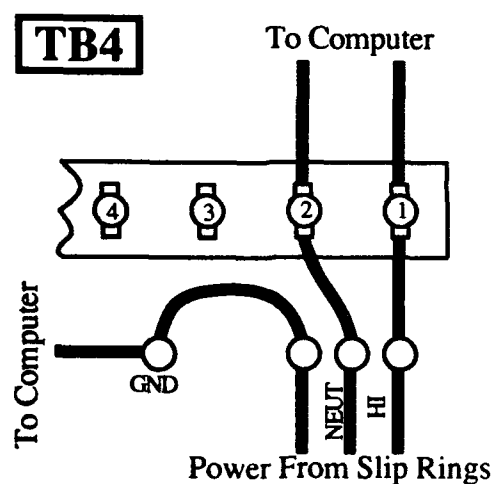


Figure 4-1. Power Conversion.

The location of the computer on the instructor's stand facilitated easy access to the computer chassis and the A/D board for wiring and any changes to the board settings. It was envisioned that the computer would eventually sit on top of the wire screen, inside the cockpit, immediately behind the pilot's seat. This



would enable the instructor's seat to be reinstalled and the GAT-1™ to retain its original appearance and function.

## **B. ANALOG/DIGITAL UMBILICAL INSTALLATION**

A one meter, 50 line ribbon cable was run from the A/D output slot on the computer chassis to the analog computer bay where it was attached to the CB-50 I/O connector block on the prototype circuit board. The pinout for the CB-50 I/O connector block is shown in Figure 3-2 . Note that analog input signals, analog output signals, digital I/O signals, digital power connections, analog and digital grounds, and I/O timing signals are all contained in the CB-50 I/O block connector.

AI GND	1	2	AI GND
A CH 0	3	4	A CH 8
A CH 1	5	6	A CH 9
A CH 2	7	8	A CH 10
A CH 3	9	10	A CH 11
A CH 4	11	12	A CH 12
A CH 5	13	14	A CH 13
A CH 6	15	16	A CH 14
A CH 7	17	18	A CH 15
AI SENSE	19	20	DAC 0 OUT
DAC 1 OUT	21	22	EXTREF
AO GND	23	24	DIG GND
ADIO 0	25	26	BDIO 0
ADIO 1	27	28	BDIO 1
ADIO 2	29	30	BDIO 2
ADIO 3	31	32	BDIO 3
DIG GND	33	34	+5 V
+5 V	35	36	SCANCLK
EXTSTROBE	37	38	START TRIG
STOP TRIG	39	40	EXTCONV
SOURCE 1	41	42	GATE 1
C T 1	43	44	SOURCE 2
GATE 2	45	46	OUT 2
SOURCE 5	47	48	GATE 5
OUT 5	49	50	FOUT

Figure 4-2 CB-50 I/O Block Connector.

## C. SIGNAL FLOW

### 1. Input Signal Flow

The National Instruments MC-MIO-16 A/D board can accept only 16 analog inputs. Since the attitude analog card J22 was to be replicated digitally, the input selection was based upon the inputs that would be necessary to complete the computation. Figure 4-3 contains the analog input channel listing

(corresponding to the array element, *volt.array#((0...15))*, variable extracted, and the location of the signal access point. For pin number locations on the analog mother board, refer to Figure 3-1.

Board No.		Array Element	Variable
J21 pin	J22 pin		
40     Nbar  39          36	31	0	Ailerion defl'n $\delta a$
	33	1	+Beta B
		2	q
	L	3	turn rate $\psi \dot{\phantom{a}}$
	36	4	+Tn
		5	$V_i$
	16	6	Rudder defl'n $\delta r$
		7	sin $\phi$
	11	8	+Vp
	Sbar	9	c.g.constant cg
	26	10	Elevator Trim $\pm\delta$ ELEV, tr
	24	11	Elevator defl'n $\pm\delta$ ELEV
	28	12	Flaps $\pm\delta$ FW
	27	13	Cl
	23	14	Alfa, stall $\alpha$ STALL
		15	sin $\theta$

Figure 4-3. Input Array.

Input leads were fabricated using light gage wire and crimped connectors. Heat shrink material was applied to the connectors to preclude any possible shorting should the leads inadvertently come in contact. The connectors

were friction fit to the pins on the rear of the analog mother board corresponding to the appropriate analog board location. The pins were connected to the locations as specified in Figures 4-3 and 3-1.

The analog voltages were referenced to  $\pm 15$  volts but the A/D board was factory configured for  $\pm 10$  volts. The signal was run through a voltage divider similar to Figure 4-4, in which the resistor values were equal. This scaled the analog voltage by 50%.

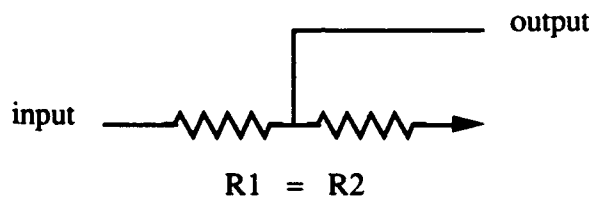


Figure 4-4. Voltage Divider.

The scaled voltages for each of the 16 channels were then sent to the connector block locations A CH0 through A CH15 (refer to Figure 4-2). From the connector block the signal entered the National Instruments A/D board in the IBM PS/2 <sup>TM</sup> Model-50. The 16 incoming signals were scanned at approximately a 16 msec rate. The 16 element input vector therefore is captured approximately 62 times per second. Figure 4-5 summarizes the input signal flow.

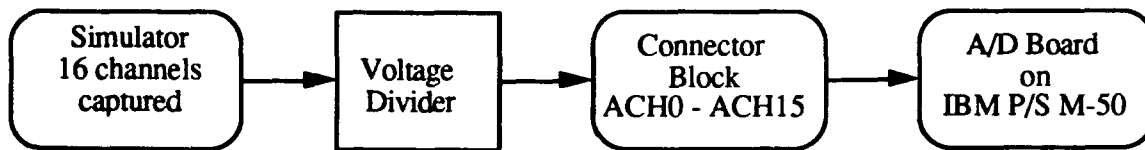


Figure 4-5. Input Signal Flow.

Once the input vector was captured, the signal was digitized then manipulated by the software contained in Appendix A. After the calculations were complete, the signal was returned to the simulator.

***a. WOG Circuit***

The weight on gear signal (WOG) had to be digitized since it had an effect on the rate equations which were being replicated. This would have been the 17th input channel. Recall that the MC-MIO-16 A/D board would only accept 16 channels. After careful inspection of the signal flow, it was determined that the WOG signal was either +15 volts while on the ground or -15 volts when the trainer simulated being airborne. This  $\pm 15$  volt logic was converted to compatible TTL<sup>1</sup> and input to the MC-MIO-16 as a digital signal of either +5 volts if on the ground and 0 volts if airborne. Figure 4-6 illustrates the hardware scheme used to level shift the  $\pm 15$  volt WOG signal to TTL levels.

---

<sup>1</sup> Transistor Transistor Logic

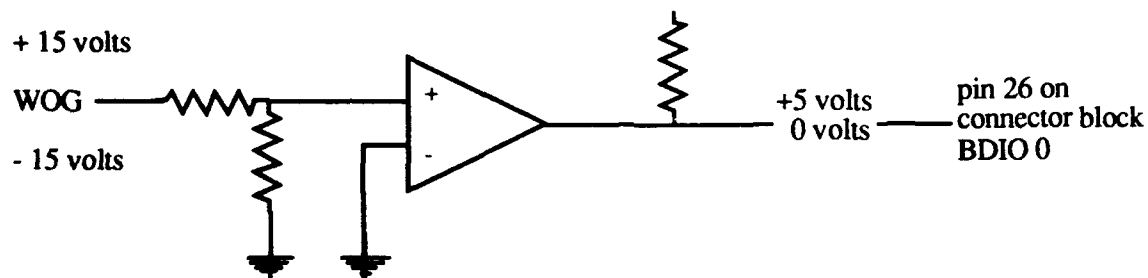


Figure 4-6. WOG Circuit.

Digital port B was configured as an input port. The WOG signal was attached to BDIO 0 (pin 26 on the connector block Figure 4-2). The command

```
dig.in.line(1, 1, 0, WOG%)
```

returns a logic state of zero if it receives the +7.5 volts (or any positive voltage). The WOG signal is therefore digitized to 1 if +15 volts (meaning the simulator is on the ground) and 0 if -15 volts (meaning the simulator is airborne). Any values multiplied by WOG would become zero once the simulator was airborne.

The WOG signal therefore went from the simulator directly to a digital input line on the A/D board. The digitized value of either 1 or 0 was used directly in the math model as such.

#### ***b. A/D Trigger Signal***

The process of acquiring the analog data began with a trigger signal to the A/D converter. A square wave trigger pulse of user specified duration was implemented using the following code:

```
input "interrupt period in milliseconds"; millis%  
delta.t# = millis% * 1.0E-3  
millis% = 0.5*millis%  
err.num = ctr.square%(1,5,4,millis%,millis%)
```

The square wave signal was sent to OUT5 (refer to Figure 4-2).

The following RTSI command was used to internally connect the trigger signal from OUT5 to the START TRIG line.

```
err.num% = rtsi.clear(1)  
err.num% = rtsi.conn(1,5,1,1)  
err.num% = rtsi.conn(1,8,1,0)
```

The START TRIG accepted the pulse which initiated the A/D conversion.

## **2. Output Signal Flow**

The National Instruments MC-MIO-16 A/D board has only two analog output channels, DAC0 OUT and DAC1 OUT (refer to Figure 4-2). One output port was dedicated to the altimeter while the other output port was time-shared among the remaining output signals. If the signal to the altimeter was time-shared it might have appeared discontinuous.

A time-sharing scheme was developed to allow the D/A board to write to multiple channels for output from the single digital output port , DAC0 OUT on the connector block. The multiplex scheme involved using the following CMOS<sup>2</sup> integrated circuit devices:

---

<sup>2</sup> Complimentary Metal Oxide Silicon

- 4024<sup>3</sup> Binary Ripple Counter
- 4011 Quad Two-Input NAND Gates
- two 4051 1-of-8 Switch
- 16 Operational Amplifiers

The software and hardware were used symbiotically to achieve the multiplexing of the output signal through a single digital output port. Figure 4-7 illustrates the complete timing circuit.

---

<sup>3</sup> CMOS device fact sheets from, Don Lancaster, *CMOS Cookbook*, Howard Sams & Co., Indianapolis, Indiana, 1979.



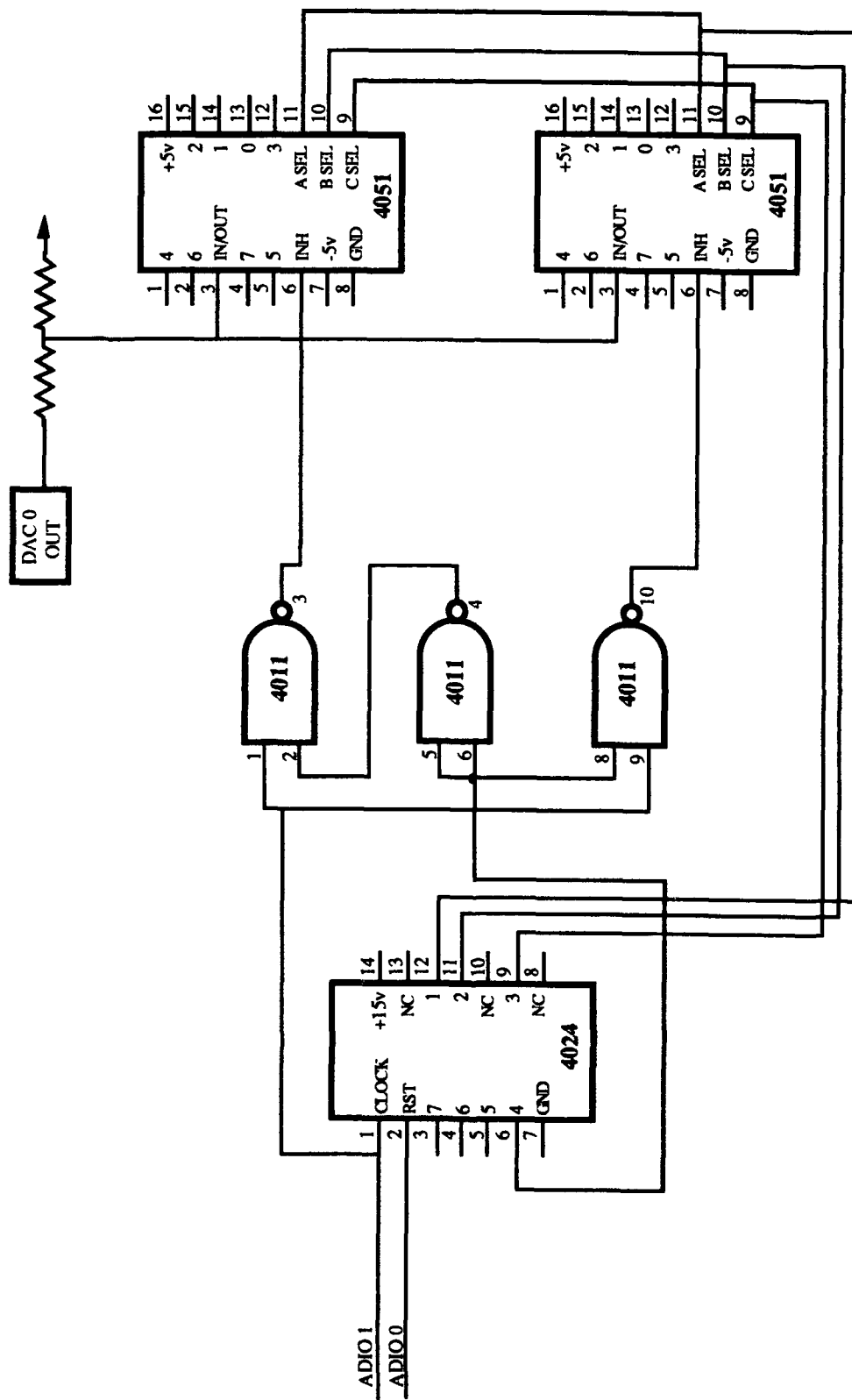


Figure 4-7. Timing Circuit.

The MC-MIO-16 board has two digital registers which can be configured for either digital input or digital output. The A port, ADIO 0-3 (pins 25, 27, 29, and 31 on Figure 4-2) was configured as a digital output port to write to the ADIO 0 and ADIO 1 lines which were used to control the multiplexing circuit. The B port, BDIO 0-3 (pins 26, 28, 30, and 32 of Figure 4-2), was configured as an input port to accept the digitized WOG signal.

```
err.num% = dig.prt.config (1, 0, 0, 1)
```

```
err.num% = dig.prt.config (1, 1, 0, 0)
```

A simple software loop sets the ADIO 0 and ADIO 1 lines. The command

```
dig.Out.Port(1,0,hi.bits%+2)
```

writes a  $2_{10}$ ,  $0010_{\text{binary}}$  to output port A, so ADIO 1 contains a  $1_{\text{binary}}$  and ADIO 0, 2, and 3 contain  $0_{\text{binary}}$ . The command

```
ao.write%(1,0,bin.val%(chan%))
```

writes the value of *bin.val%(chan%)* to the analog output to change the output voltage. *Bin.val%(chan%)* contains the analog voltage corresponding to the binary value representing that voltage.

```
hi.bits%=0
```

```
err.num%=dig.Out.Port(1,0,hi.bits%+2)
```

```
for chan%=0 to 15
```

```
err.num%=ao.write%(1,0,bin.val%(chan%))
```

```
err.num%=dig.Out.Port (1,0,hi.bits%+1)
```

```
err.num%=dig.Out.Port (1,0,hi.bits%)
```

```
next chan%
```

The ADIO 0 line is tied to the CLOCK input on the 4024 device and the ADIO 1 line is tied to the RST line on the 4024 device. The software command,

*hi.bits%=0*

*err.num%=dig.Out.Port(1,0,hi.bits%+2)*

forces the ADIO 1 line high (+1) and the ADIO 0 line low (0). That is, a binary 2 ( $10_{\text{binary}}$ ) is written. The CLOCK and RST lines on the 4024 are now at 0 and 1 respectively. Making the RST input high forces all inputs to ground where they remain until the RST returns to ground. The ADIO 0 line is also tied to the 4011 device pins 1 and 9. Both of these inputs are now set low. The 4024 device simply counts in the positive direction. The outputs change in sequential order. The counter is triggered by the clock pulse which is triggered by the ADIO 0 line which is controlled by the software loop. Simply put, the 4024 writes a binary 0, 1, 2, ..., 15 so each element of the output vector can be addressed. The counter stops at 15 because the for-next loop in which it is embedded stops at 15. An output timing diagram for channels 1, 2, 3, and 4 is shown below in Figure 4-8. The channel numbers correspond to the bit of the word being output from the 4024, where channel 1 is the least significant bit. Note that the CLOCK advances only on the low going pulse. Only channels 1, 2, 3, and 4 were used because channels 1, 2 and 3 were used to address the 4051 (via the 4011) and the fourth bit, channel 4, was used to address the particular 4051 necessary for input.

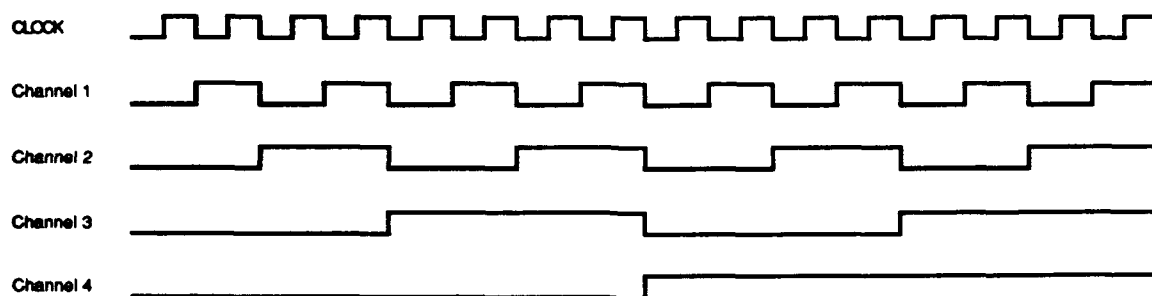


Figure 4-8. Timing Diagram.

Continuing with the first pass through the circuit, the 4024 writes a binary 0 so channels 1, 2, 3 and 4 are all set low. The channel 4 (pin 6) of the 4024 is tied to pins 5 and 6 of the 4011 NAND so the output (pin 4) is high. The pin 4 of the 4011 is tied to pin 2 of the 4011. Pin 1 of the 4011 was set low since it was tied to the ADIO 0 line so the high-low combination input to the NAND gate yields a high output at pin 3. Pin 3 is tied to the INH line, pin 6, of the 4051. A high pulse inhibits the 4051 #1 so no data is transferred. Pins 8 and 9 of the 4011 are both low since pin 8 was tied to pins 5 and 6, and pin 9 was tied to ADIO 0. The low-low combination input to the NAND gate yields a high output at pin 10. Pin 10 being tied to pin 6, the INH line of the 4051 #2 device, inhibits data transfer here as well. Figure 4-9 is a truth table for NAND logic.

Input	Input	Output
0	0	1
1	0	1
0	1	1
1	1	0

Figure 4-9. NAND Logic.

The clock now is advanced by the command,  
*err.num%=dig.Out.Port (1,0,hi.bits%+1)*

Since the clock pulse went from low to high, the outputs of the 4024 device remain the same. Pin 1 on the 4011 is now high so the high-high input yields a low output which allows the 4051 #1 to be addressed. The 4051 #1 and #2 switches are set to 0 since the A SEL, B SEL, and C SEL are all set low because they were tied to channels 1, 2, and 3 of the 4024. The 4051 #1 and #2 switches are ganged in parallel. The 4051 device is simply a switch which can be thought of as shown in Figure 4-10.

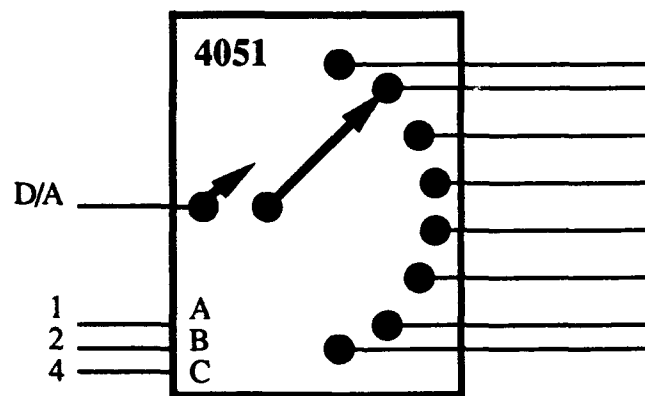


Figure 4-10. 1-of-8 Switch Concept.

Once the 4024 counts up to 8 ( $1000_{\text{binary}}$ ), channel 4 (pin 6) of the 4024 is set high. Pins 5, 6, and 8 are all therefore set high. Via the logic NAND, pin 4 is low, so pin 2 of the 4011 will also be low. Pin 3 will be high so the 4051 #1 device will be inhibited. Only the 4051 #2 device can be addressed since it will have a high-high input combinations each time the clock is advance.

The voltages, are scaled to their digital equivalent by the following commands:

```
acq.err% = ao.vscale(1,0,psi.dot*sine.theta#,bin.val%(1))
```

```
acq.err% = ao.vscale(1,0,RA*sine.phi#,bin.val%(2))
```

```
acq.err% = ao.vscale(1,0,QA*sine.phi#,bin.val%(3))
```

```
acq.err% = ao.vscale(1,0,PA#,bin.val%(4))
```

```
acq.err% = ao.vscale(1,0,QA#,bin.val%(5))
```

```
acq.err% = ao.vscale(1,0,RA#,bin.val%(6))
```

*Bin.val%(chan%)* contains the digital voltages which are reintroduced into the circuit. The command

```
err.num% = ao.write%(1,0,bin.val%(chan%))
```

takes the digital values and converts them to their analog equivalent.

Each 4051 device (Figure 4-6) has eight output channels. The outputs of the 4051 switches are tied to 16 operational amplifiers which then sequentially write to the output channels the values contained in *bin.val%(chan%)*. The information flows to the appropriate operational amplifier from the DAC 0 OUT via the 4051 device. Figure 4-11 is a timing logic table which follows the signal flow of Figure 4-7.

The operational amplifiers were configured with resistor values in a three to one ratio in order to achieve a four to one gain using the relation

$$G = 1 + R_2/R_1$$

This was done since the input signal was twice divided by two. Once as the signal entered the prototype board and again as the signal entered the 4051 device from the DAC 0 OUT

In figure 4-10 note that the very first cycle initializes the counter by writing a binary 2 to bits ADIO 0 and ADIO 1. The remaining cycles simply

advance the counter and allow the 4051 device to accept a load from the DAC 0 OUT port tied to the A/D board on the IBM P/S-2™ Model-50.

PINOUT	IN/OUT CH	LOGIC				
		CYC 1 initialize	CYC 2	CYC 3	CYC 4	CYC 5
Connector Block						
ADIO0		0	1	0	1	0
ADIO1		1	0	0	0	0
Channel		0	0	0	1	1
7-Stage Binary Ripple Counter (4024)						
pin 1	CLOCK	0	1	0	1	0
pin 2	RST	1	0	0	0	0
pin 6	CH 4	0	0	0	0	0
pin 9	CH 3	0	0	0	0	0
pin 11	CH 2	0	0	0	0	1
pin 12	CH 1	1	0	1	1	0
Counter		0	0	1	1	2
Quad 2-Input NAND Gate (4011)						
pin 1		0	1	0	1	0
pin 2		1	1	1	1	1
pin 3		1	0	1	0	1
pin 4		1	1	1	1	1
pin 5		0	0	0	0	0
pin 6		0	0	0	0	0
pin 8		0	0	0	0	0
pin 9		0	1	0	1	0
pin 10		1	1	1	1	1
1-8 Switch 4051 #1						
pin 3	IN/OUT	no load	load	no load	load	no load
pin 6	INH	1	0	1	0	1
pin 9	C SEL	0	0	0	0	0
pin 10	B SEL	0	0	0	0	1
pin 11	A SEL	0	0	1	1	0
pin 13	OUT 0	0	0	1	1	0
pin 14	OUT 1	0	0	0	0	1
pin 15	OUT 2	0	0	0	0	0
pin 12	OUT 3	0	0	0	0	0
pin 1	OUT 4	0	0	0	0	0
pin 5	OUT 5	0	0	0	0	0
pin 2	OUT 6	0	0	0	0	0
pin 4	OUT 7	0	0	0	0	0
1-8 Switch 4051 #2						
pin 3	IN/OUT	no load	no load	no load	no load	no load
pin 6	INH	1	1	1	1	1
pin 9	C SEL	0	0	0	0	0
pin 10	B SEL	0	0	0	0	1
pin 11	A SEL	0	0	1	1	0
pin 13	OUT 0	0	0	0	0	0
pin 14	OUT 1	0	0	0	0	1
pin 15	OUT 2	0	0	0	0	0
pin 12	OUT 3	0	0	0	0	0
pin 1	OUT 4	0	0	0	0	0
pin 5	OUT 5	0	0	0	0	0
pin 2	OUT 6	0	0	0	0	0
pin 4	OUT 7	0	0	0	0	0

Figure 4-11. Timing Logic.

## D. SUPPORTING SOFTWARE

Much of the software used to support the hardware has been described. The following discussion is included for completeness. While the program contained in Appendix A is annotated, the discussion further explains the code.

### 1. Explanation of Variables

The following vectors were all dimensioned to contain 16 elements.

*buffer%(15)*  
*chan.vector%(15)*  
*gain.vector%(15)*  
*volt.array(15)*  
*bin.val(15)*

#### a. *buffer%(15)*

Buffer is the array in which the acquired analog data from the flight simulator which has been converted to its digital equivalent is held from scan to scan. The data in this array are refreshed according to the parameters assigned in the *scan.start* function.

#### b. *chan.vector%(15)*

Channel vector is an integer array which contains the channel scanning sequence. The length of the array is equal to the number of channels to be scanned. For this project the number of channels scanned is the maximum allowed for the National Instruments board, 16. For simplicity, the channels were scanned sequentially in ascending order from zero to 15. The following code initializes the *chan.vector%()* and the *gain.vector%()*.



```

for i% = 0 to 15
    chan.vector%(i%) = i%
    gain.vector%(i%) = 1
next i%

```

**c. *gain.vector%(15)***

Gain vector is an integer array equal to the number of channels to be scanned with each component representing the gain value for each of the corresponding channels specified in the *chan.vector%(15)* array. As illustrated in the above code, the gain was set to unity.

**d. *volt.array(15)***

Voltage array is the vector which contains the analog voltages from the flight simulator. The 12-bit acquired data contained in the *bin.array%(15)* vector is converted into an equivalent voltage. The command

```
acq.err = daq.scale(1,1,16,buffer%(),volt.array#())
```

scales the digital data to its analog voltage equivalent. The data is manipulated in the math model as its analog equivalent. It is reconverted to a digital form by the command

```
acq.err% = ao.vscale(1,0, voltage value,bin.val%())
```

so it can be sent to the A/D board and written to the analog circuit by the command

```
err.num% = ao.write%(1,0,bin.val%(chan%))
```

Figure 4-12 is a table of the voltage array elements and their representative signals.

Voltage	Array
ailer.def	volt.array#(0)
beta	volt.array#(1)
q	volt.array#(2)/5.0
psi.dot	volt.array#(3)
thrust.net	volt.array#(4)
vel.ind	-volt.array#(5)/5.0
rudder.def	volt.array#(6)
sine.phi	volt.array#(7)/7.5
vel.p	volt.array#(8)
WOW	volt.array#(9)
elev.trim	volt.array#(10)
elev.def	volt.array#(11)
flap.def	volt.array#(12)
Cl	volt.array#(13)
alfa.stall	volt.array#(14)
sine.theta	volt.array#(15)/7.5

Figure 4-12. Voltage Array.

Notice that the dynamic pressure,  $q$ , and the indicated velocity,  $V_{ind}$ , are divided by 5.  $V_{ind}$  and  $q$  range from 0 to +10 volts. The voltage was divided by two so this yields a 0 to 5 volt range for  $V_{ind}$  and  $q$ . The scaling (division) makes  $V_{ind}$  and  $q$  equivalent to their digital counterparts of 0 to 1.

Also note that the  $V_{ind}$  voltage is negative due to the sign of the signal source. The voltages for the  $\sin\phi$  (*sine.phi*) and  $\sin\theta$  (*sine.theta*) are divided by 15. This is because they are referenced to  $\pm 15$  volts dc (+up or right, -down or left), and must be scaled accordingly. The sine must be a number between 0 and  $\pm 1$ .

**e. *bin.val%(15)***

Binary value is an array which contains the binary equivalent of the voltages in the array *volt.array(15)*. It is also the value that is written to DAC 0

OUT (refer to Figures 4-2 and 4-6). Note that *bin.val%()* is really two different arrays, depending upon where it used in the program. Recall that the limitation of a single output channel necessitated the development of the timing circuit shown in Figure 4-6 which allows as many as 16 channels to be output via the single DAC 0 OUT pin.

## 2. Explanation of Constants

The constants are divided into roll, pitch, and yaw sections of the program in Appendix A because the schematics are also separated accordingly. The constants are simply the  $1/RC$  values for the portion of circuit which is being replicated.

For example, referring to Figure 3-4 for the roll circuitry, the values for aileron deflection ( $\delta_a$ ), net thrust ( $T_N$ ), sideslip ( $\beta$ ), weight on ground (WOG), yaw rate,  $R_A$ , and feedback of roll rate,  $P_A$  all enter the summing amplifier, AR1. The inverse time constants for each of these variables are determined by the reciprocal of the product of the associated resistor and the capacitor across the summing amplifier AR1, designated C1 on the schematic. For example, the time constant for the aileron deflection input to the summing amplifier is  $1/(R6)(C1)$  or  $1/(30.9 \times 10^3 \Omega)(2.2 \times 10^{-6} \text{ F}) = 14.71 \text{ sec}^{-1}$ . The constants for the other inputs are calculated similarly.

The only slight difference in determining the constants occurs in the circuitry for the turn rate. In this circuit an additional operational amplifier, AR2, is used to incorporate the effects due to aileron drag and the change of this effects as angle of attack increases (which increases  $C_L$ ). The resulting

product of  $\delta_a C_L$  is entered into the the summing amplifier AR5. The constants associated with this input are their respective resistor ratios, 100/664 for  $\delta_a$  and 100/44.2 for  $C_L$ . These values of course are multiplied by the time constant of  $1/(R37)(C8) = 1/(243 \times 10^3)(2.2 \times 10^{-6}) = 1.87 \text{ sec}^{-1}$  since the signal passes through R37 enroute to the summing amplifier AR5.

### 3. Explanation of the Rate Equation Calculations

The input signals, with the exception of rough air inputs, to summing amplifiers AR1, AR9, and AR5 of the roll, pitch, and yaw schematics (Figures 3-4, 3-6, and 3-8) are extracted from the simulator via the prototype circuit board, connector block and MC-MIO-16 A/D board and read into the software as an input voltage vector array. These voltages are then multiplied by their time constants, summed, and integrated. An infinite loop continually captures the analog signals, performs the multiplication, summing and integration and then returns the signal to the circuit.

```

while 1 > 0
    err.num% = dig.Out.port (1,0,14)
    acq.err% = scan.start (1,buffer%(),16,1,25,4,1)
    acq.err% = daq.check (1,status%,points%)
        while status = 0
            acq.err% = daq.check (1,status%,points%)
        wend
    Code to Determine Status of WOG
    Code to Convert buffer%() array from binary to digital
    Code for Roll, Pitch, and Yaw Rate Calculations
    Code for Euler Angle Calculations

```

*Code to Output Results*  
*wend*

A simple Euler integration method was used to replicate the function of the summing/integrating amplifiers AR1, AR9, and AR5. The current value was equal to the previous value plus the newly computed incremental value times the step size. (Gerald, 1989, p.354.) The step size was set equal to the time interval,  $\Delta t$ . The *delta.t* used for the numerical integration was 16 msec.

*a. Roll Rate Calculations*

The calculations for the roll rate take the inputs with their associated time constants for sideslip ( $\beta$ ) and aileron deflection, ( $\delta_a$ ) and multiplies them by the dynamic pressure,  $q$ . Roll rate,  $P_A$ , is fed back and summed with the turn rate,  $R_A$ . The sum of  $P_A$  and  $R_A$  is multiplied by the indicated velocity,  $V_{ind}$ . The roll rate is also fed back and multiplied by WOG. WOG is also multiplied by the  $\sin \phi$ . These inputs are summed then multiplied by the step interval,  $\Delta t$ . Since the output of the summing amplifier inverts the sign of the signal, the incremental value is now subtracted from the previous value. The minus the minus values is actually adding the increment. Note that in Appendix A, the code for the integration shows a minus sign for this reason. The equation has the general form of,

(4-1)

$$P_{A_{N+1}} = P_{A_N} + \left( \frac{dP_A}{dt} \right) \Delta t$$

The code was similar for roll, pitch, and yaw. All values were computed within the infinite loop using code similar to:

$$PA = PA.old - dPA * delta.t\#$$

$$PA = PA.old$$

The actual equation used to determine the roll rate,  $P_A$ , was derived from the actual circuitry based upon the signal flow and the visually determined resistor and capacitor values. The roll rate equation was found to be,

(4-2)

$$P_A = \int_0^t \left[ q(22.1126 \beta + 14.7102 \delta_a) + v_{ind}(6.6746 P_{A_{old}} - 2.2727 R_{A_{old}}) + WOG(18.2548 \sin \phi + 6.06 P_{A_{old}}) \right] dt$$

#### ***b. Pitch Rate Calculations***

The calculations for the pitch rate were done in the same manner as the roll rate calculations. The constants were calculated and multiplied by their respective signals. The signals were combined in software to replicate the the analog signal flow. Again, the circuit board was visually inspected to determine the signal flow and the correct resistor and capacitor values. The resulting equation for pitch rate was,

(4-3)

$$Q_A = \int_0^t \left[ q \left( 29.51596 \delta_e - 0.1584 + 17.0242 C_L + 34.9650 \alpha_{\text{stall}} + 1.5101 \delta_{\text{FW}} \right) + \text{WOG} \left( \left( 15.1011 Q_{A_{\text{dd}}} - \sin \theta + 3.0303 \right) + 4.5454 \text{WOW} \right) + 7.1695 Q_{A_{\text{dd}}} v_{\text{ind}} + 0.1115 T_N \right] dt$$

### c. Yaw Rate Calculations

Like the previous two rate calculations, the yaw rate was determined from a visual inspection of the circuit board to determine the signal flow, resistor and capacitor values. The addition of the circuitry to simulate aileron drag necessitated the additional multiplication terms. The yaw rate equation determined from the analog circuit board was,

(4-4)

$$R_A = \int_0^t \left[ q \left( 12.7324 \delta_r - 16.5893 \beta - \left( 2.2624 C_L \delta_a + 0.1504 \delta_a \right) 1.8708 - 1.1364 \right) + 1.4029 R_{A_{\text{dd}}} v_{\text{ind}} + \text{WOG} \left( 10.0341 R_{A_{\text{dd}}} + 1.7825 \delta_a \right) + 0.4545 T_N \right] dt$$

Once the roll, pitch, and yaw rate equations were computed, the Euler angle rate equations were calculated. The voltage value equations

(2-78)

$$\dot{\phi} = P + \dot{\psi} \sin \theta$$

(2-79)

$$\dot{\theta} = Q \cos \phi - R \sin \phi$$

(2-80)

$$\dot{\psi} = Q \sin \phi + R \cos \phi$$

were then reintroduced back into the circuit where they were integrated by AR4, AR12, and AR8. This gave the Euler angles:

(4-8)

$$\phi = \int_0^t (P_A + \dot{\psi} \sin \theta) dt$$

(4-9)

$$\theta = \int_0^t (Q_A \cos \phi - R_A \sin \phi) dt$$

(4-10)

$$\psi = \int_0^t (R_A \cos \phi + Q_A \sin \phi) dt$$

These equations are then integrated mechanically by the gear and pulley mechanism in the base of the simulator to provide position information for the motion of the simulator.



## E. EXPERIMENTAL VERIFICATION OF NUMERICAL INTEGRATION TECHNIQUE USED

In order to verify that the numerical integration technique used was correct for this application, a simple experiment was devised.

A circuit simulating the integrator on the analog board of the flight simulator was constructed. The major inputs of  $\delta_e$  and  $C_L$  were used as inputs. The circuit also included two FETs since it was initially believed that the internal resistance of the FETs would effect the math model and should be considered. Figure 4-13 partially illustrates this circuit. A Wavetek™ signal generator produced a one Hertz square wave input of the elevator deflection.

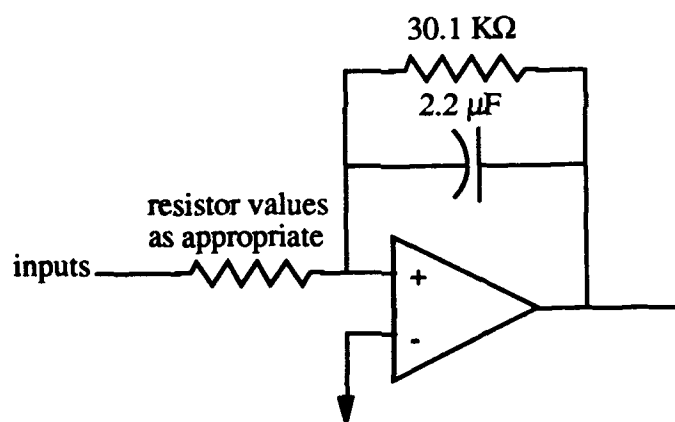


Figure 4-13. Experimental Integration Circuit.

The following code, which is identical in form to the code used to produce the roll, pitch, and yaw rates was used.

```

etest = 0
etestl.old = 0
while 1 > 0
    Code to Acquire Signal
    detest = signal*(1/RC) + etest*(1/0RC)
    etest = etest.old - detest * delta.t#
    etest.old = etest
    Code to Output Results
wend

```

The results of both the analog and digital integration were displayed on an oscilloscope. Figure 4-14 is a photograph of the oscilloscope trace. The top trace was the digital result and the bottom trace was the analog result.

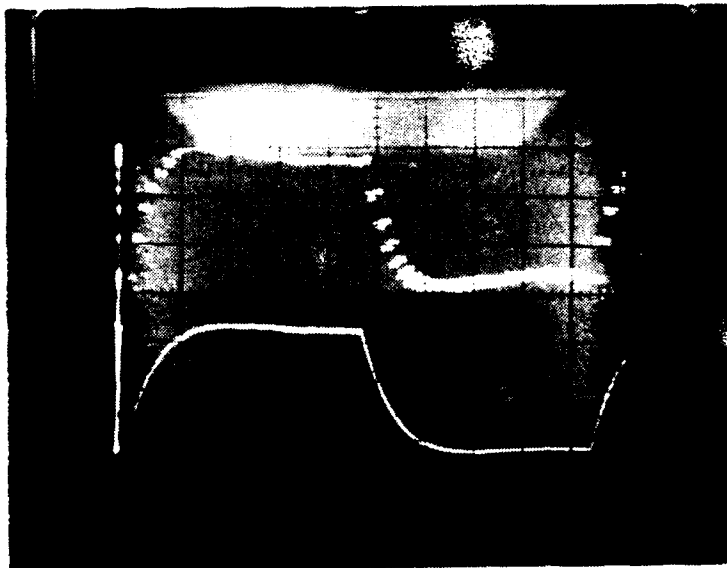


Figure 4-14. Analog and Digital Integration Oscilloscope

The oscilloscope settings were 1v/cm (vertically) and 0.1 sec/cm (horizontally). The two traces had the same size and shape. This provided verification that the simple Euler numerical integration scheme substantially replicated the analog circuit.

## **F. MATCHING WAVEFORMS**

The results of the digital integration were compared to the analog integration performed by the flight simulator. A Wavetek™ signal generator was used as a square wave input for either  $\delta_a$ ,  $\delta_e$ , or  $\delta_r$  to observe the roll, pitch, or yaw rate outputs respectively. Both the digital and analog results were displayed on an oscilloscope for analysis. In each case the digital signal tracked the analog signal.

Figure 4-15 is an oscilloscope photograph of the roll rate response. The digital signal is on the top and the analog signal is on the bottom.

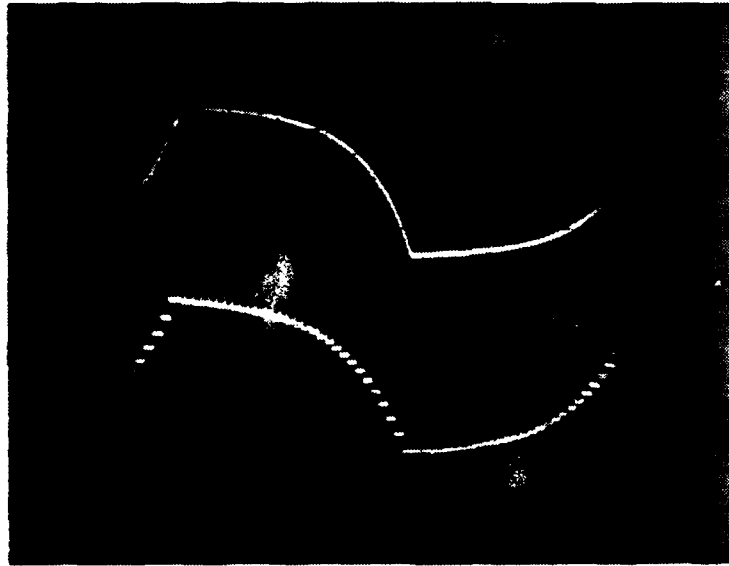


Figure 4-15. Digital and Analog Roll Rate Response to a Square Wave Input Signal.

The oscilloscope was set to 1v/cm and 0.1 sec/cm. The amplitude and shape of the digital and analog signals were virtually identical. This confirmed that the combination hardware and software fabricated accurately reproduced the roll rate computations of the actual flight simulator.

The pitch channel was investigated next. The initial results were somewhat discouraging since the wave shape and amplitude of the digital and analog signals were not closely related.

Upon further investigation, it was determined that the resistor value used in the  $C_L$  feedback was incorrectly indicated on the schematic. This effected the

RC time constant of a portion of the circuit being replicated by the software. The software was modified to reflect the actual resistor value and as shown in Figure 4-16, except for amplitude the shape of the analog and digital response wave shapes were similar.

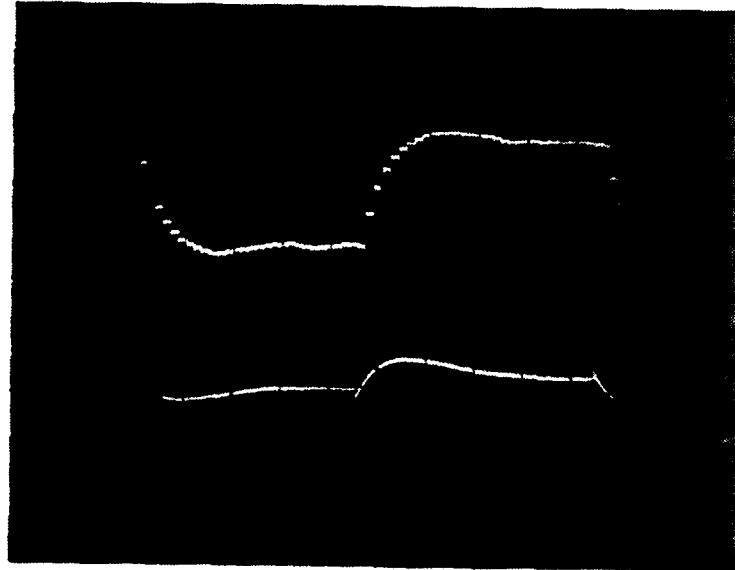


Figure 4-16. Digital and Analog Pitch Rate Response to a Square Wave Input Signal After Adjusting the Resistor Value

Equations 4-11 and 4-12 were the equations modeled by the analog circuitry of the flight simulator for  $C_L$  and angle of attack. These signals were not computed digitally but were acquired from the analog attitude card at pins 27 and 23.

(4-11)

$$C_L = 0.077 + 0.077\alpha + 0.62\delta_{FW} + 0.455 \times 10^{-3} T_N$$

(4-12)

$$\alpha = \int_0^t \left[ \frac{1845}{v_{ind}} (A_{Z_A} + g \cos \phi) + Q_A + WOG (57.3 \sin t - 10\alpha) \right] dt$$

Although the wave shape was similar for the digital and analog signals, the amplitude of the two signals differed. The digital result displayed approximately twice the gain as the analog result. The resistor and capacitor values for the pitch rate circuit were reverified. The program in Appendix A contains the resistor values determined from a visual examination of the circuit since it was discovered that the schematic was inaccurate.

After a careful review of the pitch circuit, no insight was gained as to the gain factor of two display by the digital output of pitch rate. The methodology and values used appeared to be correct.

Lastly, the yaw channel was analyzed. Like the roll channel, the wave shape and amplitude of the digitized turn rate identically matched the analog result. Figure 4-17 is an oscilloscope photograph of the digital (top) and analog (bottom) yaw rates.

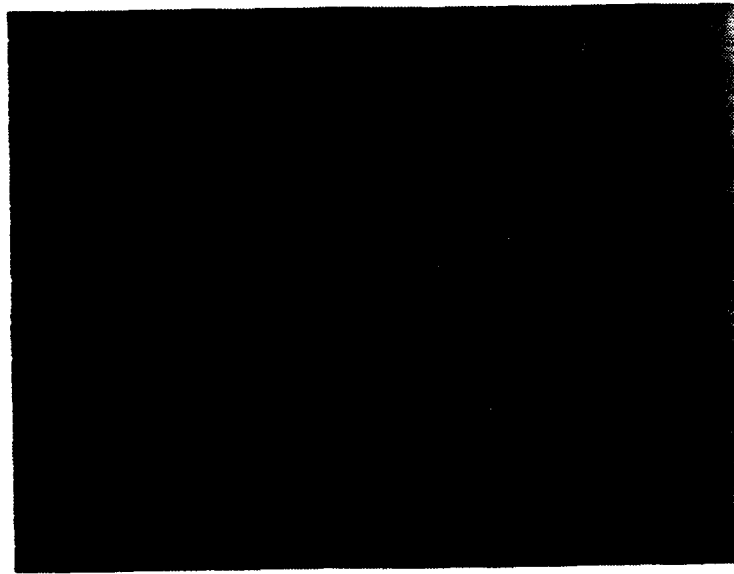


Figure 4-17. Digital and Analog Yaw Rate Response to a Square Wave Input Signal.

#### **G. CORRECTIONS TO THE SCHEMATIC**

During the visual inspection of the circuit board to verify component values and trace signal flow, several resistor values were discovered to be different from those listed on the schematics of Figures 3-4, 3-6, and 3-8. The resistor number, the schematic value and the actual value are listed in Figure 4-18. The correct resistor values are important since they effect the time constant for the circuit which effects the voltage output of the calculation. Modifying these resistor values, which modifies the constants, however is a method of changing the handling characteristics of the aircraft. For example, if more rudder authority is desired, simply change the rudder deflection time constant by

changing the value of the 35.7k $\Omega$  resistor to say 15.0 k $\Omega$ . This is easily accomplished in software but slightly more difficult to locate, unsolder, and resolder a new resistor on an analog board.

<i>Resistor Number</i>	<i>Schematic Value (Kilo Ohms)</i>	<i>Actual Value (Kilo Ohms)</i>
R1	75.00	75.00
R2		24.90
R4	22.60	22.60
R6	30.90	30.90
R8	68.10	68.10
R9	200.00	200.00
R13	665.00	665.00
R14	100.00	100.00
R15	44.20	44.20
R31	1,000.00	
R33	324.00	324.00
R37	243.00	243.00
R38	35.70	35.70
R39	27.40	27.40
R41	255.00	255.00
R42	45.30	45.30
R61	30.10	
R62	63.40	30.10
R64	150.00	
R65	100.00	100.00
R66	274.00	2,870.00
R67	100.00	24.90
R68	15.40	15.40
R69	301.00	301.00
R71	26.70	5.90
R72	13.00	13.00
R75	674.00	4,075.00
R76	1,000.00	

Figure 4-18. Resistor Values Used in Determine Appropriate Time Constants



## **H. A PICTURE IS WORTH A THOUSAND WORDS**

To better understand the physical layout, interfaces, and connections of the signal flow, the following photographs were taken. Although the quality of the photographs may be lacking clarity due to reproduction in this thesis, they serve to visualize the actual engineering.

Figure 4-19 shows the total system. The view is from the aft port quarter of the trainer. The cowling over the analog computer bay has been removed. The IBM PS/2™ Model-50 computer is visible on the starboard side. The ribbon cable is shown connecting the IBM PS/2™ to the A/D interface connector block. The wiring from the connector block to the prototype digital circuit board is visible. The prototype circuit board has been inclined for better viewing. A gang of wires flows from the rear of the analog mother board on the port side of the simulator to the prototype circuit board.



Figure 4-19. Overall System Photograph.

Figure 4-20 shows how the instructor's seat on the starboard side of the simulator was removed and the IBM PS/2™ installed. The IBM PS/2™ was screwed to the plywood platform shown. The plywood platform was bolted to the instructors seat support. Power to the digital computer was connected as described in Section A of Chapter IV.

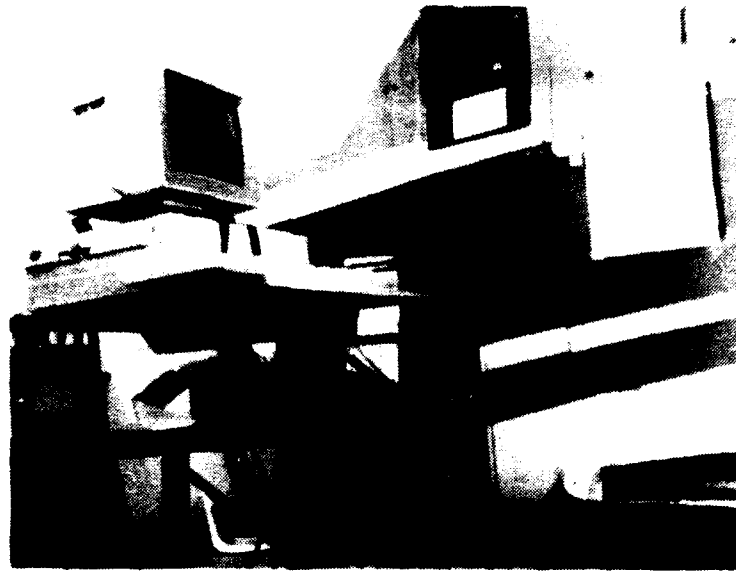


Figure 4-20. Digital Computer Installation.

Figure 4-21 is a close-up view of the connections which flow from the analog mother board. Figure 4-22 shows the gang of wires which were attached to the pins on the rear of the mother board and flow to the prototype circuit board. All the wires were tagged for identification of signals.

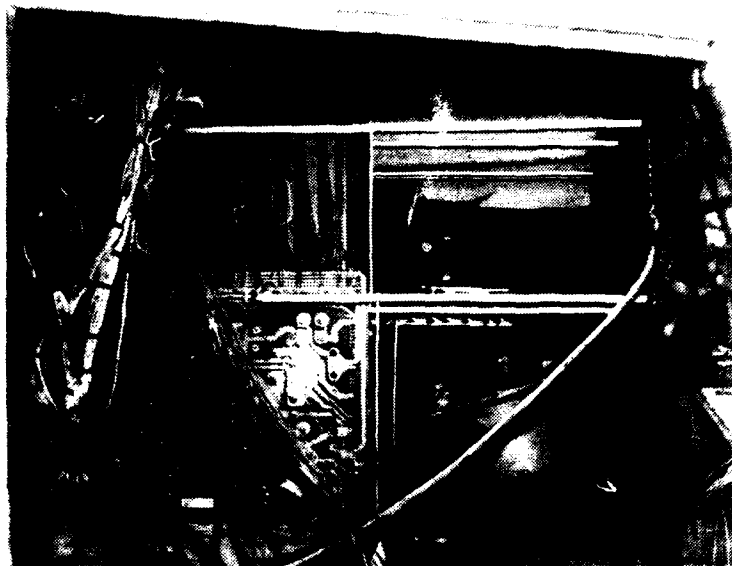


Figure 4-21. Analog Mother Board Close-Up.

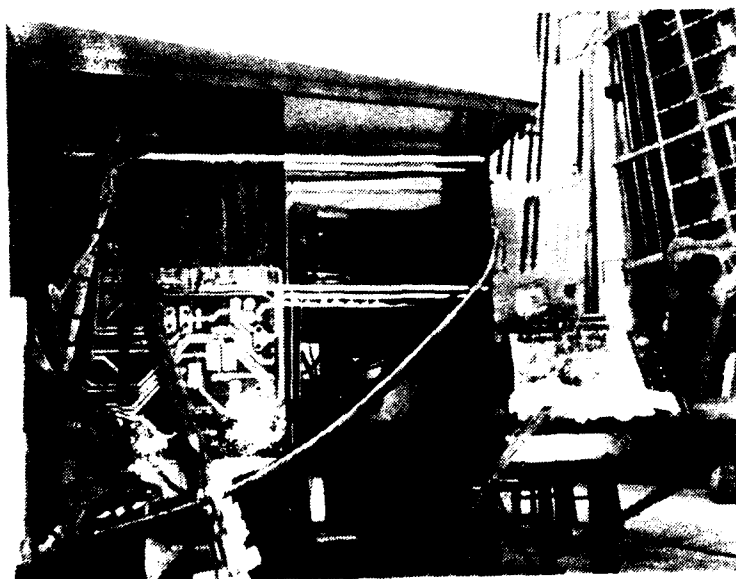


Figure 4-22. Analog Mother Board and Prototype Circuit Board Close-Up.

Figure 4-23 shows a close-up photograph of the prototype circuit board. This board contained the multiplexing circuit to time-share the data transfer ports on the A/D board. Towards the top of the circuit board are the CMOS integrated circuits. The signal from the simulator entered the board at the bottom of the photograph and left the board to the A/D connector block near the top of the photograph.



Figure 4-23. Close-Up of the Prototype Circuit Board.

## **V. RESULTS AND CONCLUSIONS**

The results of this engineering project are promising. With the exception mentioned in Chapter III, the objective of replicating the attitude control portion, in particular the roll, pitch, and yaw rate equations, was achieved. This section will describe the results and offer some conclusions.

### **A. RESULTS**

#### **1. Digital Tracked Analog Signal**

As explained in Section IV-F, the digitally computed signal tracked the analog signal in roll, pitch, and yaw rate. The wave shape response to a one Hertz square wave input of the digital signal identically matched the analog response wave shape in roll and yaw. The pitch signal digital response however displayed a gain factor of approximately twice the analog signal. This meant that the digital signal would be more responsive in pitch command control inputs than the actual analog behavior. In short, the handling characteristics of the original trainer would be slightly different.

#### **2. Unexplained Gain**

The circuit was modeled using the resistor and capacitor values contained on the circuit. The internal resistance of the FETs however, was not modeled. The experiment explained in Section IV-E verified that neglecting the relatively small FET resistance would not adversely effect the results.

Although the waveforms and amplitudes matched, some unexplained gain was present. The source or reason for this gain could not be uncovered. Its effect on the model was not considered to be significant.

### **3. Difficulty Relating Constants from Circuit to Euler Equations of Motion**

The equations actually implemented, (4-2), (4-3), and (4-4) were different than equations, (2-81), (2-82), and (2-83) provided by Singer-Link as the Euler rate equations. No particular scaling factor could be determined to relate one to the other. Additionally, the Singer equations contained terms not present in the circuit and consequently not digitally modeled.

## **B. AREAS FOR FUTURE MODIFICATION**

During the course of this project, many possible areas for enhancement were discovered. *These embellishments would add to the trainer's utility as a teaching and research tool as well as serve as an excellent vehicle to gain an appreciation of the subtleties and concepts of good avionics design.*

### **1. Construct a Special Purpose A/D Circuit**

Although a PS/2™ Model-50 IBM general purpose computer was used for proof of concept of this project, future modifications should consider replacing the PS/2™ Model-50 with a microprocessor and an A/D converter. The hardware and interfaces could be greatly simplified and the relatively simple code could be contained on the microprocessor. A considerable amount of processing overhead was contained in the Lab Windows™ software. The Lab Windows™ software and National Instruments® hardware offered many many functions not utilized nor needed for this project.

## **2. Digitize All Analog Boards**

Once all the boards have been replicated in software, the possible modifications become almost limitless. The only boards which should remain in the simulator would be the power amplifier boards. These would amplify the inputs to the motion drive motors. Rather than simply manipulating the Euler equations, the core forces creating these forces and moments could be manipulated. Different aircraft lift curves could be easily added and the performance monitored.

As a next step, the relative wind analog card J20 would be the next card to replicate digitally. This card contains the lift, angle of attack, vertical speed, and other information used as an input for the attitude and other cards.

The software contained in Appendix A could be modified so that the RC time constants which are used to compute the rotation rates and angular positions are loaded from a data file. The RC time constants give the trainer its handling characteristics.

Lastly, it would be nice to be able to fly the trainer either digitally or in the analog mode. The circuit could be modified to isolate the analog cards if the digital computer were on line. In this manner, the digital computer would perform the flight simulation. If the digital computer were not on line, then the trainer would revert to the analog mode.

## **3. Add X-Y Plot**

The GAT-1B originally had a course plotter for the instructor to monitor student progress. The GAT-1B at the Naval Postgraduate School however, does not have one. Since no plotter was installed, the schematic,



Figure 3-8, shows no potentiometer in the yaw circuit. The potentiometer would relate aircraft heading to computer to indicate a track. A circuit similar to the one shown in Figure 5-1 would have to be constructed. Synchro data from the heading of the simulator would be converted to analog data then digitized for manipulation and computation.

#### **4. Add Visual**

Digitized attitude information could be transferred to another digital computer which is dedicated to the calculation and presentation of the display. The digital computer used to acquire and convert the analog information vector could not be used due to the time intense computational requirements for presenting visual information. The computer used for the analog conversion would be slowed down too much if it had to perform the visual as well as the A/D conversion and the flight attitude computations.

#### **5. Multi-Engine**

Although the GAT-1B is currently configured as a single engine aircraft simulator, there is no reason that multi-engine characteristics could not be added. In software, this would entail modifying the inputs to the aircraft equations of motion. Additional hardware, such as a potentiometer, would be necessary to simulate the power setting of the additional engine.

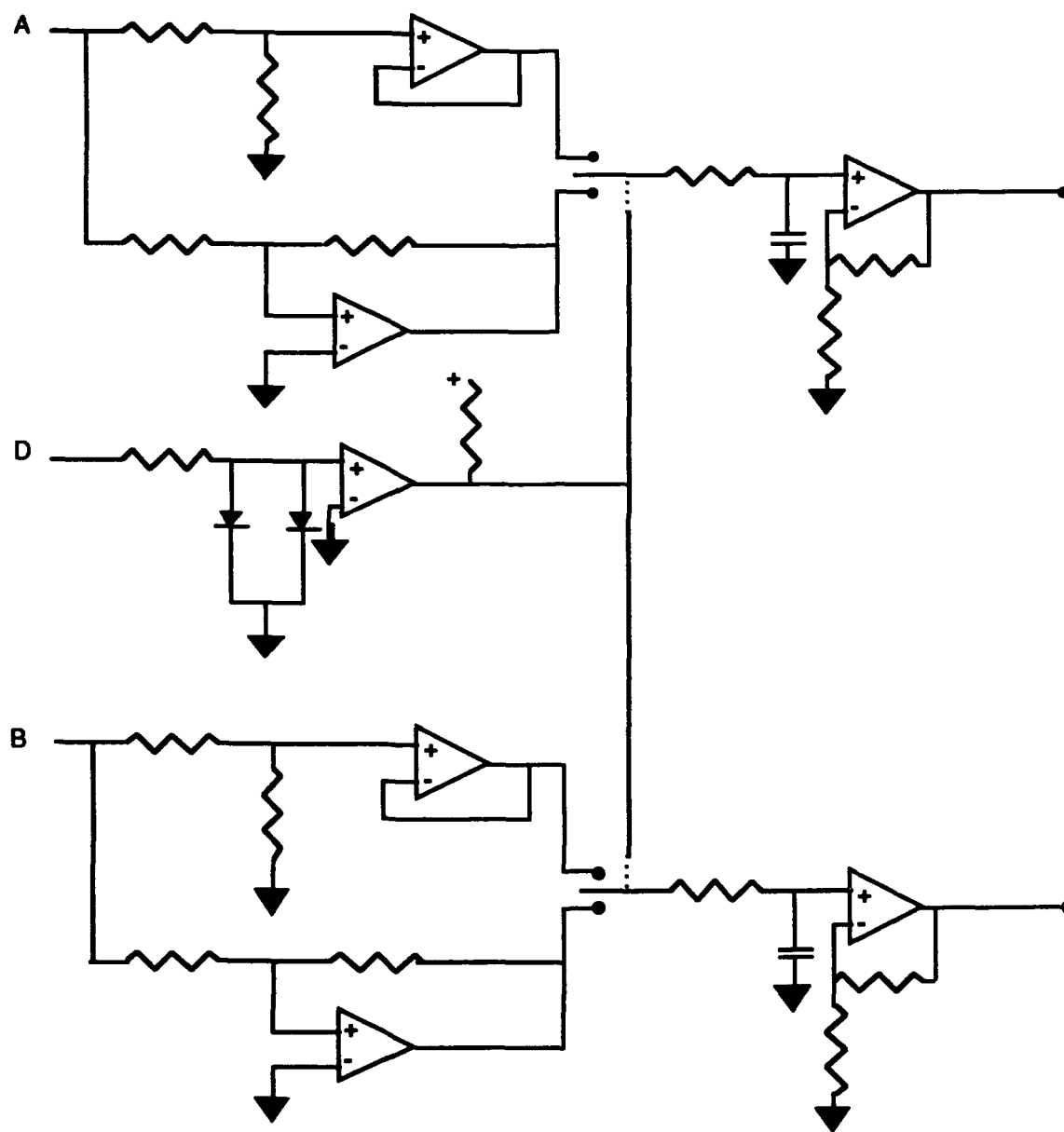


Figure 5-1. Synchro to Analog Converter Circuit.

## **6. Helicopter Equations of Motion**

If the equations dictating the aircraft motion were already in software, minor modifications would have to be made for the simulator to attain the performance characteristics of a helicopter. Hardware changes to the simulator would be necessary for the additional helicopter specific inputs necessary for these equations.

## **C. CONCLUSIONS**

This project began with the need for a clear understanding of the objective. The analog circuitry was studied at length. Interface hardware had to be designed, tested, and validated. Software had to be written, assessed and validated. The fundamental math model replicating the analog circuit had to be validated.

Many constraints also had to be considered. Software was written to execute as quickly as possible. Update rates became important to achieve continuity of kinesthetic feel. Parts availability and funding (lack of) became intertwined with the engineering solution.

This project clearly proved the viability of converting the GAT-1B™ flight simulator to a fully digital flight simulator. Signals were extracted and manipulated. The digital replication compared favorably to the analog response.

This project also demonstrated the multi disciplined nature of simulation engineering. All engineering disciplines, psychological and behavioral sciences come together in a successful simulation. A simulation engineer has to have working knowledge in multiple fields.

A digitized trainer could serve as an important laboratory device in such courses as AE 2036, Performance and Stability, AE 3340, Dynamic Stability of Aerospace Vehicles, AE 3341, Control of Aerospace Vehicles, and AE 4323 Flight Test of Aerospace Vehicles.

There is no substitute for actually experiencing the effects that certain parameter changes have on the handling characteristics of an aircraft. An academic exercise does not leave the student with a full appreciation for the dynamics involved.

This project clearly demonstrated the fundamental principle of all good avionics design. Data, received from whatever source or sensor via an interface, is multiplied and accumulated (digitally processed). The results are then used to indicated a particular condition and affect the functioning of the system.

```

rem DIGITAL FLIGHT SIMULATOR -- Attitude Card J22, GAT-1B
rem =====
rem =====
cls

dim buffer%(15), chan.vector%(15), gain.vector%(15)
dim volt.array(15), bin.val%(15)

rem      Clear, Initialize, and Configure Data Acquisition Board
rem      =====
err.num%=daq.clear(1)
board.code%=1
acq.err%=init.da.brds(1,board.code%)
acq.err%=daq.config(1,1,0)

rem      Set Analog Input and Output Configuration
rem      =====
err.num%=ai.config(1,1,10,0)
err.num%=ao.config(1,0,0,10.0,0)

rem      Configure Digital Port, A as Output, B as Input
rem      =====
err.num%=dig.prt.config(1,0,0,1)
err.num%=dig.prt.config(1,1,0,0)

rem      Set Square Wave Trigger Pulse for Timing
rem      =====
input "interrupt period in milliseconds.";millis%
delta.t#=#millis%*1.E-3
millis%=0.5*millis%
err.num%=ctr.square%(1,5,4,millis%,millis%)

rem      Set Real Time System Integration Bus
rem      =====
err.num%=rtsi.clear(1)
err.num%=rtsi.conn(1,5,1,1)
err.num%=rtsi.conn(1,8,1,0)

rem      Initialize Channel and Gain Vectors
rem      =====
for i%=0 to 15
    chan.vector%(i%)=i%
    gain.vector%(i%)=1
next i%

```

```
err.num%=scan.setup(1,16,chan.vector%(),gain.vector%())
```

```
rem      Values for Constants --- 1/RC
rem      =====
```

```
rem      Roll Rate (PA) Constants
rem      =====
```

```
roll.beta.con = 1/(22.6*2.2*1.E-3)
roll.ailer.def.con = 1/(30.9*2.2*1.E-3)
roll.RA..vel.ind.con = 1/(200.0*2.2*1.E-3)
roll.PA..vel.ind.con = 1/(68.1*2.2*1.E-3)
roll.thrust.net.con = 0
roll.PA..WOG.con = 1/(75.0*2.2*1.E-3)
roll.sine.phi..WOG.con = 1/(24.9*2.2*1.E-3)
```

```
rem      Pitch Rate (QA) Constants
rem      =====
```

```
pitch.elev.def.con = 1/(15.4*2.2*1.E-3)
pitch.Cl.con = 1/(5.9*2.2*1.E-3)
pitch.alfa.stall.con = 1/(13.0*2.2*1.E-3)
pitch.flap.def.con = 1/(301.0*2.2*1.E-3)
pitch.thrust.net.con = 1/(4075.0*2.2*1.E-3)
pitch.thrust.net..q.con = 0.0
pitch.elev.trim.con = 1/(24.9*2.2*1.E-3)
pitch.QA..vel.ind.con = 1/(30.1*2.2*1.E-3)
pitch.cg.konstant.con = 1/(1000.0*2.2*1.E-3)
pitch.QA..WOG.con = 1/(30.1*2.2*1.E-3)
pitch.fuse.mom.con = 7.5/(2870.0*2.2*1.E-3)
pitch.unknown.con = 7.5/(150.0*2.2*1.E-3)
pitch.WOW..WOG.con = 1/(100.0*2.2*1.E-3)
```

```
rem      Yaw (a.k.a turn rate, RA) Constants
rem      =====
```

```
yaw.rudder.def.con = 1/(35.7*2.2*1.E-3)
yaw.beta.con = 1/(27.4*2.2*1.E-3)
yaw.Cl..ailer.def.con = 1/(243.0*2.2*1.E-3)
yaw.RA..vel.ind.con = 1/(324.0*2.2*1.E-3)
yaw.thrust.net.con = 1/(1000*2.2*1.E-3)
yaw.RA..WOG.con = 1/(45.3*2.2*1.E-3)
yaw.rudder.def..WOG.con = 1/(255.0*2.2*1.E-3)
yaw.Cltd1.con = 100.0/44.2
yaw.Cltd2.con = 100.0/665.0
yaw.vert.stab.con = 4.7/(400.0*2.2*1.E-3)
```

```
rem      Initialize Roll, Heading and Pitch Rates
rem      =====
```

```
PA=0
QA=0
RA=0
PA.old=0
QA.old=0
```

RA.old=0

```
rem      Infinite Loop to Acquire Data and Output Results
rem      =====
while 1>0
err.num%=dig.Out.port(1,0,14)
    acq.err%=scan.start(1,buffer%(),16,1,25,4,2)
    acq.err% = daq.check (1,status%,points%)
        while status% = 0
            acq.err% = daq.check (1,status%,points%)
        wend

rem      Determine the Status (0 or 1) of WOG
rem      =====
err.num%=dig.in.line(1,1,0,WOG%)

rem      print:for i%=0 to 15:print buffer%(i%);:next i%

rem      Scaling the Voltage (converting from binary to volts)
rem      =====
acq.err%=daq.scale(1,1,16,buffer%(),volt.array#())

rem      Table of Voltage Array Elements
rem      =====
ailer.def =      volt.array#(0)
beta =          volt.array#(1)
q =             volt.array#(2)/5.0
psi.dot =       volt.array#(3)
thrust.net =    volt.array#(4)
vel.ind =       -volt.array#(5)/5.0
rudder.def =    volt.array#(6)
sine.phi=       volt.array#(7)/7.5
vel.p =         volt.array#(8)
WOW =           volt.array#(9)
elev.trim =     volt.array#(10)
elev.def =      volt.array#(11)
flap.def =      volt.array#(12)
Cl =            volt.array#(13)
alfa.stall =    volt.array#(14)
sine.theta =    volt.array#(15)/7.5

cg.konstant = 0.0

Cltd = -Cl/5.0
if Cltd <0 then
    Cltd = 0
end if

cos.phi=sqr(1-sine.phi^2)
```

```

rem      due to diode in circuit for alfa stall computations
rem      if alfa.stall > 0 then
rem          alfa.stall = 0
rem      end if

rem      The input vevtor is routed through a 50% voltage divider.
rem      sine.phi and sin.theta are dividied by 7.5 to scale them to +/- 1
rem      q and vel.ind are divided by 5 to make them equivalent to their
rem      time divided counterparts.

rem      Roll Rate (PA) Calculations
rem      =====
dPA1=q*(beta*roll.beta.con+ailer.def*roll.ailer.def.con)
dPA2=(-RA.old*roll.RA..vel.ind.con+PA.old*roll.PA..vel.ind.con)
dPA3=-thrust.net*roll.thrust.net.con

dPA4=WOG%*(sine.phi*roll.sine.phi..WOG.con+PA.old*roll.PA..WOG.con)
dPA=dPA1+vel.ind*dPA2+dPA3+dPA4
PA = PA.old - dPA*delta.t#
PA.old=PA

rem      Pitch Rate (QA) Calculations
rem      =====
dQA1=(elev.def*pitch.elev.def.con-pitch.fuse.mom.con+cl*pitch.Cl.con)
dQA2=(alfa.stall*pitch.alfa.stall.con+flap.def*pitch.flap.def.con)

dQA3=(thrust.net*pitch.thrust.net..q.con+elev.trim*pitch.elev.trim.con)

dQA4=QA.old*pitch.QA..vel.ind.con*vel.ind
dQA5=(thrust.net*pitch.thrust.net.con)
dQA6=cg.konstant*pitch.cg.konstant.con
dQA7=(QA.old*pitch.QA..WOG.con-sine.theta*pitch.unknown.con)

      if dQA7 < 0 then
          dQA7 = 0
      else
          dQA7 = dQA7
      end if

dQA8=(WOW*pitch.WOW..WOG.con)
dQA9=(dQA7+dQA8)*WOG%
dQA=q*(dQA1+dQA2+dQA3)+dQA4+dQA5+dQA6+dQA9
QA = QA.old - dQA*delta.t#
QA.old=QA

rem      Heading Rate (RA) Calculations
rem      =====
dRA1=(rudder.def*yaw.rudder.def.con-beta*yaw.beta.con)

```



```

dRA2=Cltd*ailer.def*yaw.Cltd1.con+ailer.def*yaw.Cltd2.con
dRA2=-dRA2*yaw.Cl..ailer.def.con-yaw.vert.stab.con
dRA3=RA.old*yaw.RA..vel.ind.con*vel.ind
dRA4=(RA.old*yaw.RA..WOG.con+rudder.def*yaw.rudder.def..WOG.con)
dRA5=thrust.net*yaw.thrust.net.con
dRA=q*(dRA1+dRA2)+dR.3+dRA4*WOG%+dRA5
RA = RA.old - dRA*delta.t#
RA.old=RA

rem      Euler Angle Calculations
rem      =====
THETA.dot = QA*cos.phi - RA*sine.phi
PHI.dot = PA + psi.dot*sine.theta
PSI.dot.dot = RA*cos.phi+QA*sine.phi

hi.bits%=0

rem      Output results
rem      =====
acq.err% = ao.vscale(1,0,psi.dot*sine.theta#,bin.val%(1))
acq.err% = ao.vscale(1,0,RA*sine.phi#,bin.val%(2))
acq.err% = ao.vscale(1,0,QA*sine.phi#,bin.val%(3))
acq.err% = ao.vscale(1,0,PA#,bin.val%(4))
acq.err% = ao.vscale(1,0,QA#,bin.val%(5))
acq.err% = ao.vscale(1,0,RA#,bin.val%(6))

err.num%=dig.Out.Port(1,0,hi.bits%+2)
for chan% = 0 to 15
    err.num%=ao.write%(1,0,bin.val%(chan%))
    err.num%=dig.Out.Port (1,0,hi.bits%+1)
    err.num%=dig.Out.Port (1,0,hi.bits%)
next chan%
wend

end

```

## LIST OF REFERENCES

- Anderson, John D., *Introduction to Flight*, New York, McGraw-Hill Book Company, 1985.
- Caro, P.W., *Some Factors Influencing Transfer of Simulation Technology*, The Royal Aeronautical Society, Third Flight Simulation Symposium, *Theory and Practice in Flight Simulation*, London, 1976.
- DOS LabDriver Software Reference Manual*, Austin, Texas: National Instruments Corporation, 1989.
- Etkin, Bernard, *Dynamics of Flight*, 2nd ed., New York, New York: John Wiley and Sons, 1982.
- Gerald, Curtis F., and Wheatley, Patric O., *Applied Numerical Analysis*, Fourth Edition. Reading Massachusetts: Addison-Wesley Publishing Company, 1989.
- Halfman, Robert L., *Dynamics - Particles, Rigid Bodies, and Systems*, Reading, Massachusetts: Addison-Wesley Publishing Company, 1962.
- Keegan, J.B., *The Design of Simulators as Aids to Instruction*, The Royal Aeronautical Society, Third Flight Simulation Symposium, *Theory and Practice in Flight Simulation*, London. 1976.
- Lab Windows® User Manual*, Austin, Texas: National Instruments Corporation, 1989.
- Lab Windows® User Manual Supplement, The Data Acquisition Library*, Austin, Texas: National Instruments Corporation, 1989.
- Link General Aviation Trainer GAT-1 Operation and Maintenance Manual*, Binghamton, New York: Singer-Simulation Products Division, 1973.
- Link General Aviation Trainer GAT-1B Systems Descriptons*, Binghamton, New York: Singer-Simulation Products Division, 1972.
- Link General Aviation Trainer GAT-1 Illustrated Troubleshooting Guide (serial no. 150 and up)*, Binghamton, New York: Singer-Simulation Products Division, date unknown.

Mitchel, F. H., Sr., and Mitchel, F. H., Jr., *Introduction to Electronics Design*, Englewood Cliffs, New Jersey: Prentice Hall, 1988.

Nelson, Robert C., *Flight Stability and Automatic Control*, New York, New York: McGraw-Hill Book Company, 1989.

Ostendorf, William, ed., *Principles of Naval Weapons*, Pensacola: Naval Education and Training Command, 1982.

Parish, Lex, *Space-Fight Simulation Technology*, Indianapolis: Howard W. Sams & Co., Inc., 1969.

Rolfe, J.M., and Staples, K.J. *Flight Simulation*, Avon, Great Britain: The Bath Press, 1986.

Roskan, Jan, *Airplane Flight Dynamics and Automatic Flight Control*, Ottawa, Kansas: Roskam Aviation and Engineering Company, 1979.

The Comptroller General of the United States, *Greater Use of Flight Simulators in Military Pilot Training Can Lower Costs and Increase Pilot Proficiency (B-157905)*, Washington, D.C.: United States General Accounting Office, 1973.

Wolko, Howard S., ed., *The Wright Flyer - An Engineering Perspective*. Washington D.C.: Smithsonian Institution Press, 1987.

## BIBLIOGRAPHY

Anderson, John D., *Fundamentals of Aerodynamics*, New York, New York: McGraw-Hill Book Company, 1984.

Anderson, John D., *Introduction to Flight*, New York, New York: McGraw-Hill Book Company, 1985.

Bertin, John J., and Smith, Michael L., *Aerodynamics for Engineers*, 2nd ed., Englewood Cliffs, New Jersey: Prentice Hall, 1989.

The Comptroller General of the United States, *Greater Use of Flight Simulators in Military Pilot Training Can Lower Costs and Increase Pilot Proficiency (B-157905)*, United States General Accounting Office, Washington, D.C., 1973.

Donohue, Paul F., *An Aerodynamic Performance Evaluation of the NASA/Ames Research Center Advanced Concepts Flight Simulator*, Master's Thesis, Naval Postgraduate School, Monterey, California, June 1987.

*DOS LabDriver Software Reference Manual*, Austin, Texas: National Instruments Corporation, 1989.

Etkin, Bernard, *Dynamics of Flight*, 2nd ed., New York, New York: John Wiley and Sons, 1982.

Gerald, Curtis F., and Wheatley, Patrick O., *Applied Numerical Analysis*, Reading, Massachusetts: Addison-Wesley Publishing Company, 1989.

Halfman, Robert L., *Dynamics - Particles, Rigid Bodies, and Systems*, Reading, Massachusetts: Addison-Wesley Publishing Company, 1962.

*Lab Windows® User Manual*, Austin, Texas: National Instruments Corporation, 1989.

*Lab Windows® User Manual Supplement, The Data Acquisition Library*, Austin, Texas: National Instruments Corporation, 1989.

*Link General Aviation Trainer GAT-1 Operation and Maintenance Manual*, Binghamton, New York: Singer-Simulation Products Division, 1973.

*Link General Aviation Trainer GAT-1B Systems Descriptions*, Binghamton, New York: Singer-Simulation Products Division, 1972.

*Link General Aviation Trainer GAT-1 Illustrated Troubleshooting Guide (serial no. 150 and up)*, Binghamton, New York: Singer-Simulation Products Division, date unknown.

Martinson, Steven Paul, *An Inexpensive Real-Time Flight Simulator for the United States Marine Corps' Airborne Remotely Operated Device*, Master's Thesis, Naval Postgraduate School, Monterey, California, June 1988.

Meriam, J. L., and Kraige, L. G., *Dynamics*, 2nd ed., New York, New York: John Wiley and Sons, 1986.

Mitchel, F. H., Sr., and Mitchel, F. H., Jr., *Introduction to Electronics Design*, Englewood Cliffs, New Jersey: Prentice Hall, 1988.

Naval Training Equipment Center, *Proceedings of the Eighth NTEC/Industry Conference for New Concepts for Training Systems*, Orlando, Florida: Chief of Naval Education and Training, 1975.

Nelson, Robert C., *Flight Stability and Automatic Control*, New York, New York: McGraw-Hill Book Company, 1989.

North Atlantic Treaty Organization (Organisation Du Traite De Atlantique Nord) Advisory Group for Aerospace Research and Development, *AGARD Conference Proceedings No. 79 on Simulation*, London England, 1971.

North Atlantic Treaty Organization (Organisation Du Traite De Atlantique Nord) Advisory Group for Aerospace Research and Development, *AGARD Conference Proceedings No. 198 on Flight Simulation/Guidance Systems Simulation*, London, England, 1976.

Naval Postgraduate School NPS52-87-034, McGhee, *An Inexpensive Real-Time Three-Dimensional Flight Simulation System*, by Robert. B., and others, July 1987.

Parish, Lex, *Space-Fight Simulation Technology*, Indianapolis, Indiana: Howard W. Sams & Co., Inc., 1969

Roskan, Jan, *Airplane Flight Dynamics and Automatic Flight Control*, Ottawa, Kansas: Roskam Aviation and Engineering Company, 1979.

The Royal Aeronautical Society, Third Flight Simulation Symposium, *Theory and Practice in Flight Simulation*, London, England: 1976.

Vassos, Basil H., and Ewing, Galen W., *Analog and Digital Electronics for Scientists*, New York, New York: John Wiley & Sons 1985.

Whalen, Harold R. III, *A Preliminary Software Design for a Personal Computer Based Antisubmarine Warfare Tactical Flight Simulator*, Master's Thesis, Naval Postgraduate School, Monterey, California, September 1985.

Wolko, Howard S., ed., *The Wright Flyer - An Engineering Perspective*. Washington D.C.: Smithsonian Institution Press, 1987.

Zyda, Michael, J., and others, "Flight Simulators for Under \$100,000," *IEEE Computer Graphics & Applications*, January 1988.

## INITIAL DISTRIBUTION LIST

		No. Copies
1.	Defense Technical Information Center Cameron Station Alexandria, Virginia 22304-6145	2
2.	Library, Code 0142 Naval Postgraduate School Monterey, California 93943-5002	2
3.	James P. Hauser, Code 67HS Department of Aeronautical and Astronautical Engineering Naval Postgraduate School Monterey, California 93943-5000	2
4.	Louis V. Schmidt, Code 67SC Department of Aeronautical and Astronautical Engineering Naval Postgraduate School Monterey, California 93943-5000	1
5.	LCDR George D. Duchak, USN Space and Naval Warfare Systems Command Washington, D.C. 20363-5100	4
6.	Chairman Department of Aeronautical and Astronautical Engineering Naval Postgraduate School Monterey, California 93943-5000	1
7.	Anthony M. Cook (FS) Assistant Chief, Flight Systems and Simulation Research Division M/S 243-1 Room Number 105 NASA Ames Research Center Moffet Field, California 94035	1